REGIONALISATION OF SEISMIC VELOCITIES FOR PRECISE EARTHQUAKE LOCALISATIONS IN KENYA. /1

by

KATAKA MILTON OBOTE.

A thesis submitted as partial fulfillment for the award of Master of Science Degree at the University of Nairobi.

College of Biological and Physical Sciences
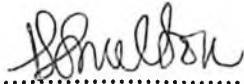Faculty of Science
Department of Geology

UNIVERSITY OF NAIROBI, 1996

(i)

DECLARATION

I Milton Obote Kataka, hereby declare that this is my own work and has not been presented

for a degree at any other University.

MILTON OBOTE KATAKA.

This thesis has been submitted for examination with our knowledge as University supervisors.

Dr. RAIMUND STANGL

Dr. JUSTUS O. BARONGO

ABSTRACT

The essential part of this study has involved the determination of seismic velocities for different regional waves using natural earthquake data. The analysis was based on available catalogues. The whole territory of Kenya was taken into consideration for the period 1964-1990. Travel time collected from 1964-1990 are based on the bulletins from the International Seismological Centre (ISC) whose accuracy in localisations have been assumed to be better than the other reporting agencies for reasons mentioned in the text. The data from the catalogues have been used to compute velocities by least-square fit approach and correction of the Nairobi M_L magnitudes has been done by correlating them to the mb_{ISC} magnitudes.

Eight major sectors were established from the seismicity map of Kenya adopted from Olang (1992). The sectors have been taken to be relatively narrow to meet the assumption that the geological structure is constant in whole the sector. A profile was established in each sector dividing it into two equal parts. The events were considered as if they were recorded on this line. These sectors covers all parts of Kenya. Some of them are in the direction of Kenya Rift International Seismic Project (KRISP) and the others ended up filling the gaps left by the KRISP90 results.

The epicentral distances and azimuths have been calculated. The seismograms have been read and the travel times computed for each phase. These travel times have been plotted against the epicentral distances after obtaining their reduced travel times. In this case events were plotted from one station with increasing epicentral distances. This is a reverse of the conventional method usually used. The velocities have been used to do the modelling of a one-dimensional flat earth model.

Profile 1, extending towards the north eastern part of Kenya lying in the Rift Valley had a Pn of 7.93 km/s. The region extending towards the Western Rift Valley (Profile 2) reflected a Pn velocity of 8.03 km/s, Sn of 4.72 km/s, Pg of 6.31 km/s and Sg of 3.63 km/s. The area extending towards the Lake Victoria (profile 3) has velocities of, 8.27 km/s for Pn, 4.77 km/s for Sn, 6.34 km/s for Pg and 3.63 km/s for Sg. The profile 4 which extends towards the southwestern part of Kenya and north eastern part Tanzania resulted in the following velocities, Pn of 8.13 km/s, Sn of 4.72 km/s, Pg of 6.34 km/s, and Sg of 3.64 km/s. The region extending towards the southern part of Kenya and northern part of Tanzania (profile 5) resulted in a Pn of 8.06 km/s, Sn of 4.66 km/s, Pg of 6.38 km/s and Sg of 3.67 km/s. The region extending to the coastal part of Kenya (profile 6) had Pg of 6.41 km/s and Sg of 3.67 km/s. Profile 7 extends towards the north eastern part of Kenya resulted in Pg of 6.28 km/s.

A unified dataset including all data resulted in a Pn of 8.12 km/s, Sn of 4.68 km/s, Pg of 6.35 km/s and Sg of 3.65 km/s. On average the localisations from this model is close to that of the Nairobi East model (NAI-EAST) from KRISP refraction study. The travel times obtained from the unified model were in agreement with NAI-EAST. The computed

travel times had a difference of less than 1.5 secs. This can be explained from the poor known source depths and errors in phase readings.

The velocities for the various phases and time intercepts for Pn and Sn have been used to compute velocity-depth functions for the selected profiles. The lower crustal velocities and the upper mantle thicknesses have been taken from the KRISP90 experiments as these two parameters could not be resolved from the data. The Moho depths and the S wave velocities in the lower crust have then been modelled for the corresponding profiles. The profiles 1, 6, 7, and 8 could not be modelled because, the first three had no observed Sn while the later had no ISC localised events. The modelled profiles had an average thickness of 35-37 km. The KRISP90 models have been retained for profiles 1, 7 and 8.

It has been observed that there is need for regionalisation of seismic velocities for the Kenyan crust. The Finnish velocity model has been found to be useful for the profile extending towards the coastal region through the Chyulu hills. It mislocates events with an error of 50-60 km for the other regions. The East African model (EAF) which has been used in the two workshops (of Dar- es-salaam and Nairobi) sponsored by International Programs for Physical Sciences (IPPS), with some minor modifications can be used to localise events from western part of Kenya extending towards the Western Rift Valley. The events from the Eastern Rift Valley are better located with the KRISP90 model for the rift valley. The Unified velocity depth model and those from profiles 4 and,5 can be used for regions tending towards Lake Victoria especially the Homa Bay area and those of from southern part of Kenya extending into Tanzania. This therefore indicates that the unified model can not be used as an average model for the Kenyan crust.

The Nairobi local magnitude ML_{NAI} is over estimated compared to mb_{ISC} on Richter scale. Nairobi local magnitude can be corrected to mb_{ISC} with the formula:
$$mb_{ISC} = (0.78 \pm 0.3)M_{L(NAI)} + 0.39 \pm 0.01$$

ACKNOWLEDGEMENTS

(v)

Lastly but not least, I would like to thank Prof. Gaciri, chairman Geology Department, and members of staff for their encouragement and very productive pieces of advice during my course.

(vi)

TABLE OF CONTENTS

(vii)

(ix)

LIST OF TABLES

LIST OF FIGURES

CHAPTER ONE

Introduction.

Kenya is part of the East African Rift Zone which is tectonically active (Girdler, 1972). Geophysical studies have recently been made in this area (KRISP WORKING GROUP, 1991) and seismological studies have increased both in number and significance since the development of seismograph networks in Africa in the 1950's (Rodrigues, 1970; Shah, 1986). Most of these studies are centred in the Rift Valley due to the interesting geological and tectonic features (see figure 1.1). But a lot is desired in this field to unravel the misunderstandings and overgeneralizations which have often been attributed to the area.

The limited number of seismograph stations and poor management of the few installed have been the major problems in these studies. The first modern seismographs were installed in Eastern Africa in 1953 by Institute pour La Recherche Scientifique en Africa Centrale (IRSAC). An improvement was made in 1963 with the installation of the World Wide Standardized Seismograph Network (WWSSN), (Shah, 1986). For the last three decades or so, detection and location of earthquakes in Africa improved in general. The increasing number of seismograph stations and later on, the fast computation of earthquake locations with computers have made things much easier and enabled localisations with errors of ± 100 km as was found in East Africa (Gutenberg and Richter, 1954; Rothe', 1954). It is hoped that the new digital network in Kenya with those in the neighbouring countries will bring very promising results as far as detection and localisations are concerned. The Eastern Africa Regional Workshops Group Meetings currently sponsored by the International Programs for Physical Sciences

Despite this improvement the accuracy is still debatable. This is wholly dependent on the poorly known crustal structure of the country which in turn influences the localisation accuracy.

Precise locations of earthquakes have been one of the major problems to seismologists. To achieve an improvement, a dense network of seismic stations is necessary. In Africa however, there is normally one station in many countries, therefore events can not be accurately located.

All seismological studies assume certain starting models before the interpretation is done (e.g. Jeffreys-Bullen and Gutenberg-Richter tables). These models represent an average for the whole Earth and therefore do not apply everywhere in the Earth, because the crustal thickness and composition is not the same everywhere. For example, the model formerly used in Kenya assumes the thickness of the crust to be about 40 km. In Kenya however, the crust is much thinner in many parts of the country as per the values given by various results of the Kenya Rift International Seismic Project KRISP experiments (KRISP WORKING GROUP, 1991) show. Therefore, the localisations of earthquakes using this model will not be precise.

Information about the crustal structure in Kenya comes mainly from the studies of the three refraction seismic experiments carried out in Kenya. The KRISP experiments i.e KRISP68, KRISP85, and KRISP90. The first two refraction studies were constrained to the Rift Valley (KRISP WORKING GROUP, 1991). The most recent seismic experiment (KRISP90) not only confirmed the findings of the previous experiments but also gave a completely new picture of the crustal structure in and across the Rift Valley. The detailed information about P- and S-wave velocities in the crust is now available. With this information and with existing seismic

(IPPS), where SEISAN software by Havskov and Utheim (1992) is in use for the analog data has made it possible to locate a larger number of earthquakes than before that have occurred in the Eastern African region and will lead to the release of quarterly bulletins. This is bound to give very promising results in the near future. But the SEISAN package cannot be used for local earthquakes in any country without care, as it may not represent the crustal structure properly.
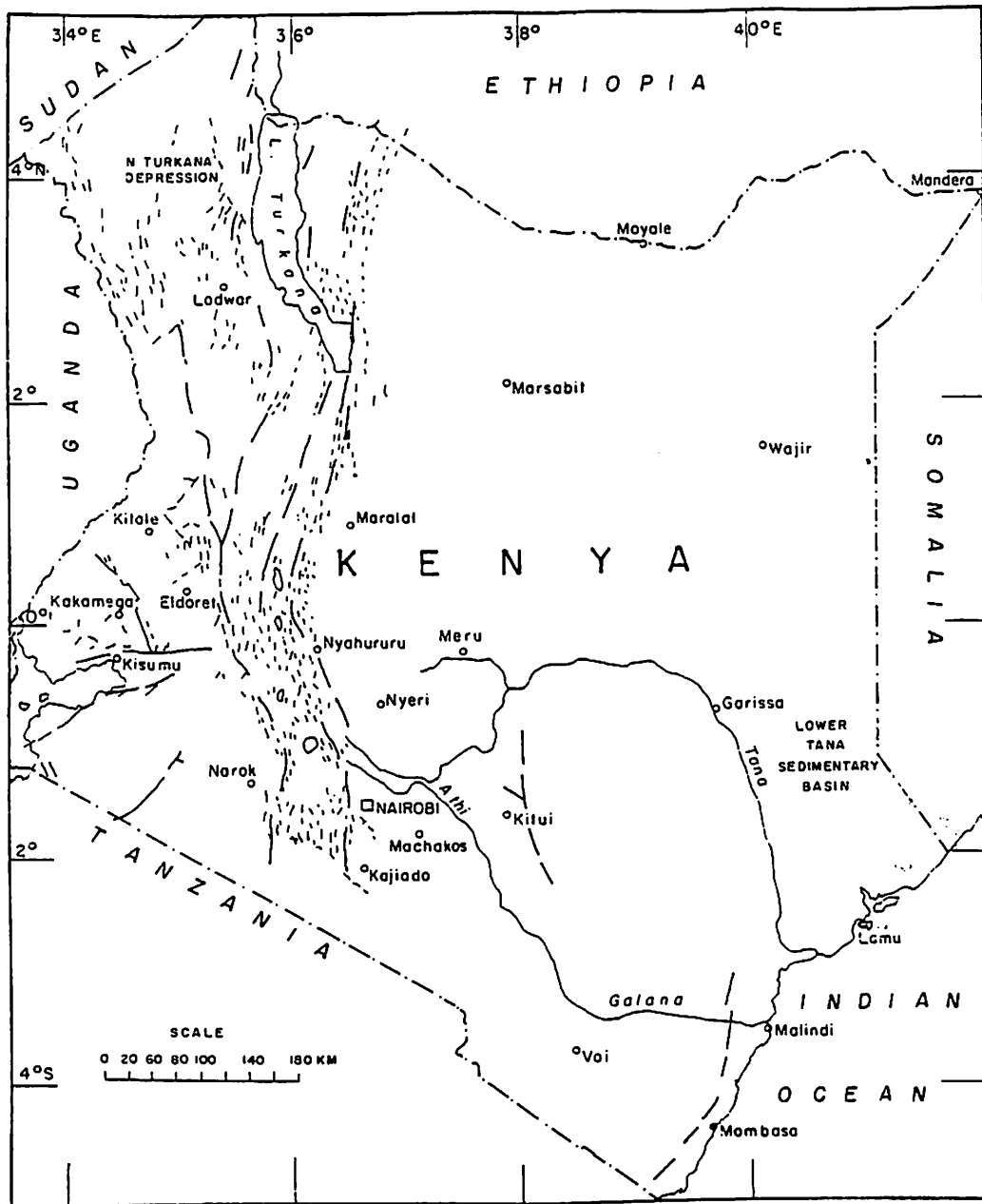
Figure (1.1) Map of Kenya with its main tectonic features.The dashed lines represents the major faults, while the small dots represents the minor faults and the circular dark dots represents the locations of the proposed Kenya network (adopted from G.D S'ouza)

data, we can obtain reasonably good models for several regions (or one) in Kenya to locate earthquakes more precisely.

With the projected digital network in Kenya, it will be possible to study the seismicity over a wide range of magnitudes. The network will also allow the study of source mechanisms for particular larger earthquakes and relate them to the tectonic processes in Kenya. The precise locations of earthquakes however, requires a good knowledge of the crustal structure. From the work of Rodrigues (1970) and Olang (1992), it can be seen that the choice of the travel time base has a strong influence on the calculated locations. In the previous studies, travel time tables for global earth models have been used. As mentioned above, the crustal structure in Kenya differs much from these standard models, thus reducing their value for locating earthquakes in the area.

In this study, the one-dimensional models obtained will allow a precise location of earthquakes recorded from this network. In order to obtain a broader database, the seismic data from Nairobi station between 1964 to 1990 have been reanalysed.

1.1 OBJECTIVES AND METHODOLOGY

The principle aim of this study is to obtain convenient velocity-depth models for different regions in Kenya to determine the epicentral distance from observed arrival times of seismic crustal waves with the highest precision possible.

This study will use collected seismological data, group them in profiles, obtain velocities of the

well located events, obtain velocity depth models, compare them with the previous studies and find out if regionalisation is necessary (possible), these models established fills the gaps left by the KRISP experiments. The main contribution of the present study is the regionalisation of wave velocities which has been achieved by analysing the events located by International Seismological Centre (ISC). From the seismicity map of Olang (1992), see Figure 3.6 in section 3.3.2, eight major sectors (fans) were delineated. Selected events in each sector were picked and travel times were established (for details refer to section 3.3.4) for curve plotting which led to the interpretation.

The main objectives of the study are:

1. To collect seismological data from 1964 to 1990 using records from the seismograph station in Nairobi (NAI) belonging to the Nairobi World Wide Standardized Seismological Network (WWSSN).

2.   Group the data into profiles.

4.   Obtain wave velocities from well located events and compare them with previous studies, to reveal if there is need to regionalise them.

5.   Establish models for precise earthquake localisations for various parts of the country.

6.   Relocate the earthquakes and analyse the residuals with regard to other models.

7.   The best model will then be established, for routine use of future data analysis henceforth.

The study started in its first phase with an analysis of all earthquakes above a local magnitude of 3 on the Richter scale for the period between 1964 and 1990, to extend Olang's (1992) dataset. As Olang's (1992) readings of the arrival times have not been available, a reanalysis

of the events given by Olang (1992) was necessary. In that way, a complete database for all earthquakes above magnitude 3 on the Richter scale in Kenya was obtained for the period 1964 to 1990. Based on the dataset a regionalisation of the earthquakes was done in the following way:

1. From the epicentral map of local earthquakes of Olang (1992), several sectors were established by taking into account the grouping (frequency) of earthquakes and the geology. The sectors (fans) were taken as open triangles centred in Nairobi and the events inside them were used for phase picking (refer to section 3.3.4 for details).

2. Travel times for the well located earthquakes were computed and velocities for several P- and S- phases estimated in those regions where there were sufficient data.

3. A literature review was used to obtain velocity depth functions for those regions in Kenya and adjacent areas with insufficient earthquake data.

The analysis and interpretation was done by means of microcomputer programs. This was done mainly by graph plots from the data obtained and calculation of regression coefficients. For a brief description of the programs used see section 1.5.

The results of the locations were compared with other models (Gutenberg-Richter 1942 and Jeffrey's-Bullen, 1958) and the "best fit" for each region was obtained. These models are the ones which will be used later to relocate earthquakes by means of the new digital network.

1.2 Study area.

All earthquakes which occurred in any part of the territory of Kenya were taken into account.

The area covered was the whole of Kenya which lies between 4^0 45" S to 5^0 0" N and 33^0 58" E to 41^0 15" E . The neighbouring countries, Uganda, Tanzania, Sudan and Ethiopia were used for their strong events as well. Only events in the specified profiles from their respective sectors have been used.

1.3 The Nairobi seismograph station

The Nairobi seismograph station was installed and operated by the Mines and Geology Department from 1963 to 1964 and operated by the Geology department of the University of Nairobi from 1964 onwards (Loupekine, 1971). The Nairobi station started its operation in June 1963 as part of the WWSSN network and is situated on longitude 36^0 48" 13" E and on latitude 1^0 16" 26" S at an altitude of 1692 metres. The instrument consists of three short period Bennioff and three long period (Sprengnether) seismometers which are of electromagnetic type. This station was previously recording with galvanometers on photographic paper and was changed into a heat stylus system in 1988.

1.4   Data file

APPENDIX I shows the unified magnitude, azimuths calculated from the epicentral coordinates giving a homogeneous catalogue. It is homogeneous in the sense that the local magnitude of Nairobi has been converted to the ISC body wave magnitude following unification formula and the unification formula obtained in this study (section 5.5). The arrival times are available in a special report, Kataka and Stangl (1994).

1.5 Computer Programs

Analysis and interpretation of data were done by microcomputers at two seismic laboratories; i.e. at the Department of Geology (University of Nairobi) and Department of Seismology, Uppsala University. The following computer programs were used:

(a) EPIDIST (Stangl, 1984), to calculate the azimuth and the epicentral distance to the located earthquakes.

(b) LOTUS 123 and MATLAB software packages used in constructing graphs of travel times and in the regression of data to obtain velocities in the crust and mantle and plots for magnitude correction.

(c) TRAVTIME (Stangl, 1986), to model the observed travel times and velocities.

(d) TRAVTAB (Stangl, 1992) to compute travel time tables for the obtained crustal models.

(e) SEISAN (Havskov and Utheim, 1992), for comparing the locations from different models and relocating the events from the established models.

(f) EQMAP (Lomax, 1989), for the plotting of the relocated events to give a new seismicity map.

CHAPTER TWO

PREVIOUS WORK

2.1 Seismicity of Kenya

The frequency of occurrence of earthquakes in Africa prompted the writing of early travellers

and explorers who indeed experienced a lot of problems in their communications. Isolated cases

of tremors were first reported in 1906 by Montessus de Ballore without any seismicity

attachment (Shah 1986). Seismic activity in East African Rift valley was studied by Sieberg

(1904) and later detailed by Krenkel (1921). Their work is based on macroseismic

investigations. Gutenberg and Richter (1949; 1954) produced the first epicentral maps using data

from distant seismograph stations. They were the first to use instrumental data and listed a

number of earthquakes for the region of interest ranging in magnitude from 6.0 to 7.0. Their

accuracy of the epicentral locations, however cannot be considered to be significantly adequate.

Studies relating mainly on the seismicity of the Western Rift were carried out by Sutton and

Berg (1958), De Bremaeker et al (1959) using data of the seismograph station network of the

Institute Pour La Recherche Scientifique en Africa Centrale (IRSAC). Wohlenberg (1968) gave

epicentre locations for period 1958 to 1963 for the Eastern rift as well.

Gorshkov (1961) summarised all reviews of seismicity of East Africa in a rather general report

on seismicity of Africa as a whole. He concluded that the majority of the epicentres in East

Africa fall within the graben structure. He considered that the accuracy of the location of the

epicentres prior 1958 is sufficiently high to warrant such an assertion.

Dopp (1964) used epicentres located by IRSAC network which were used for the profile construction to the stations. The epicentres had been located by use of the difference in the arrival times of P and S phases, (S - P times) so that the determined velocities were in agreement with the Jeffreys-Bullen (1958) values as these were the tables used. Dopp (1964) gave values of 5.57 km/s for Pg at a mean depth of 16 km and 6.7-6.82 km/s for an intermediate layer.

Sykes and Landisman (1964) recomputed the epicentres for the period January 1955 through March 1964 for the entire area of the East Africa Rift System. The improved locations with an error of ±10-20km for the best located events revealed a better correlation with the major tectonic features.

Fairhead (1968) used joint epicentre determination method to study the accuracy of epicentral locations of larger earthquakes in East Africa. His results were in line in terms of accuracy with the US-Coast and Geodetic Survey (USCGS) locations. The study of Fairhead and Girdler (1971) was done between the period January 1963 to December 1970 on seismicity of Africa and they found that the Western Rift is more seismically active than the Eastern Rift Valley.

Gumper and Pomeroy (1970) studied the frequency content of the Sn-phase and velocities of seismic waves in both rift and stable continental regions of Africa. Lahr and Pomeroy (1970) investigated the aftershock activity of the Toro earthquake of 20th Mar. 1966.

Wohlenberg (1968; 1969; 1970) studied the earthquake activity of the central part of the East Africa system between 4^0 N and 12^0 S and 23^0 E and 44^0 E, for the period 1958 to 1963,

using instrumental data from the IRSAC network and in some special cases from the Nairobi

station (WWSSN). He found out that; firstly, almost all tectonic structures are seismically active

and secondly, a number of active zones are not connected with any known tectonic structures

(e.g Malagarosi area and region between Eyasi and Rukwa Rifts of Tanzania) Shah (1986).

Loupekine (1971) compiled a catalogue of felt earthquakes for Kenya. A catalogue for Tanzania

which includes historical and macroseismic data was produced by Ambraseys (1972). A detailed

catalogue of earthquakes which includes felt earthquake data was compiled for Ethiopia by

Gouin (1979). Rodrigues (1970) gave a summary of macroseismic data for Tanzania, Uganda

and Kenya and includes an analysis of information contained in the earthquake catalogue of East

Africa which was compiled by the Geology Department, University of Nairobi in 1976.

Hamilton et al (1973) operated a network to locate earthquakes associated with geothermal

prospects. Earthquakes were mostly observed in the southern half of the lake Hanington (now

called Lake Bogoria which is situated in the Rift Valley of Kenya) in the general vicinity of

geothermal activity.

A microseismic survey in the Stiegler's gorge area in Tanzania was done by Bungum and Nnko

(1984), between the period 1978 and 1987. Many regional earthquakes were located of

magnitude 0-4. Molnar et al (1970) made a microearthquake study along the rift floor in

Ethiopia and revealed a surprisingly low level of activity compared with that found in Kenya

rift.

Bungum and Ringdal (1982) reviewed all information available at Norway Seismic Array

(NORSAR) on tectonics and seismicity of Kenya with emphasis on the Turkwel gorge area. For a period of 70 years till the end of 1981 they found 715 earthquake reports with data from the newly established World Wide Standardised Seismological Station Network (WWSSN) of US-Coast and Geodetic Survey (USGSS) which considerably enhanced the accuracy of epicentral locations in Africa.

Shah (1986) in her Ph.D thesis established that seismicity was not so much related to the geological structures. The study showed that, the eastern rift valley appears to be significantly less seismic than the western rift valley and the northern Tanzania. The most generally accepted explanation for this is that the lithosphere in Kenya is rather thin and weak, with a very high rate of heat flow from the partly fluid asthenosphere. Crustal stress in Kenya is dissipated in large number of very small shocks, and does not build up to the degree that it does in the more rigid parts of the region (Scholz, 1990). She found out that, on a wider scale, the seismic activity in East Africa is in comparison with one of a mid-oceanic ridge. In the study she came out with two seismicity maps one from macroseismic data and the other from instrumental data for East Africa as shown in Figs. 2.1 a and b below.
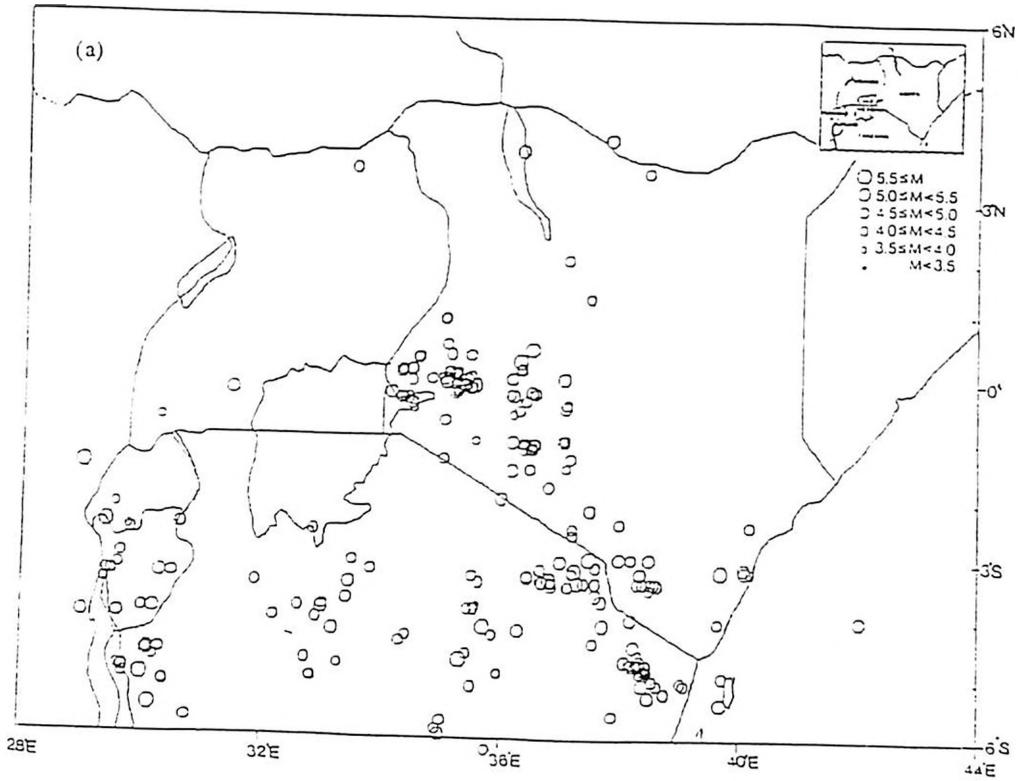
Figure 2.1 (a) Macroseismic epicenters (1880-1979) from Shah's catalog.
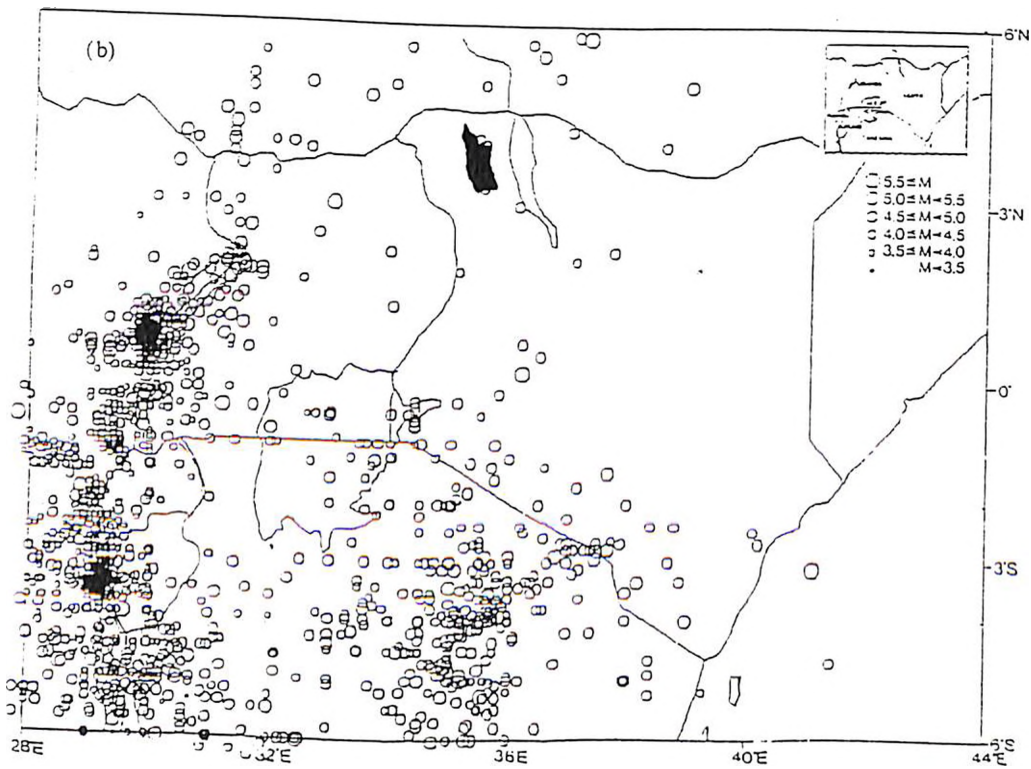
Figure 2.1 (b) Instrumental epicenters (1913-1979) from Shah's catalog.

Olang (1992) located earthquakes in Kenya using the Gutenberg and Ritchter tables. He also

computed the Isomagnitudes from the seismicity of Kenya. His findings were different in terms
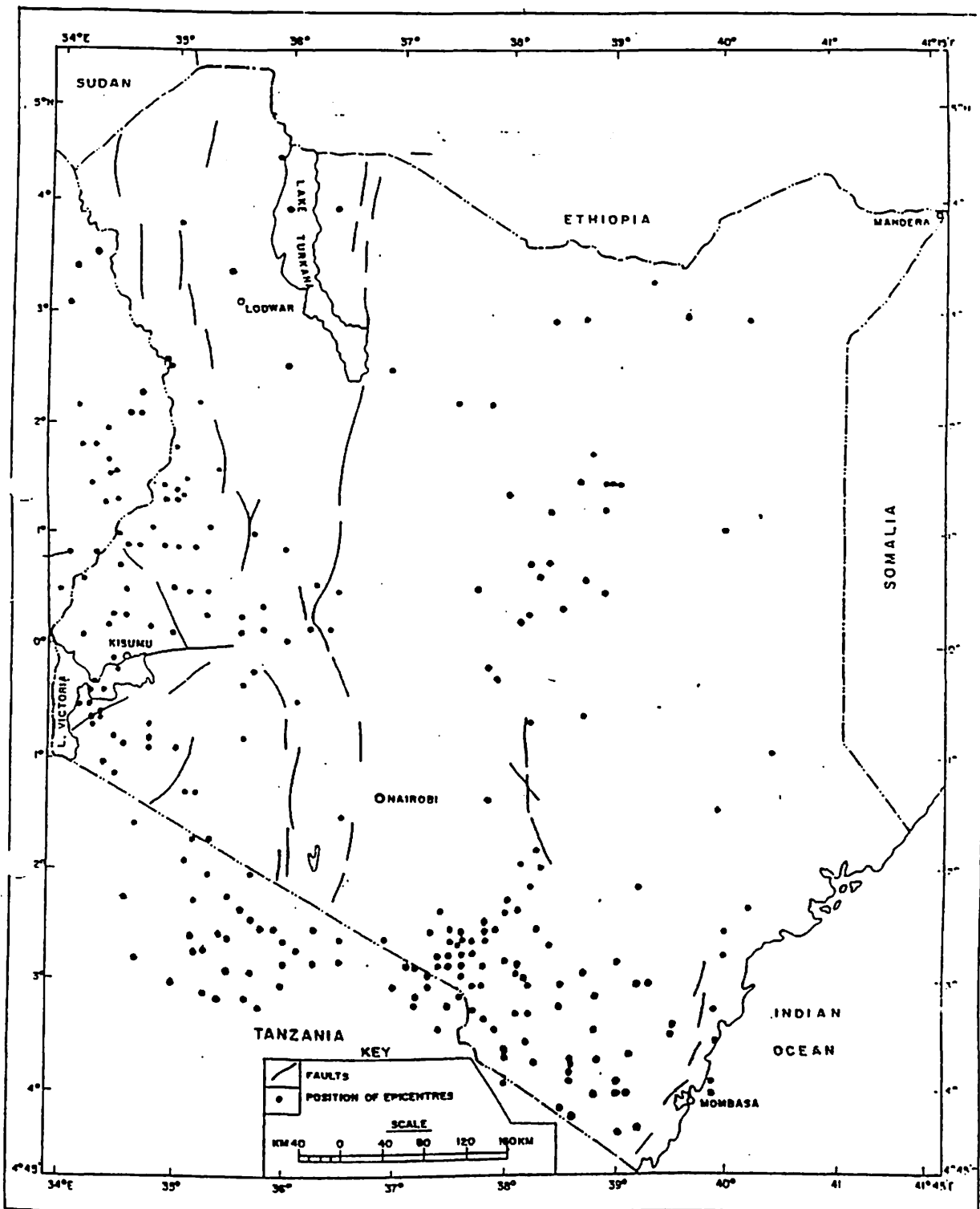
Figure 2.2 shows the seismicity of kenya from Olang's (1992) localisations (using Gutenberg and Richter tables)

of seismicity from that of Shah (1986). The study showed that the volcanic ranges are more seismically active than the rift valley. This is clearly seen in his seismicity map (see Fig. 2.2 above).

2.2 Explosion Seismology

The Kenya Rift International Seismic Project of 1968, 1985 and 1990 (KRISP68, 85 and 90) gave the crustal structure and velocities in many parts of Kenya. The data from KRISP90 were analysed mainly by using a two-dimensional ray tracing method (refer to Fig. 2.3 and 2.4a,b,c profiles for details). The study of KRISP90 confirmed the findings of the former experiments and also gave a clear cut picture of the crustal structure of large parts of Kenya (refer to Fig. 2.3 and 2.4 a, b, c).

In these studies the refracted seismic waves Pn and Sn and some reflected phases have been observed. In addition to this, the frequency content and amplitudes for P- and S- waves for various azimuthal paths have been studied. From the variation of the velocities and wave character the inferences on the crustal and upper mantle structure were drawn. The results depicted crustal thinning along the rift axis from 35 km in the southern part (lake Magadi) to 20 km in the northern part (lake Turkana), (KRISP WORKING GROUP 1991).

A layer with velocity of approximately 6.8 km/s Fig (2.4a,b,c) is identified at the base of the crust beneath all three lines, except at the northern end of the axial profile. To the eastern part of the Rift lies the Mozambique orogenic belt, the base of the crust is marked by increasing velocity gradient (due to the increase in the mafic content in the rocks) KRISP WORKING GROUP (1991).

An anomalous upper mantle characterised by a low Pn velocity (Fig. 2.4a) of 7.5-7.7 km/s observed along the complete length of the axial profile but is confined to the region beneath the rift itself, it becomes normal upper mantle with a Pn velocity of 8.0-8.1 km/s beneath the rift flanks Fig (2.4c).

The cross-section along line D, Fig (2.4 b) shows considerable variation in the crustal thickness. Beneath the western flank, crustal thickness varies from 37 km to 40 km, with modest thickening beneath the path of the Mozambique orogenic belt west of the rift. At the rift's Western boundary near the Elgeyo escarpment the crust thins considerably to 30 km below the rift axis at lake Baringo. It thickens again to 35 km beneath the eastern flank at the same latitude (Fig. 2.4 b).

The model (in Figs 2.4 a,c) supports the previous estimate for the crustal thickness of 18.5 km beneath lake Turkana (KRISP WORKING GROUP 1991). The model was vertically exaggerated considerably, to show crustal thinning from 35 km, beneath the apex of the Kenya dome to 20 km beneath lake Turkana.
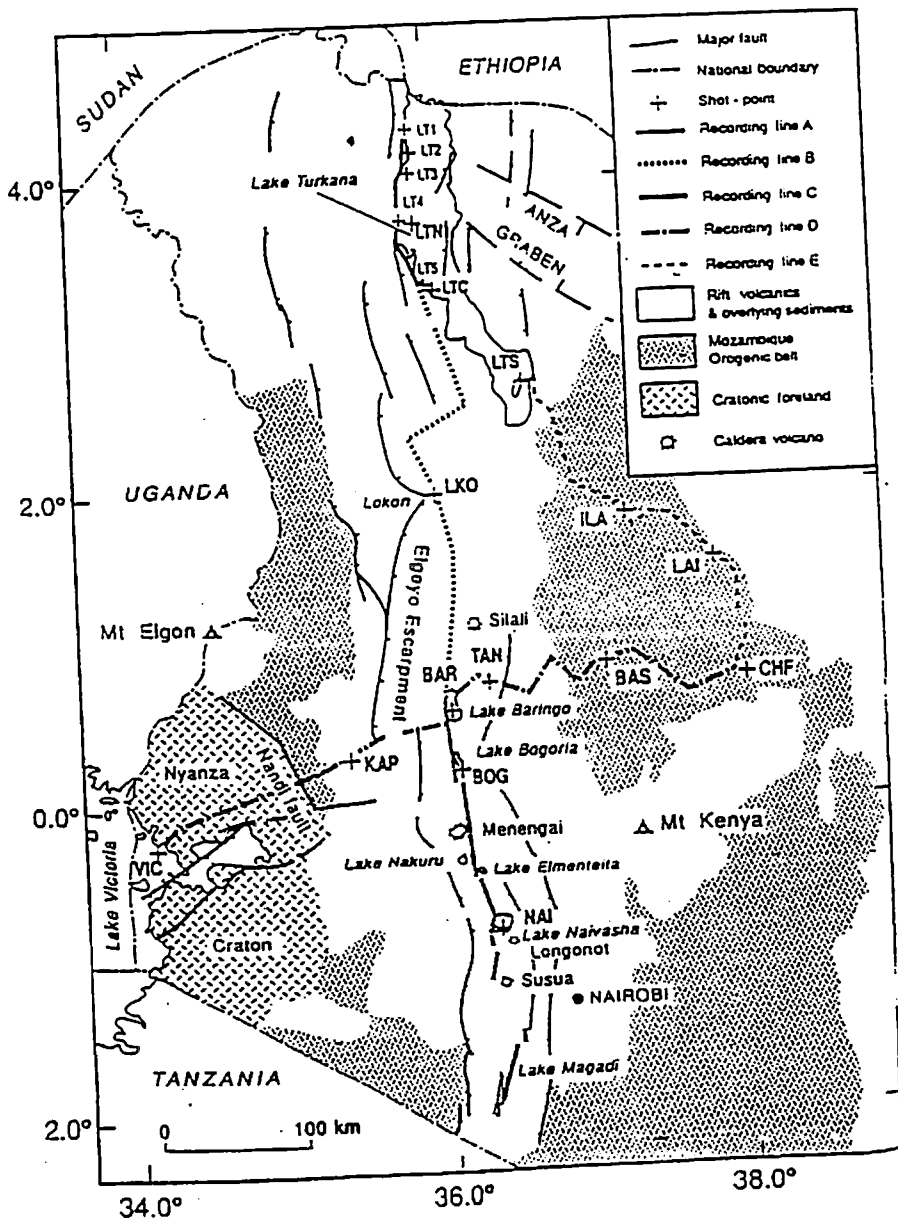
Figure (2.3) shows location map of KRISP90 adopted from KRISP WORKING GROUP (1991)
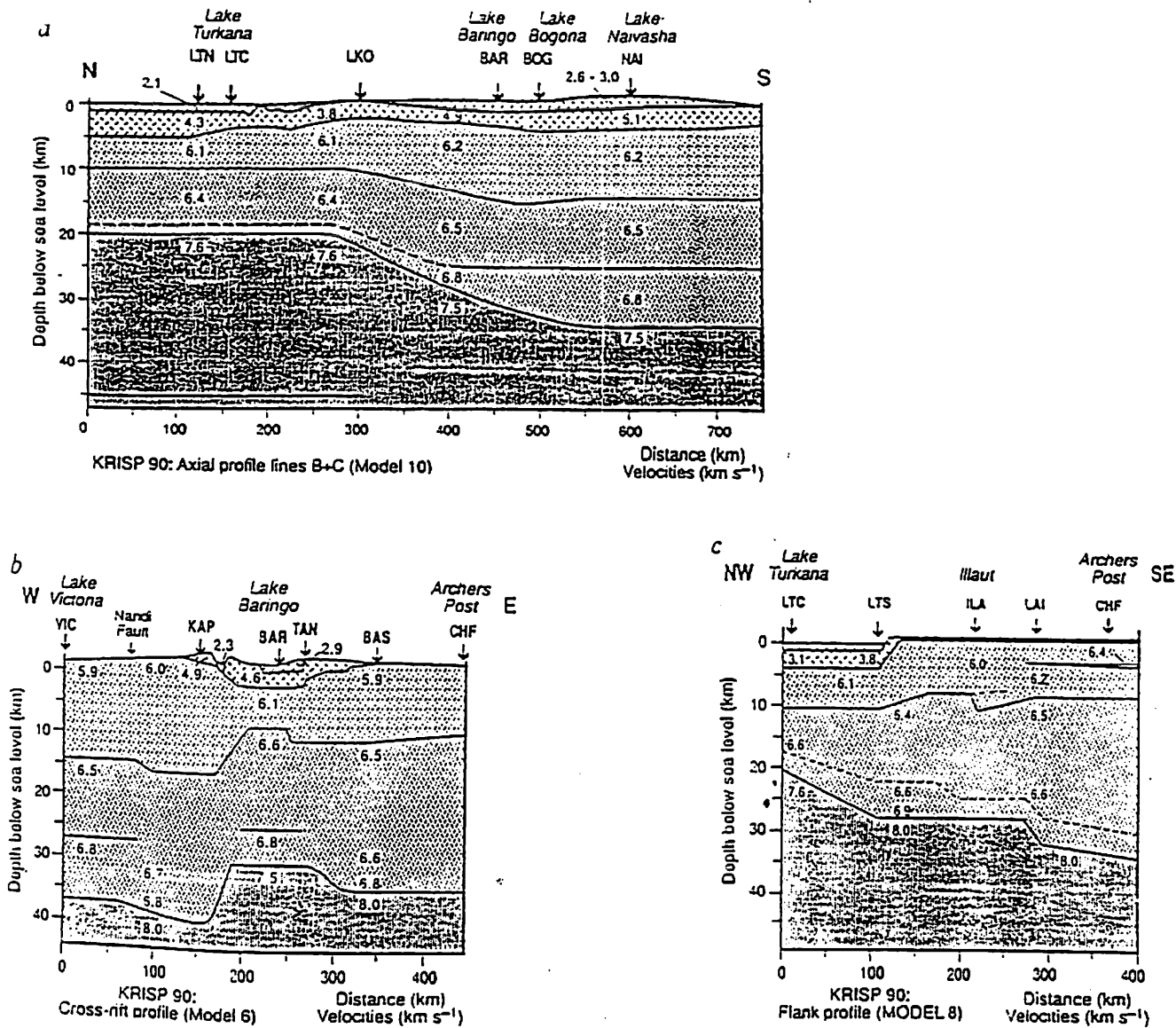
Figure (2.4a,b,c) Schematic velocity models showing the refraction interpretation. (a) The axial profile, (b) The cross profile & (c) The flank profile. Velocities are shown in kilometers per second (After KRISP WORKING GROUP, 1991)

CHAPTER THREE

PROPAGATION OF SEISMIC WAVES IN KENYA

3.1 Introduction and objectives

This chapter tries to unravel the seismic velocities in the crust and the uppermost mantle in Kenya, from the observed arrival times of seismic waves. The principle compressional waves i.e Pn and Pg and the strongest waveform onsets from local and regional earthquakes, mainly Sn and Sg are used.

After a brief introduction into basic earthquake parameters (in section 3.2), the process of computing the seismic velocities is described in section 3.3 and the results for various profiles are presented in section 3.4.

The localisation of regional seismic events can be considered in three steps, with increasing precision as far as available travel times are concerned:

(1) Use of world-wide travel time tables e.g from JEFFREYS and BULLEN (1958)

(2) Use of regional travel time tables derived from observations within region concerned, usually of an extent of about 10^0 to 20^0

(3) Use of local travel time-tables derived from a dense network of observations within the region and with different travel times and structures along different profiles (directions)

The purpose of this study is mainly to add information on point (2) in addition to the previous work in the region by various researchers, whereas the purpose is not to derive any local structure like (3) but to try to obtain generalized crustal structures for various regions in Kenya using any available information either from earthquake data or from refraction

seismic experiments.

3.2 Basic earthquake parameters

A source of seismic waves, be it an earthquake or an explosion is defined by latitude and longitude of the epicentre (a point on Earth's surface vertically above the source), depth of the source or focal depth, time of the event or origin time and the size of the event; magnitude or seismic wave energy. The first four parameters only require measurements of the arrival times of the waves on various seismograms (kinematic parameters) and the fifth requires the amplitude and the period (dynamic parameters).

3.2.1 The propagation of seismic waves in the Earth's crust and uppermost mantle

In seismology, mostly a two layered crust is used to locate earthquakes. This is of course an oversimplification of the Earth. In this layered structure, the velocity and the thickness is assumed to be constant. As shown in Figure (3.1) below (for a one layered crust), the rays leave the focus F and are recorded at stations S_1, S_2 and S_3. Since the source radiates both P and S waves, there will be direct longitudinal and transverse waves recorded along the earth's surface. These waves have rays such as FS_2 (see Figure 3.1) and are encoded Pg and Sg. The subscript g indicates the travel path, which for seismic events is in the crust (most of the crustal earthquakes are confined in the granitic layer). A reflected ray such as FRS_1 is also possible from the Moho, and its corresponding P and S are labelled PmP and SmS, respectively.

As the epicentral distance increases, the angle of incidence i and the angle of refraction i_r

also increase. At a certain epicentral distance, i_r = 90, which means that the energy of the refracted ray does not penetrate into the mantle but travels along the Moho discontinuity (c.f the ray path $FR_2R_3S_3$). The corresponding angle of incidence is called critical angle denoted i_c. The P and S waves are called headwaves recorded at station S_3 and labelled Pn and Sn respectively. The Pn are only seen after the critical distance, which for continental crust is about 100 to 200 km (Kulhánek, 1990). Such waves appear as shown in a typical seismogram shown below in Fig. (3.2)
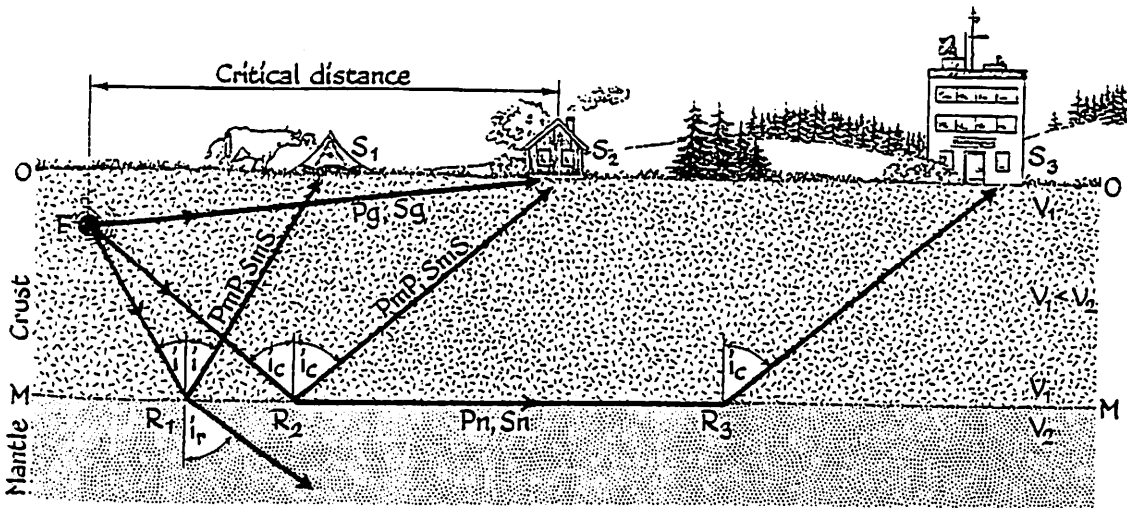
Figure (3.1) Propagation of P and S seismic rays in a two layer flat earth. Symbol O and M designate the Earth's free surface and Moho discontinuity respectively. S_1, S_2 and S_3 are stations, i is angle of incidence, i_r angle of refraction, i_c is the critical angle and V is velocity of propagation of P or S. R_k are points of reflections at the Moho discontinuity for rays that travel to the k station (Adopted from Kulhánek 1990).
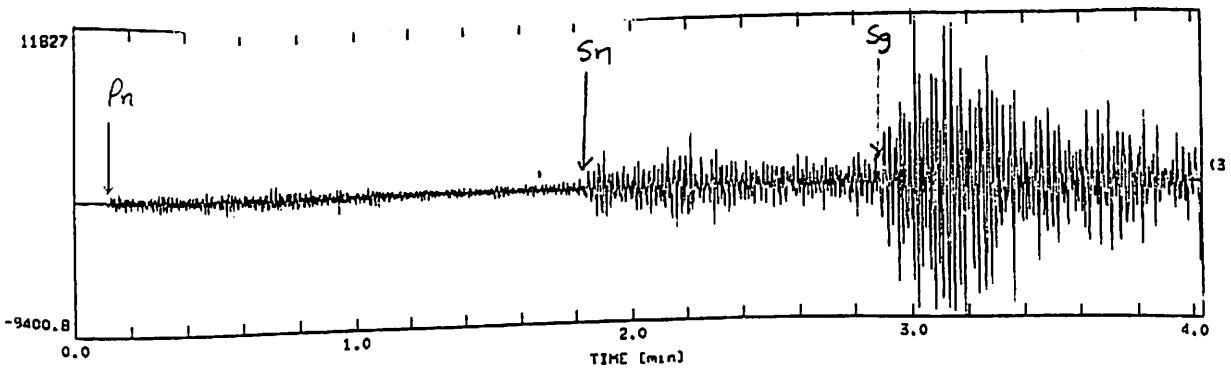
Figure (3.2) A typical local event recorded by one of the Nairobi digital station, at approximately 1300 km away from the station located at L. Tanganyika region (The Pg phase is not clear on this seismogram).

3.2.2 Localisation of earthquakes

The parameters mentioned in section 3.1 like origin time, latitude, longitude, source depth and magnitude have to be determined from seismic records. To achieve a precise localisation of an earthquake, it is necessary to have a good knowledge of the crustal structure. This is especially true if only one station is used to locate the events, as it is impossible to get all parameters with such a method. With this method, the direction between the station and the event can only roughly be determined with an error of ± 5^0 (azimuth). The source depth cannot normally be determined from the travel time data. The distance however, depends strongly on the travel time tables used (or equivalently the model of the seismic velocities used). If more than three readings of P- and S- arrival times from different stations are available the location of an event can be found in an iterative process. In such a process a, trial epicentre is assumed and the travel time differences between the theoretical and the observed times are used to get an improved location (Lee and Lahr, 1971) for the event. This process can be repeated until the changes are smaller than a given unit. The observed lateral variations of the crustal structures and velocities have to be approximated by a one-dimensional model. Ray tracing technique can be used to test such a model.

With P and S arrival time readings from three stations one can compute the origin time and the V_p/V_s ratio (Wadati-method see below; Wadati, 1931) and epicentral coordinates as the depth. In most cases, a simple one layered model with constant velocities of V_p and V_s are assumed.

The arrival times of the P and S phases are picked. The hypocentral distances can then be expressed as;

$$S = K * (t_{S1} - t_{P1}) \quad \ldots \ldots \ldots \ldots \ldots \ldots \ldots \ldots \quad (3.1)$$

where

S = hypocentral distance, $K = (V_P * V_S)/(V_P - V_S)$ (K is about 8.2 in Kenya), t_{pi} = arrival time of Pg, t_{Si} = arrival time of Sg. Given a minimum of three stations P_i =1,2,3; with P- and S- arrival times given as: $\{t_{p1}, t_{s1}, t_{p2}, t_{s2}, t_{p3}, t_{s3}\}$. P- velocity α and S- velocity β are assumed to be constant or of constant average for the rays concerned. The hypocentre H is then given by the intersection of three spheres with radii: $s_i = K (T_{si} - T_{pi}) = K(t_{si} - t_{pi})$; i = 1, 2, 3. Since the source is at depth h_0, three circles around P_1, P_2 and P_3 with radii s_1, s_2, and s_3 respectively, do not intersect in the epicentre E, but rather form a circle segment triangle. E, however, is found to be the intersection of three secants (as viewed below). If we consider the spheres around P_1 and with radii s_1, source depth h_0 can be derived as sketched (see Fig. 3.3 below), preferably using the nearrest station (here P_1).
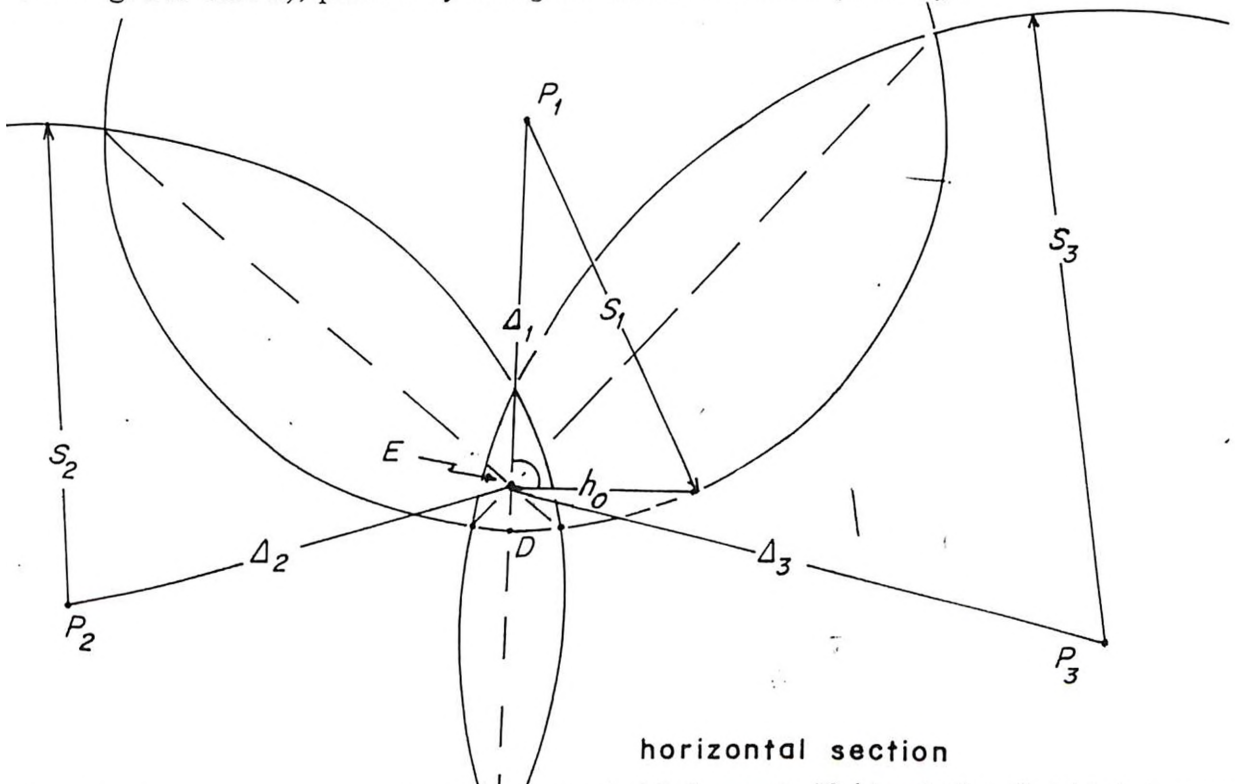
Figure (3.3) A sketch showing 3-station S-P circle method for hypocentral S determination. ($\Delta_3 > \Delta_2 > \Delta_1$ is assumed). P_1, P_2 and P_3 are the stations while s_1, s_2, and s_3 are the radii respectively.

This method is used for shallow earthquakes and for distances of less than 100 km normally.

The source depth can be computed from

$$h=\sqrt{S^2-\Delta^2} \ldots\ldots\ldots\ldots\ldots\ldots\ldots\ldots\ldots (3.2)$$

If readings of two corresponding seismic phases (e.g Pg and Sg) are available from at least three stations the origin time can be computed (Wadati-Method).

From equation 3.3 below one can find the V_P/V_S ratio

$$\epsilon=\frac{\alpha}{\beta}=\frac{V_P}{V_s} ratio \ldots\ldots\ldots\ldots\ldots\ldots\ldots\ldots (3.3)$$

where, α=P velocity and β= S velocity. With equation 3.1 for the hypocentral distance derived from the travel time of the P-wave (Pg) and equation 3.4 one can obtain equation 3.5 giving the S-P travel time difference as a function of the P-arrival time.

$$S=\alpha*(T_P)=\alpha*(t_P-t_o) \ldots\ldots\ldots\ldots\ldots\ldots\ldots (3.4)$$

$$(t_S-t_P)=(\epsilon-1)*(t_P-t_o) \ldots\ldots\ldots\ldots\ldots\ldots\ldots (3.5)$$

Where, T_P = travel time of P phase, T_S = travel time of the S phase, t_p = arrival time of P wave, t_s = arrival time of S wave, t_o = origin time.

From a graph of $(t_{si}-t_{pi})$ against t_{pi}, (see Fig. 3.4 below) the origin time can therefore be obtained. This will give a straight line (equation 3.5) and the point where $(t_{si}-t_{pi})$= 0 gives the origin time. The slope of the graph being $(\epsilon-1)$.
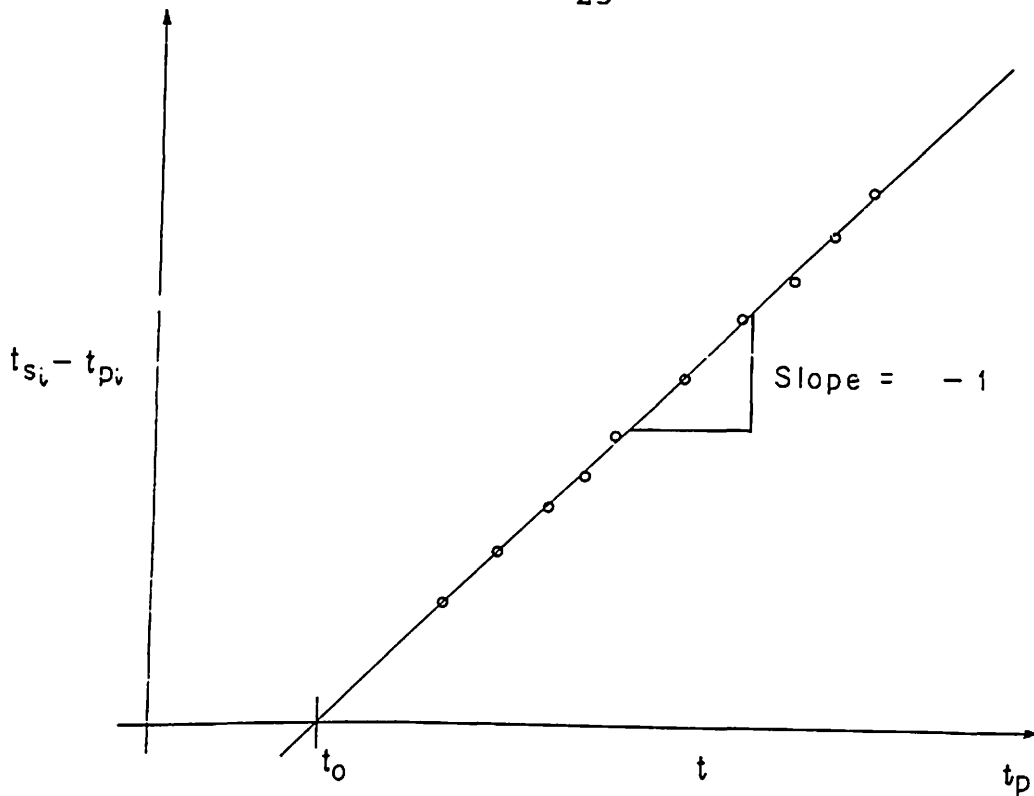
Figure (3.4) Shows a graph of t_{si}-t_{pi} against t_{pi} (Wadati Method). The time intercept t_0 is the origin time while t_{pi} and t_{si} are the arrival times of P and S phases.

When four stations or more are available, all parameters can be obtained i.e latitude, longitude, origin time and focal depth as it has been shown above. The HYPO71 program of Lee and Lahr (1971) or SEISAN software by Havskov and Utheim (1992) can be used. This softwares assumes a flat earth and layered structure of constant velocity. The programs requires structural models and that is why there is a need to establish the models from this study.

3.2.3 Computation of travel time curves of teleseimic and local earthquakes

It has already been observed at the beginning of the century when the first travel time tables were constructed, that the time of .ravel for body waves (from a given teleseimic distance and focal depth) are nearly the same irrespective of the geographical region (Kulhánek, 1990). This implies a laterally homogeneous (spherically symmetric) structure of the earth.

Small deviations, in the order of 2.0 seconds of the observed travel times from those listed in the tables are to a great extent due to structural deviations from spherical symmetry (after allowance is made for the earth's elliplicity) Kulhánek (1990). The greatest symmetric divergence have been observed between propagation paths under the oceanic and continental regions (Bullen and Bolt, 1985). Some workers advocated for construction of regional or even azimuth dependent travel times (Båth, 1979a) to improve the accuracy of Teleseismic source locations. However, these proposals are yet to be seen (Kulhánek, 1990). Broadly speaking, in seismolgical practice, the global teleseismic travel time tables which consider the Earth to be spherically symmetric are used. The situation is quite different when analysing seismograms from nearby earthquakes i.e. shocks at an epicentral distance of 10^0 or less. In contrast to the mantle and core, the crust shows significant regional variations in the structure which heavily influences travel times of all crustal waves. For example, the crust is about 40 km thick in continental areas and the P wave velocity varies from 6 km/s to 7.5 km/s. On the other hand, the oceanic crust is about 5 km thick and the layering practically disappears. The speed of the Pn wave is around 8 km/s (Kulhánek, 1990). Thus to be able to identify the arriving waves on seismograms and to determine correctly the source parameters (location and origin time), accurate regional tables applicable in a specific region must be available. Further allowance is sometimes made for local geological structure beneath the station, the height of the station above sea level etc. Because of the need for accurate phase identification on seismograms, the travel time tables of the identified model will have to be computed from this study for future use in the Kenyan seismic network (refer to APPENDIX II).

In a real situation, for accurate estimation of seismic wave velocity, explosion seismology is the only solution. But earthquake seismology can be used when there is a substantial

degree of frequency of earthquakes occurring in a particular region in such a way that a choice of only well located earthquakes with increasing epicentral distance from the station for the velocity studies are taken (Båth, 1973). This is the basis of this study.

3.3 Calculation of wave velocities from earthquake data

Well located events were used for the velocity determination. The procedure started with grouping of the events into profiles by selecting sectors from Nairobi WWSSN station (for details see section 3.3.2). Epicentral distances and azimuths were then computed for all selected events. The seismograms were then read and the travel times computed from the known origin times given in ISC bulletins. These were later reduced with the corresponding reduction velocities for different phases, to get reduced travel times in order to enhance the time resolution to enable a better check of the data scattering. Velocities for the different seismic phases were then computed for these data points by fitting a straight line to them using a least square fit approach. First velocity-depth functions have been computed to match the observed travel times mainly to check the plausibility of the readings. Wherever it was necessary, outliers have been checked to reduce the data noise and the fits have been repeated. The process is summarized in the flowchart below. Details about the procedures can be found in the following subsections, the results for the different profiles will be shown in section 3.4, the modelling is discussed in chapter 4.

28

FLOW CHART

```
┌─────────────────────────────┐
│ Seismogram reading from the │
│ short  periods .            │
└─────────────────────────────┘
              │
              ▼
┌─────────────────────────────┐
│ Establishment of the sectors│
│ from the seismicity map .   │
└─────────────────────────────┘
              │
              ▼
┌─────────────────────────────┐
│ Epicentral distance and     │
│ azimuth calculation using   │
│ EPIDIST Program .           │
└─────────────────────────────┘
              │
              ▼
┌─────────────────────────────┐
│ Travetime calculation  and  │
│ plotting for a selected     │
│ Profile.                    │
└─────────────────────────────┘
              │
              ▼
┌─────────────────────────────┐
│ Reduced traveltime          │
│ calculation and plotting    │
│ for a selected profile.     │
└─────────────────────────────┘
              │
              ▼
┌─────────────────────────────┐
│ Least  square  fit          │
│ calculation .               │
└─────────────────────────────┘
              │
              ▼
┌─────────────────────────────┐
│ Checking and eventually     │◄──────┐
│ removing of  outliers .     │       │
└─────────────────────────────┘       │
              │                        │
              ▼                        │
┌─────────────────────────────┐       │
│ Modelling the seismic       │       │
│ velocities with TRAVTIME    │       │
│ Program .                   │       │
└─────────────────────────────┘       │
              │                        │
              ▼                        │
        ◄ Data scattering OK ► ──► [NO]┘
              │
            [YES]
              │
              ▼
┌─────────────────────────────┐
│ Velocity Models for different regions │
└─────────────────────────────┘
```

Figure (3.5) Flowchart showing a summary of the procedures that have been used in this study.

3.3.1 Seismogram reading from the short period records

In this study the velocities of Pn, Sn, Pg and Sg are to be determined. Pg and Sg being waves which are first arrivals at less than 150 km Båth (1973) and usually travel directly from the focus to station. On local earthquakes seismograms, the Sg usually gives the highest amplitudes. Beyond this distance waves arrive which strike the boundary between the crust and the upper mantle, the Mohorovicic discontinuity. These are the Pn and Sn which travel at the critical angle as head waves (as mentioned above in section 3.1).

The criterion used in this study for distinquishing the two phases, Pn and Pg is that up to about a distance of 200 km or so Pg is the first arrival after which it is overtaken by Pn. This crossover distance however is dependent on the crustal model used and on the focal depth (Kulhánek, 1990). In this study 150 km was supposed to be more likely. The Sn identification was carried out by using Jeffreys-Bullen tables (Jeffreys and Bullen, 1958). The time of arrival was chosen as that of the most prominent phases close to the expected arrival time. At times the Sn onset was clear and this procedure was not undertaken.

The basic requirement for a reliable estimate of seismic wave velocity from earthquake data is that the origin time, arrival time and epicentral position be known as accurately as possible. The analog seismograph station in Nairobi allows a precision of $\pm$ 0.1 sec, in reading arrival times of earthquakes up to 10^{0}.

A correct identification of phases is important and a necessary condition in order to get reliable crustal models. Information sources like the already existing travel time tables (Jeffreys and Bullen, 1958) and amplitude relations must be used as preliminary hints only.

This has been taken into account in this study. The arrival time readings of all earthquakes used in this study are published in a special report of the Department of Geology (Kataka and Stangl, 1994). This report contains all strong events (ML ≥ 4.0) located by the Nairobi WWSSN station irrespective of whether they are located by ISC or not.

3.3.2 Establishment of sectors from seismicity map

In determining the regional velocity distribution in Kenya, sectors were constructed from Nairobi WWSSN station into different directions using the map of located earthquakes from Olang (1992) as shown in Fig. 3.6. These sectors (fans) are open triangles centred in Nairobi and were chosen to be as narrow as possible. The criteria for the width of each sector have been the grouping of events in the map and the geological structure. Wider fans have more . earthquakes generally but cover regions of different geology. The Fig. 3.5 shows eight sectors centred at NAI WWSSN station. These sectors runs in defined azimuths from the NAI WWSSN station.
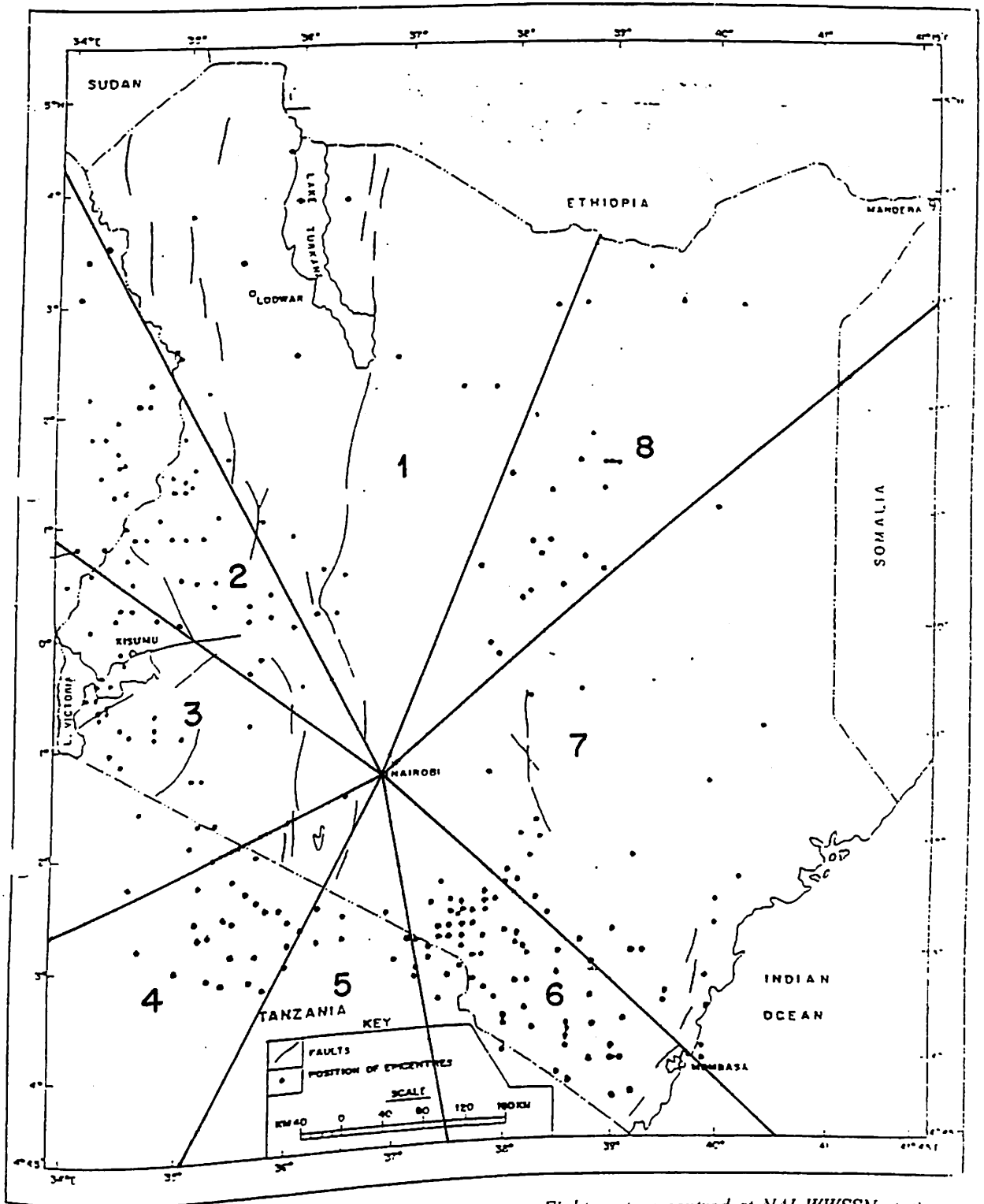
Figure (3.6) The seismicity of Kenya with established sectors. Eight sectors centred at NAI WWSSN station are represented. These sectors run in all directions from NAI station at various azimuths as described in the text. The line bisecting these sectors represents the profiles as it has been explained in the section below.

The profiles were taken to be straight lines running from Nairobi dividing the sectors into two equal parts as shown in Fig. 3.7. Open circles are representing the located events in the sector and the dashed line represents the corresponding profile. The travel times of the events were plotted as if the events were lying on the chosen profile (see Fig. 3.7 below).
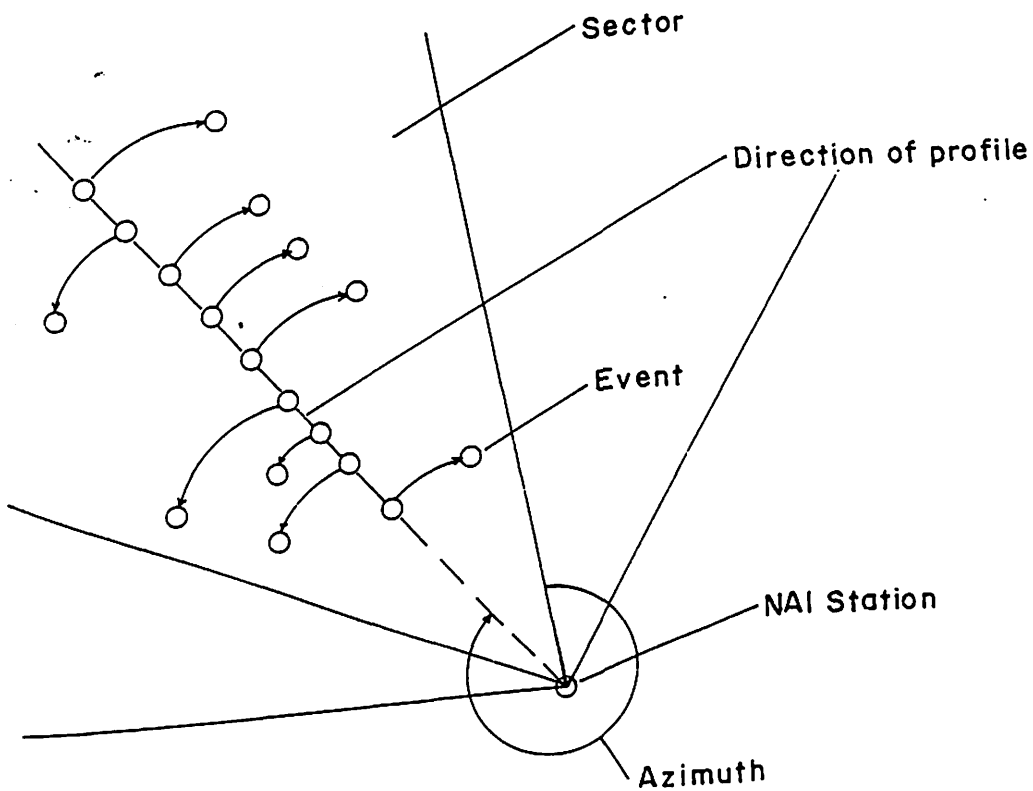
Figure (3.7) A sketch of a sector with a constructed profile at an azimuth of 45°. The open circles represents located events, the dashed line represents the profile and the triangle represents the sector.

Eight sectors were established partly covering the area of the KRISP90 experiment (see Fig. 2.3) but also filling gaps left by the KRISP experiments. Profile 1 trends along the rift valley towards the north, in the rift valley at an azimuth of 356°, profile 2 trends towards the northwest, extending towards the western rift valley at an azimuth 319°, profile 3 extends

towards the Lake Victoria at an azimuth of 279^0, profile 4 extends south west of the rift valley towards the stable craton of Tanzania at an azimuth of 221^0, profile 5 extends towards the southeastern part of Kenya and in the northeastern part of Tanzania at an azimuth of 196^0, profile 6, extends towards the coastal region through the Chyulu hills at an azimuth of 149^0, profile 7, extends towards the eastern part of Kenya (Garissa area) at an azimuth of 88^0, and the profile 8 trends towards the north eastern part of Kenya at an azimuth of 44^0.

Out of all the profiles only number 8 could not be analysed as there was no earthquake located by ISC in this sector. The total length of each profile does not exceed 1000 km. This limit is necessary since at larger distances, the first arrivals corresponds to waves that have penetrated deeper into the mantle and such earthquakes will no longer be located in Kenyan territory. The earthquakes selected in these profiles are those whose origin times have accuracy of better than ± 1.0 sec.

3.3.3 Epicentral distance and azimuth calculation

In order to get travel time data, only well located earthquakes can be used. These are earthquakes which have to be recorded by at least four stations. These have been obtained from the earthquakes with magnitudes of $ML \geq 4.0$ from Kenya and neighbouring countries. On comparison of all available data, the agency providing the most reliable epicentre determination was selected, that is the ISC agency. ISC gives standard deviations in the origin time, coordinates and the focal depth determinations, which indicate high quality of the given solution. The ISC collects data from a world-wide network of stations including a few in Africa and thus their locations seem to be quite reliable. Finally, it is one of the two international agencies (besides USGS) that provides data for East Africa in which

Kenya is part of the region. Here, ISC is prefered agency because it reports more events in the investigated area than USGS does.

Although the origin time depends on the focal depth, the calculations of the epicentral locations do not vary significantly when the sources are shallow (Rodrigues, 1970). Most of the earthquakes occurring in East Africa are not likely to occur deeper than 30 to 40 km (Rodrigues, 1970). This can be clearly seen in APPENDIX I for the earthquake locations with focal depth given by ISC bulletins. Very few of them occur at a focal depth greater than 33 km. Previous studies done in parts of Kenya also support this. From the local earthquakes that were monitored around Lake Bogoria area, Tongue (1992) revealed that the hot springs were consistent with the low seismic velocities encountered locally (Tongue, 1992) and the observation showed that 90% of the observed earthquakes occured at depth shallower than 12 km (Young et al 1991). Therefore the assumption that these earthquakes are well located has some justification since most of these earthquakes can be presumed to be shallow events.

From these selected events, located by the ISC the epicentral distances and the azimuths were then calculated using the EPIDIST program (Stangl, 1984), which uses their respective coordinates, by means of following basic relation of spherical trigonometry. If (θ) and (φ) are the coordinates of the epicentre and (θ') and (φ') those of the station, the following parameters can be defined (Willmore 1979);

$$A = \sin\theta\cos\varphi \quad B = \sin\theta\sin\varphi \quad C = \cos\theta \quad \text{and} \quad \text{..............................(3.6)}$$

$$A'= \sin\theta'\cos\varphi' \quad B = \sin\theta'\sin\varphi' \quad C=\cos\theta' \text{...(3.7)}$$

If (Δ) is the epicentral distance in degrees then,

$$\cos(\Delta) = AA' + BB' + CC' \quad\text{...(3.8a)}$$

OR

$$2(1-\cos(\Delta))=(A - A')+(B - B')+ (C - C') \quad\text{................................(3.8b)}$$

These two formulas give correct epicentral distance and azimuth calculations.

In determining the azimuth from a station to an epicentre measured from north to east one can use

$$\sin\alpha = \cos\theta\sin(\varphi-\varphi')/\sin\Delta \quad\text{...(3.9)}$$

to obtain azimuth from epicentre to station, interchange θ', φ' with θ, φ

3.3.4   Travel time calculation and plotting for a selected profile

The travel times T for the various seismic phases were calculated by subtracting the origin time t_0 from the arrival times t (i.e $t-t_0$). The travel times were plotted against the epicentral distance as is shown in an example from profile 4 in Fig. 3.8.

The procedure adopted in the construction of travel time curves here is essentially the reverse of the conventional travel time plot in which the travel times of a seismic wave for one event at a number of stations are plotted as a function of epicentral distances. In this reversed method, one station is used for several events along a profile. This reversed method has earlier been used by Dopp (1964) in his study of seismic velocities in the Western Rift and by Rodrigues (1970). The method had to be used in this study because during the period 1964-1990, Kenya had only one seismograph station (NAI station) belonging to the WWSSN

network. Therefore, the data were taken from one station and the profiles constructed by choosing well located earthquakes at increasing epicentral distances from the station.
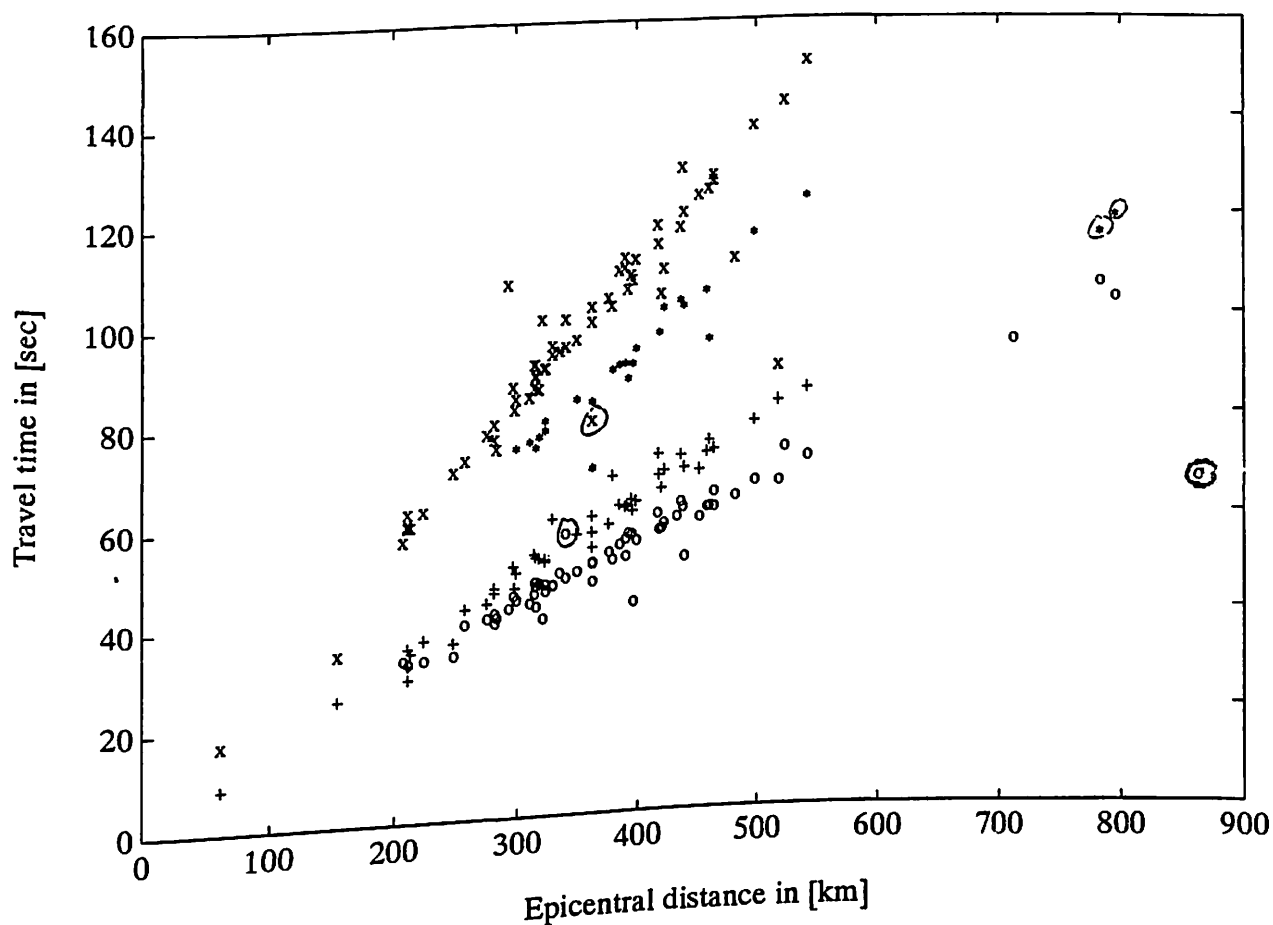
Figure (3.8) A plot of travel times of all phase against the epicentral distances for profile 4; 'o'represents the Pn, '+' represents the Pg, '*'represents Sn, 'x'represents Sg outliers are encircled in the plot.

With the calculated epicentral distances, reduced travel times were plotted against the epicentral distance (Fig. 3.9). The reduced travel times were obtained by subtracting an epicentral term Δ/V_r from the travel time ($T_R = T - \Delta/V_r$) in seconds. The reduction velocity was usually chosen so that a good time resolution for each phase could be obtained. The reduced travel time was preferred instead of the real travel time in order to enhance the time resolution and check for false readings.
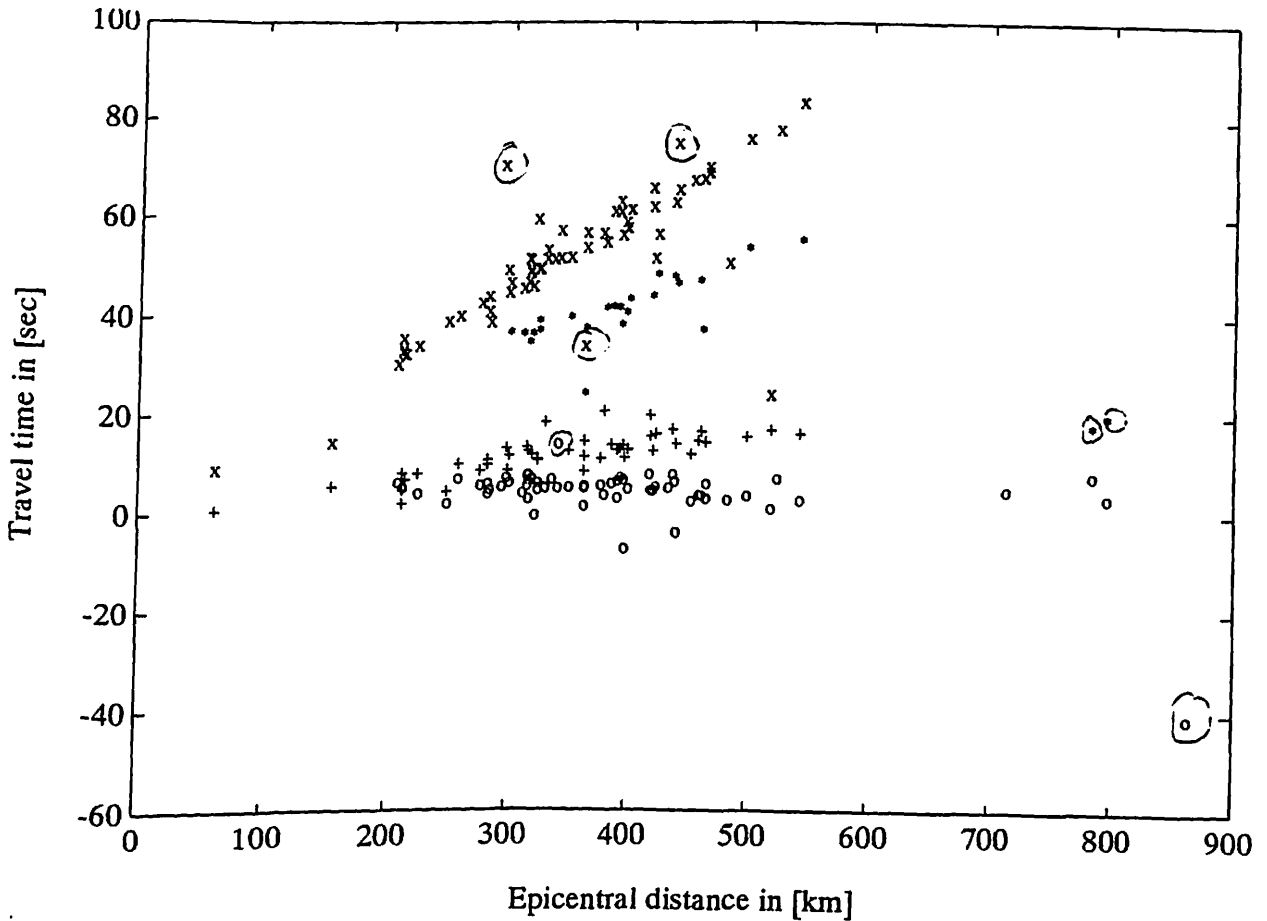
Figure (3.9) A plot of reduced travel times of all phases against epicentral distance for profile 4 (Legend is same as in Fig. 3.8).

A first fit of the travel times were made by means of least square fits for each phase in order to obtain the velocities and intercept times. These fits helped in checking the data points as the velocities can be strongly affected by outliers.

The plots of the reduced times also helped in checking the plausibility of the readings. Fig. 3.9 for example shows the plot of the reduced travel time (reduced with a velocity of 8 km/s) against epicentral distance in km for profile 4. Fig. 3.9 shows a considerable scattering for Pn data points ('o's in the plot) and also a wrong association of a Sn reading for a Pg (encircled x in Fig. 3.9). Outliers which were more than ±2.5 secs away from the average reduced travel time of a phase were reread to improve the travel times and also correct wrong phase associations. Those which could not be improved were discarded. This led to datasets with a minimised scattering as can be seen in Fig. 3.10 for the same data.

datasets with a minimised scattering as can be seen in Fig. 3.10 for the same data.
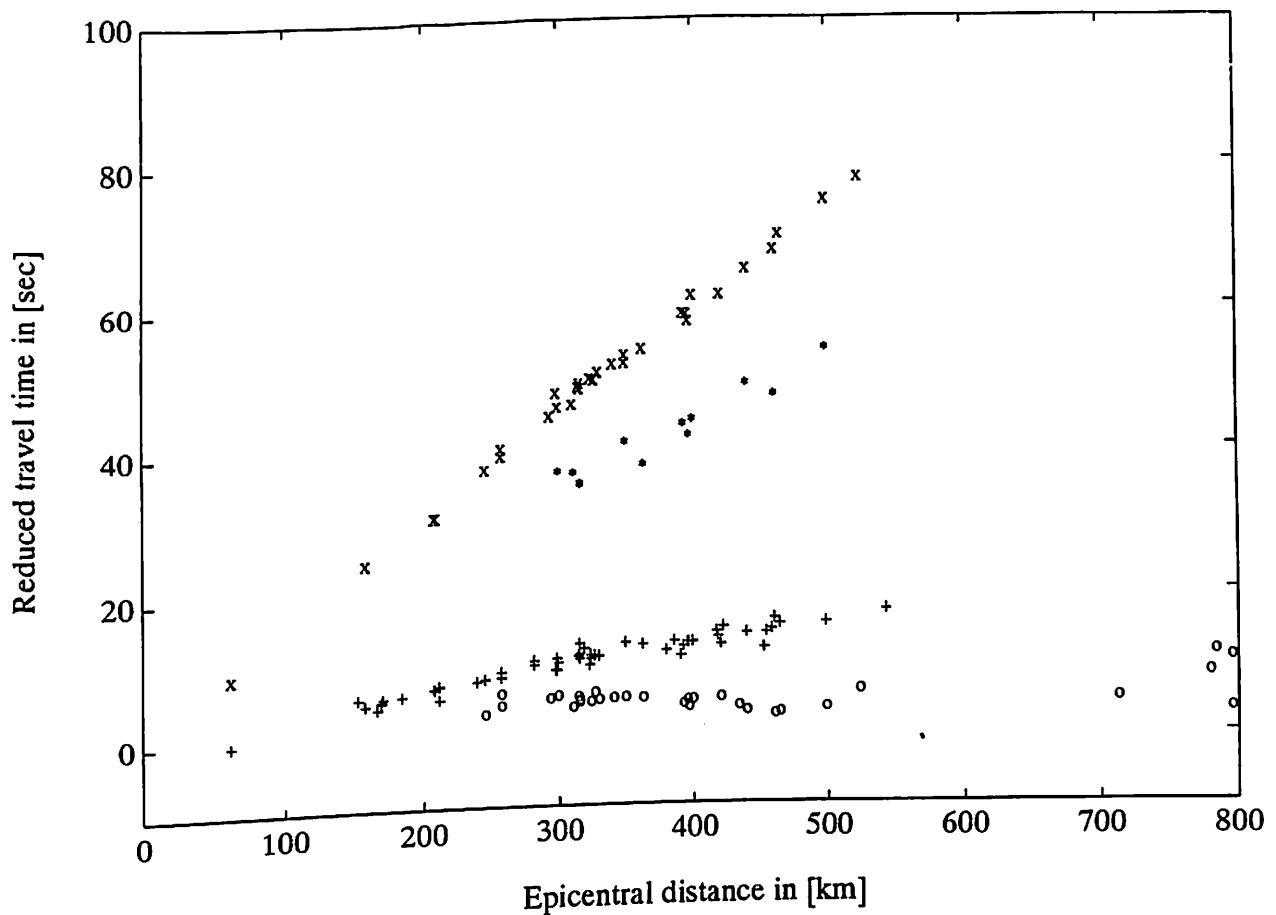
Figure (3.10) A plot of reduced travel times against epicentral distance for profile 4, after outliers are discarded (Legend is same as in Fig. 3.8).

The following reduction velocities (in km/s) have been used, 6 for Pg, 3.46 for Sg, 8 for Pn, 4.62 for Sn.

The velocities obtained for each profile were then used for a first modelling of the crustal structure with TRAVTIME (Stangl, 1986). A two layer crust was used to satisfy the data. The main aim of this first modelling was a plausibility control of the phase associations. Seismograms were reread whenever necessary to check the outliers and the whole procedure of plotting and fitting was repeated.

Since most of the events had no source depth given in the ISC bulletin a correction to a

particular source depth could not be computed. The effect of the unknown source depth on the scatter of the data is discussed in the next paragraph. Further details about the modelling and the established models can be found in section 4.1.

3.3.5 Problems encountered with the fits for Pg and Sg

Pg and Sg fits gave normally small positive intercepts of less than 0.5 secs. For some profiles however this intercepts were even negative but very small (less than -0.5 secs.). Small negative intercepts can be explained by errors in the data set. New regression coefficients were calculated by forcing the intercepts to zero. This however had very little effect on the velocities indicating the stability of the fit.

The velocity of the direct wave Pg is given by the relation $V = (\sqrt{\Delta^2 + h^2}/t)$ in a homogeneous upper crust where h is the focal depth and Δ is the epicentral distance. Usually h cannot be greater than the thickness of the upper crust otherwise no Pg can be recorded. A direct wave however still exists but does not follow the above given relation. At distances greater than 1000 km, h can be ignored to leave the relation $V = \Delta/t$.

In the absence of sediment layers the time differences between the direct wave travelling from a surface focus and one at a particular depth (10 km for example) are less than 0.1 secs, for distances greater than 250 km as shown in Fig. 3.11a. The straight line represents a wave travelling at a surface focus and the hyperbola is for a wave travellinng at a depth of 10 km. Even if thick sediments (of say 2 km with wave velocity of 4 km/s and below the sediments the wave velocity being 6 km/s) are present, the time difference is less than 0.25 secs (see Fig. 3.11b for details above). The straight line at 0.75 secs represents a surface focus while
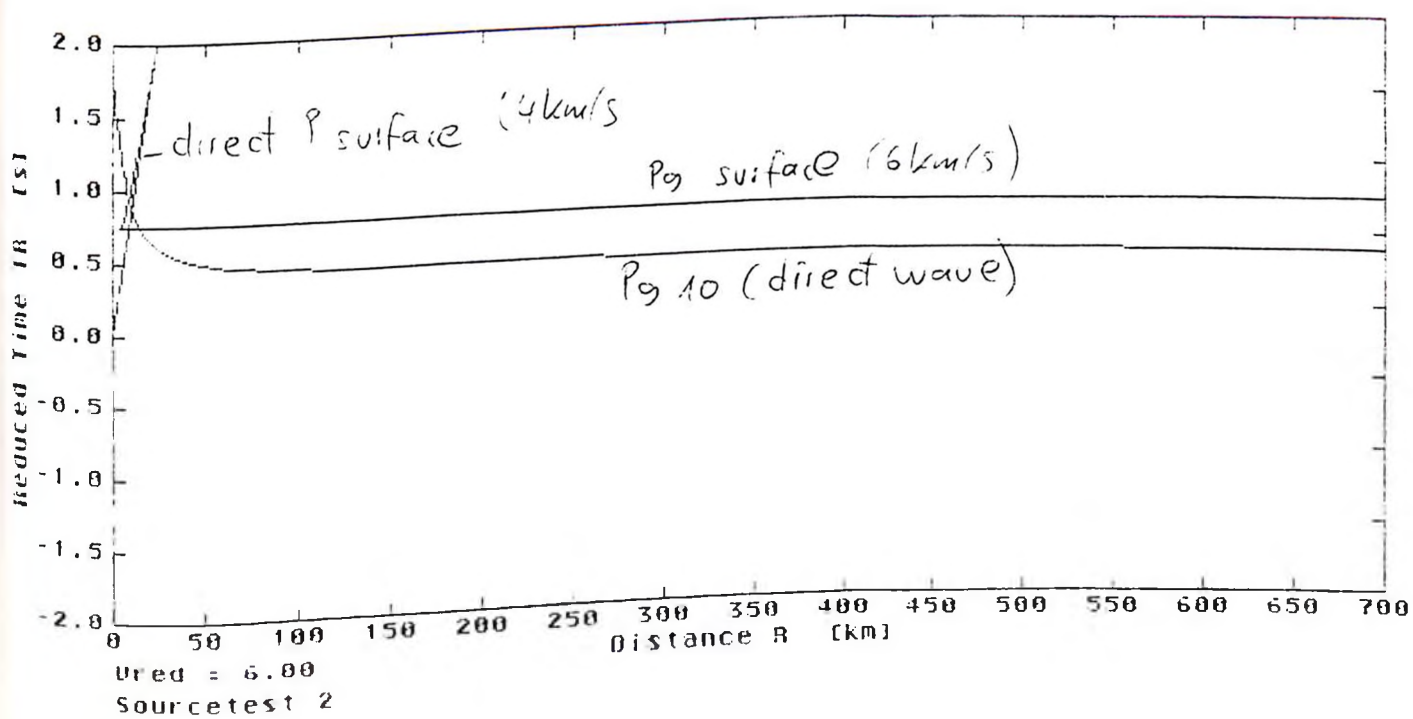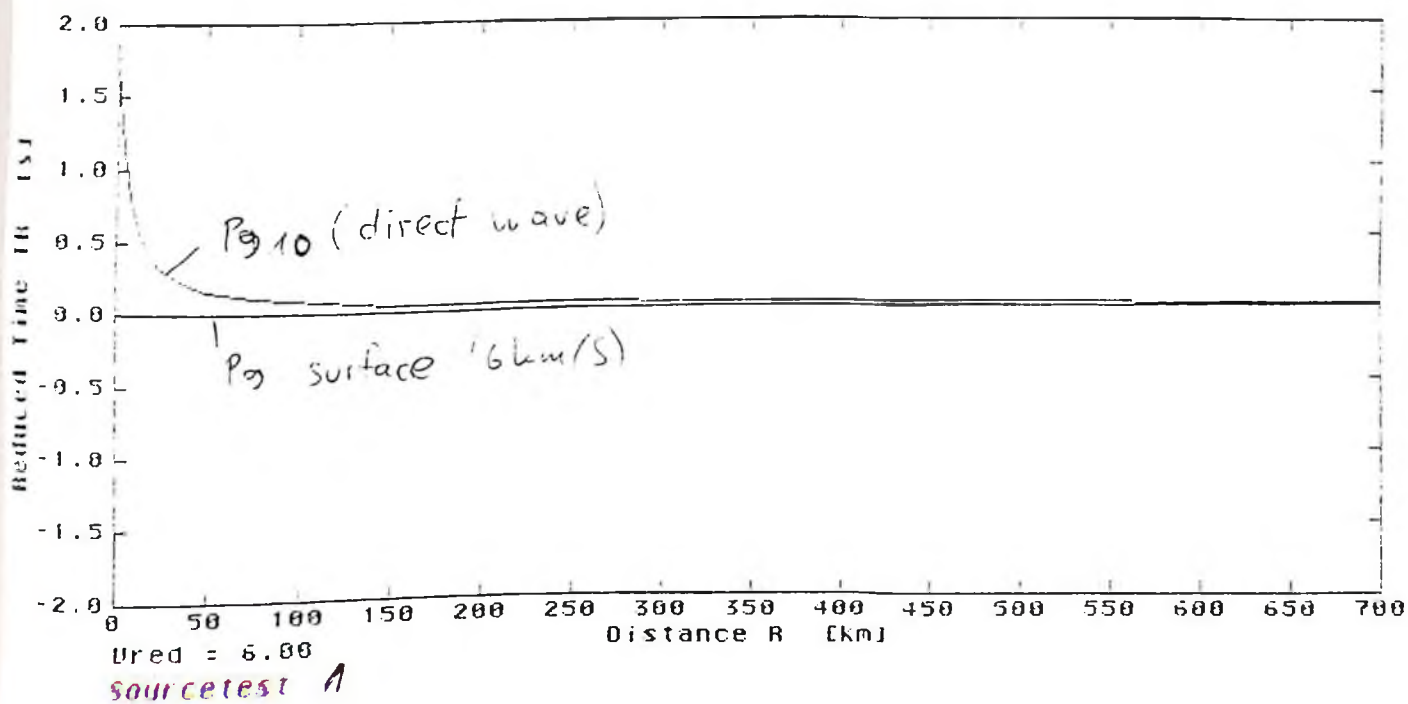
Figure (3.11) Comparison of reduced travel times for an event at the surface and one at a depth of 10 km. a) model without sediments, b) model with 2 km of sediments.

the hyperbola at 0.5 secs represents an event at a depth of 10 km. It can be seen that the velocities are almost the same. The travel times of these phases could be fitted with straight lines without making big errors. For these reasons a focal depth of 10 km has been assumed for all the events in this analysis.

3.4   Data analysis for the selected profiles

The establishment of the profiles was based on the epicentral locations of earthquakes from the seismicity map of Kenya (Olang, 1992) as was mentioned in section 3.3.2 above. The density of the earthquake data was not unique for all the profiles. Even within a profile not all distance ranges have been covered fully.

The data obtained from the seismogram readings amount to about 240 P- phases and 190 S- phases, these are too extensive to be printed here. Instead they are available in the a special report (Kataka and Stangl, 1994) refer to section 3.3.1 for details.

In this analysis various plots have been made for different phases. Some events in these plots could be observed as outliers. The seismograms for these outliers have been reread to check for this discrepancies. Those which could not be improved were discarded and an effort has been made to give possible reasons for them being outliers but some times no explanation could be given to them. For example, from the plot of combined phases of all the profiles, it could be clearly seen that profile 6 and 7 gave most of the outliers especially for the Pn phase. The travel times were about 1-2 seconds late compared to the rest but no explanation could be given to this sort of discrepancies. These events have been discarded to give plots in Figs. 3.31 - 3.34 which contains all profiles combined (unified dataset).

3.4.1 P- and S- wave velocities of Profile 1

The profile extends towards the northwestern part of Kenya at an azimuth of 35° from NAI station. This profile lies in sector 1 which covers the rift valley extending northwards towards Lake Turkana. This sector is covered by the rift volcanics and a small area on the west is covered with the complex metamorphosed rocks (belonging to the Mozambique belt).

This sector has twenty events, out of which only seven appear in the ISC localisations. The seismograms were saturated and therefore only the first break (taken as the Pn in most cases) could be read. From the analysis two events located at a distance of about 700 km appeared as outliers. This was explained as a phase belonging to a different branch that has penetrated deep in the mantle hence should have a different velocity. The profile reflects a velocity of 7.93 km/s for Pn as seen in Fig. 3.12 below. This is have shown low velocity coparable to the results from KRISP90 refraction experiments which found low anomalous velocities of 7.5-7.7 km/s in the rift valley (KRISP WORKING GROUP, 1991). The quality of the fit is poor however. Two events lie out of the narrow band of the rift valley therefore this analysis can not be representative of the anomalous low velocities of the Kenyan rift region.
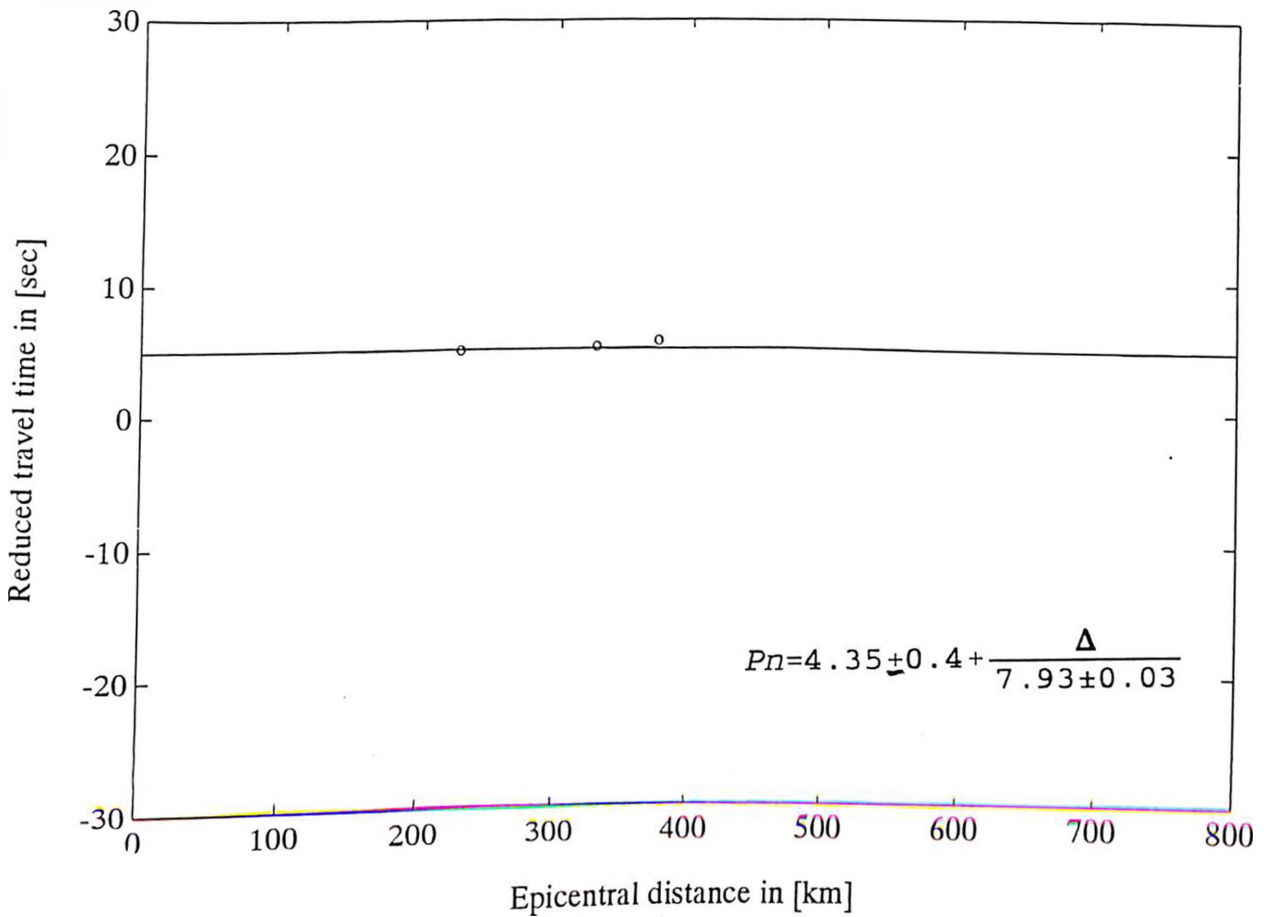
Figure (3.12) Profile 1 plot of reduced travel times against epicentral distances for Pn phase upto 650 km (The apparent velocity and time intercepts are shown in the plot).

3.4.2 P- and S- wave velocities for profile 2

The profile crosses the rift valley, passing through the rift volcanics and the complex metamorphosed rocks of the Mozambique belt tending towards the western rift valley at an azimuth of 319^0 fron NAI station.

This profile lies in sector 2 which has forty eight events from the seismicity map, but only eleven of them appear in the ISC localisations. The profile reflected the velocities; Pn of 8.03 km/s, Sn of 4.72 km/s, Pg of 6.31 km/s and Sg of 3.63 km/s. These are represented in

the Figs. 3.13, 3.14, 3.15 and 3.16 below.

A total of nine events were analysed for the Pn. There were three outliers in the plot. One of the outliers could not be explained, but the other two occurred at distances greater than 650 km therefore, they were assumed to belong to another branch of the travel time curve since the waves must have penetrated much deeper in the mantle hence should have different velocities.
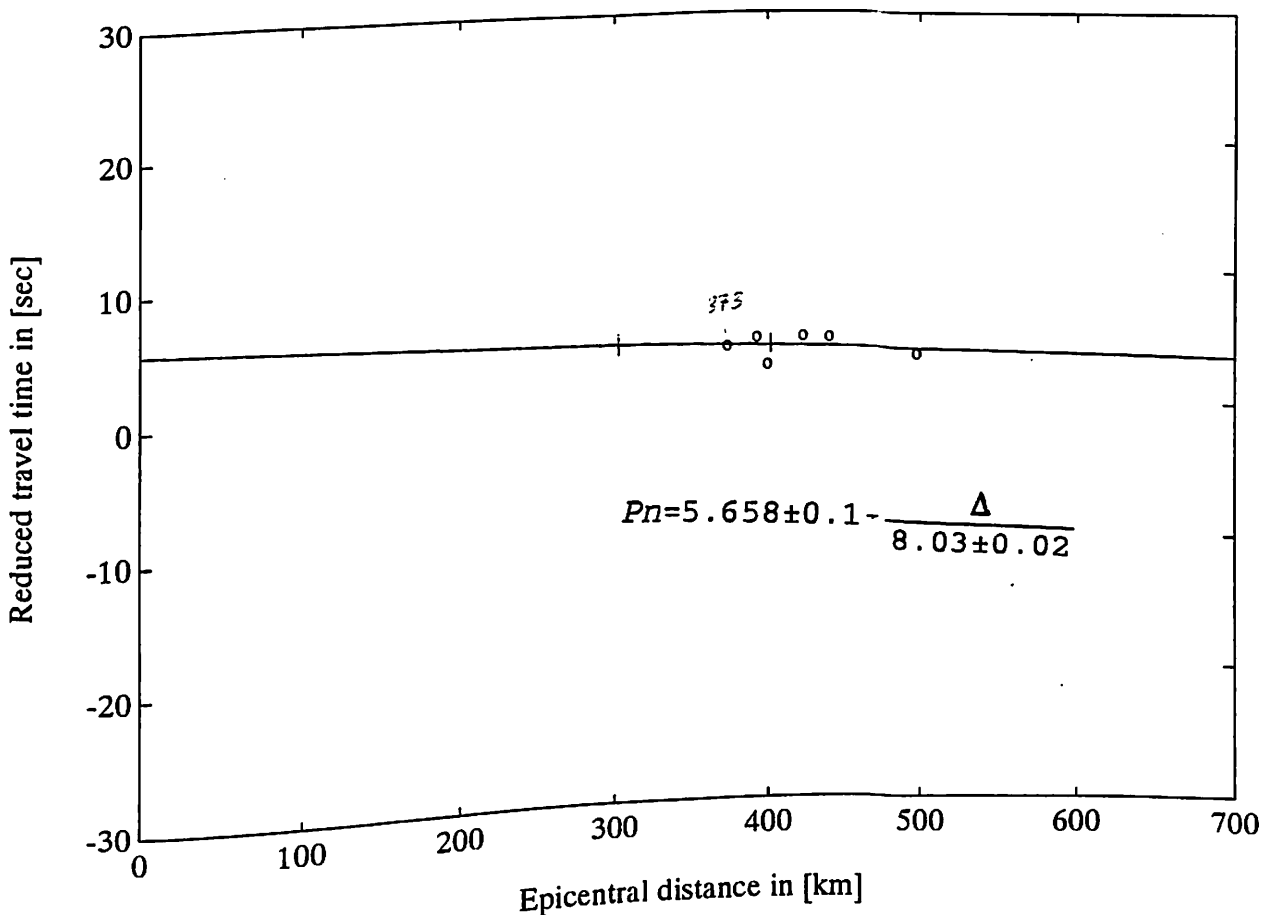
Figure (3.13) Profile 2 plot of reduced travel times against epicentral distances (upto 650 km) for Pn phase with outliers removed from the plot (The apparent velocity is listed in the plot).

Sn phase had a total of nine events in the analysis. Three of these events were outliers in the plot. Two events occurred at distances greater 650 km and therefore have been assumed

to belong to a different phase. One outlier at a distance of 396 km could not be explained and was removed from the data. The plot is represented in Fig. 3.14 below.

Figure (3.14) Profile 2 plot of reduced travel times against epicentral distance (upto 600 km) for the Sn phase (Legend same as in Fig. 3.13).

Pg phase had a total of six events from the profile. The scatter was not very significant, hence all the events have been used in the plot. The plot resulted in a very small positive time intercept which could not be attributed to the presence of the sediments as there is no evidence from both the refraction experiments (KRISP Working Group, 1991) and from the geology of the area. Therefore the intercept was forced zero and new coefficients were computed, see Fig. 3.15 below.

A plot of reduced travel time of Pg for profile 2

$$Pg = \frac{\Delta}{6.31 \pm 0.02}$$

Figure (3.15) Profile 2 plot of reduced travel times against epicentral distance for the Pg phase (Legend same as in Fig. 3.13).

Sg phase had five events from the analysis. The scatter from the plot was not significant hence all of the events have been used in the determination of the coefficients. The plot had a small negative time intercept therefore the intercept was forced to zero and new coefficients have been obtained. The plot obtained is shown in the Fig. 3.16 below.

Figure (3.16) Profile 2 plot of reduced travel times against epicentral distance for the Sg phase (Legend same as in Fig. 3.13).

3.4.3 P- and S- wave velocities for profile 3

The profile crosses the rift valley extending towards Lake Victoria, at an azimuth of 279° NAI station. The profile transects the Kavirondo rift structures before crossing through a stable precambrian formation.

This profile belongs to sector 3. The sector has forty events from the seismicity map, but only twenty six appears in the ISC localisations. This therefore implies that a lot of events from Olang's seismicity map may have been mislocated. This could be as a result of miscalculation of the azimuth or the low magnitude range used. Olang's data consists of events with local magnitudes of 3-4. These magnitudes are too low for them to be located by ISC.

The Pn phase had a total of twenty three events in this profile. Thirteen of these occurred at a distance range of 780-820 km. Two events at this distance range were outliers and had to be removed from the data. A least-square fit of all remaining events resulted into a Pn velocity of 8.43 km/s. When the events beyond 780 km were removed a velocity of 8.27 km/s was obtained. The two calculations imply that the events at distance range of 780-820 km must be belonging to another seismic phase other than Pn and had therefore to be removed from the plot given in fig. 3.17.

$$Pn = 6.526 \pm 0.1 + \frac{\Delta}{8.27 \pm 0.03}$$

Figure (3.17) Profile 3 plot of reduced travel times against epicentral distance of Pn phase (Legend same as in Fig 3.13).

Sn phase had a total of eighteen events from the analysis. There was a considerable scatter for events at a distance range of 780-820 km. This distance constituted of thirteen events.

Out of these thirteen events, four of them had to be removed. For the remaining events a velocity of 4.67 km with intercept of 8.29 was obtained. A computation without the events beyond 780 km distance led to a velocity of 4.77 km/s (see Fig. 3.18).

The plot with equation:

$$Sn = 7.6536 \pm 0.1 + \frac{\Delta}{4.77 \pm 0.3}$$
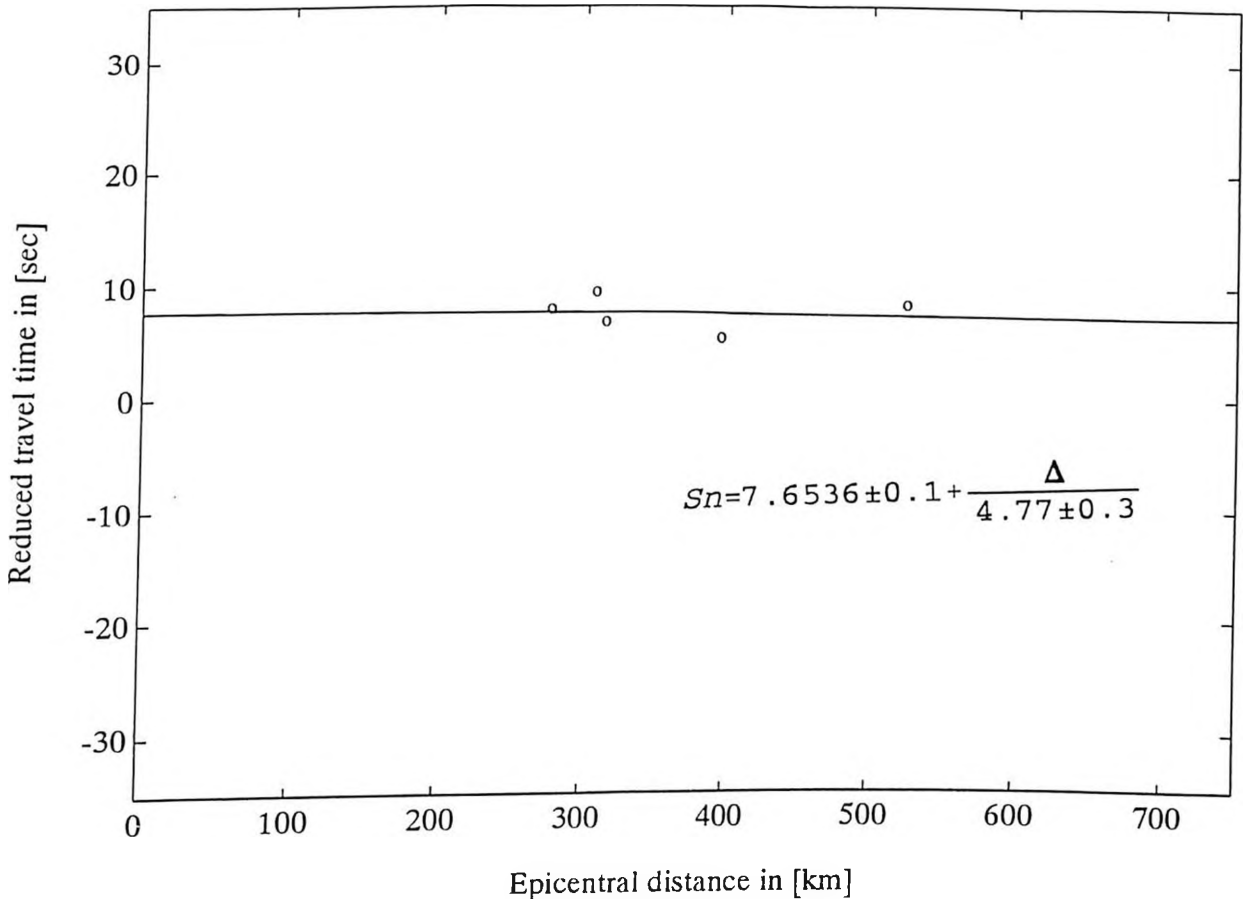
Figure (3.18) Profile 3 plot of reduced travel times agianst epicentral distance of Sn phase (Legend as in Fig. 3.13).

The Pg phase had nine events in the plot with one of them being an outlier. This event was therefore discarded. This plot resulted in a small positive time intercept of 0.35 secs suggesting the existence of sediments in the profile. But due to the fact that there is no evidence of sediments in the area from both refraction experiments done within the vicinity of this profile and the geology of the area, the intercept was forced to zero to get new coefficients. This then resulted in a velocity of 6.27 km/s (see Fig. 3.19 for details).
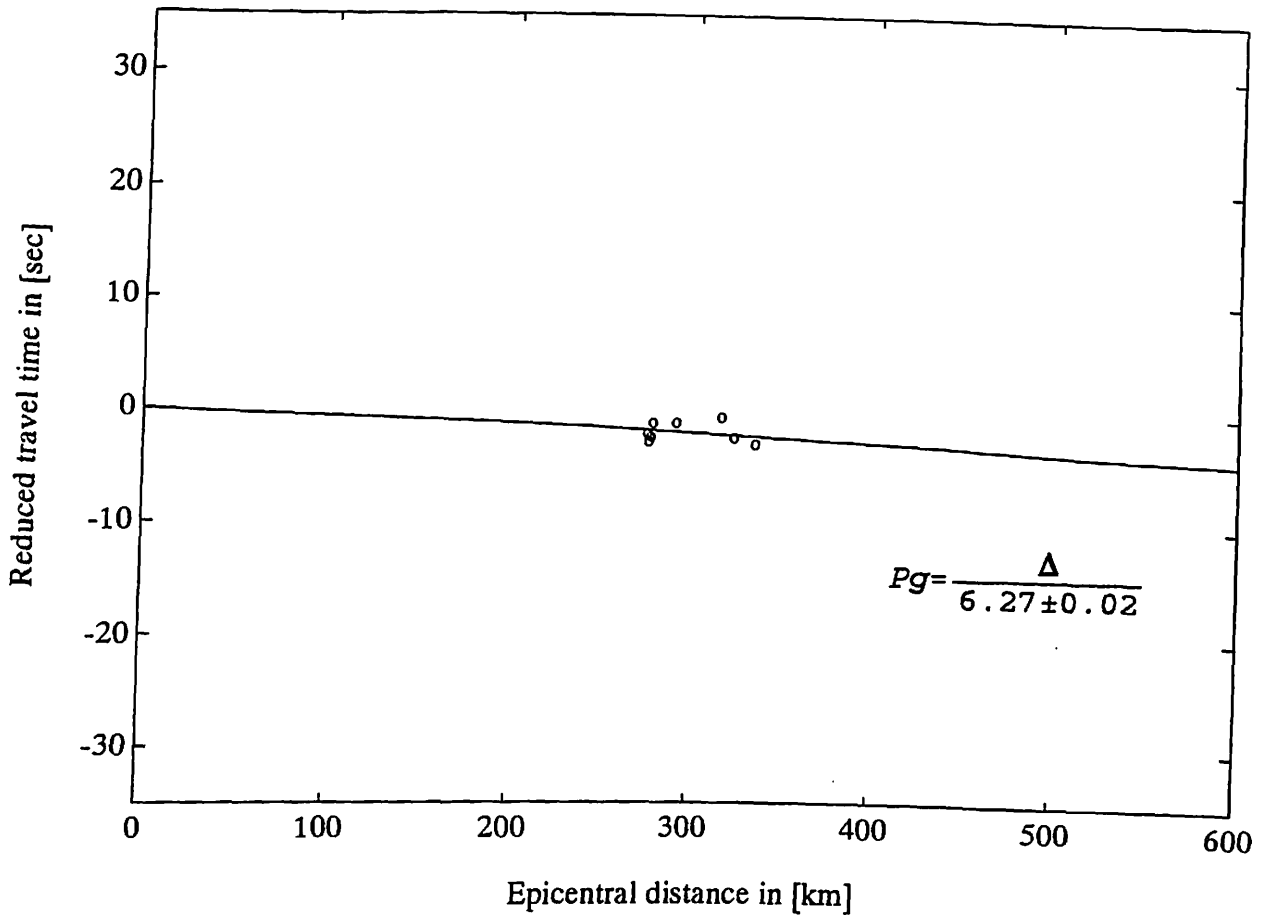
Figure (3.19) Profile 3 plot of reduced travel times against epicentral distance of Pg phase (Legend as in Fig. 3.13).

Sg phase had nine events in the analysis. The scatter of the data points was not very significant. One of the events had to be removed as an outlier. A plot made for this profile resulted into a small positive time intercept after removing the outlier. The intercept was therefore later forced to zero (for same reasons already mentioned above under the Pg phase) and a velocity of 3.63 km/s was obtained, see Fig. 3.20 for details.
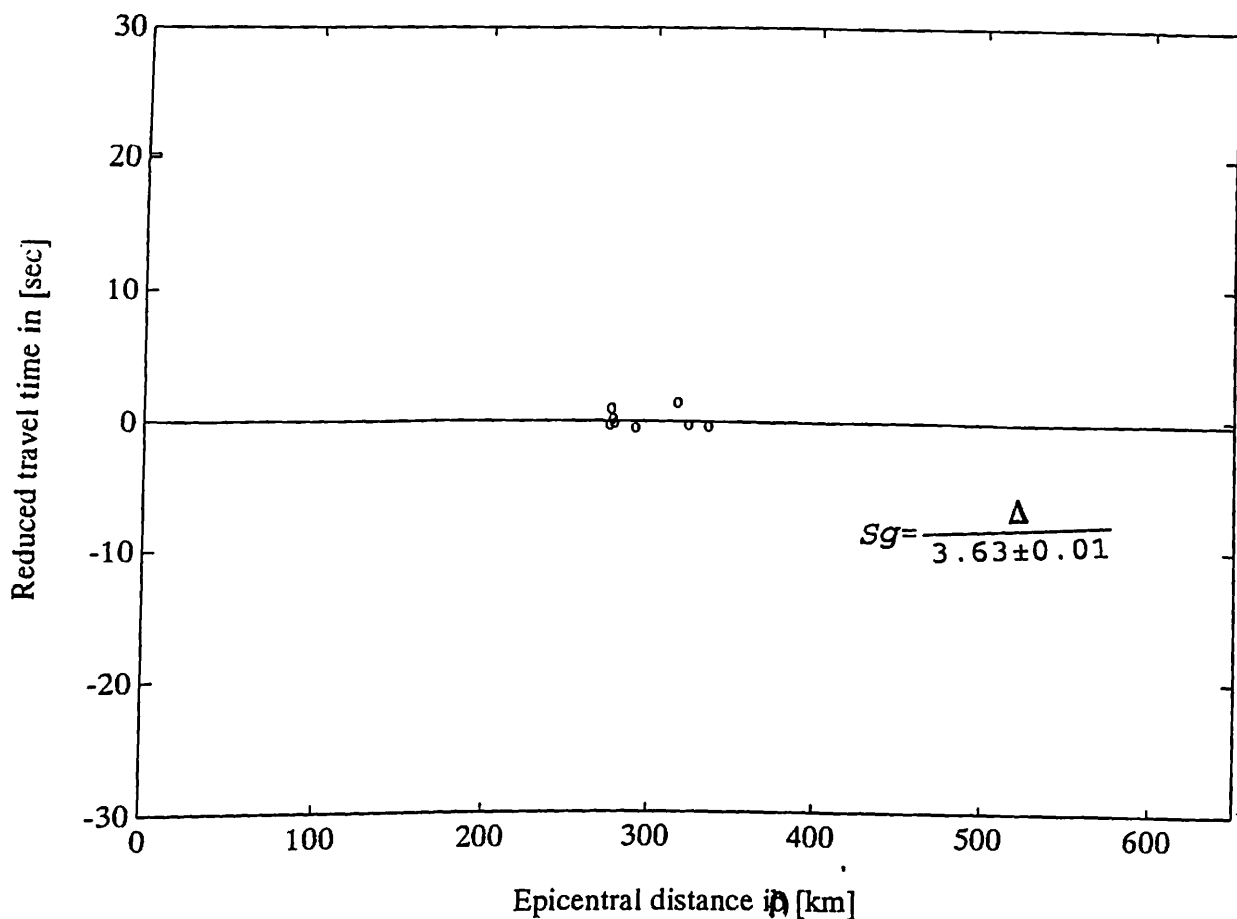
Figure (3.20) Profile 3 plot of reduced travel times against the epicentral distance of Sg phase (Legend same as Fig. 3.13).

3.4.4 P- and S- wave velocities for Profile 4

The profile runs from Nairobi towards the southern part of Kenya and the northern part of Tanzania at an azimuth of 221^0. The greater length of this profile is within the rift valley (which is covered with volcanics), although the term 'rift' cannot really be used to describe tectonic structure in Tanzania (Rodrigues, 1970).

This profile lies in sector 4 which has a total of twenty six events from the seismicity map. But thirty five events were found have been located by ISC. This implies that most of Olang's (1992) may have been mislocated for reasons already mentioned in section 3.4.3. The results are shown in Figs. 3.21, 3.22, 3.23 and 3.24 below.

Pn phase had twenty eight events for the analysis. There was a negligible scatter apart from one outlier at a distance of 796 km (which has been assumed to belong to a different branch). The rest of the events have been used in the regression analysis to give a velocity of 8.13 km/s, as shown in Fig. 3.21 below.
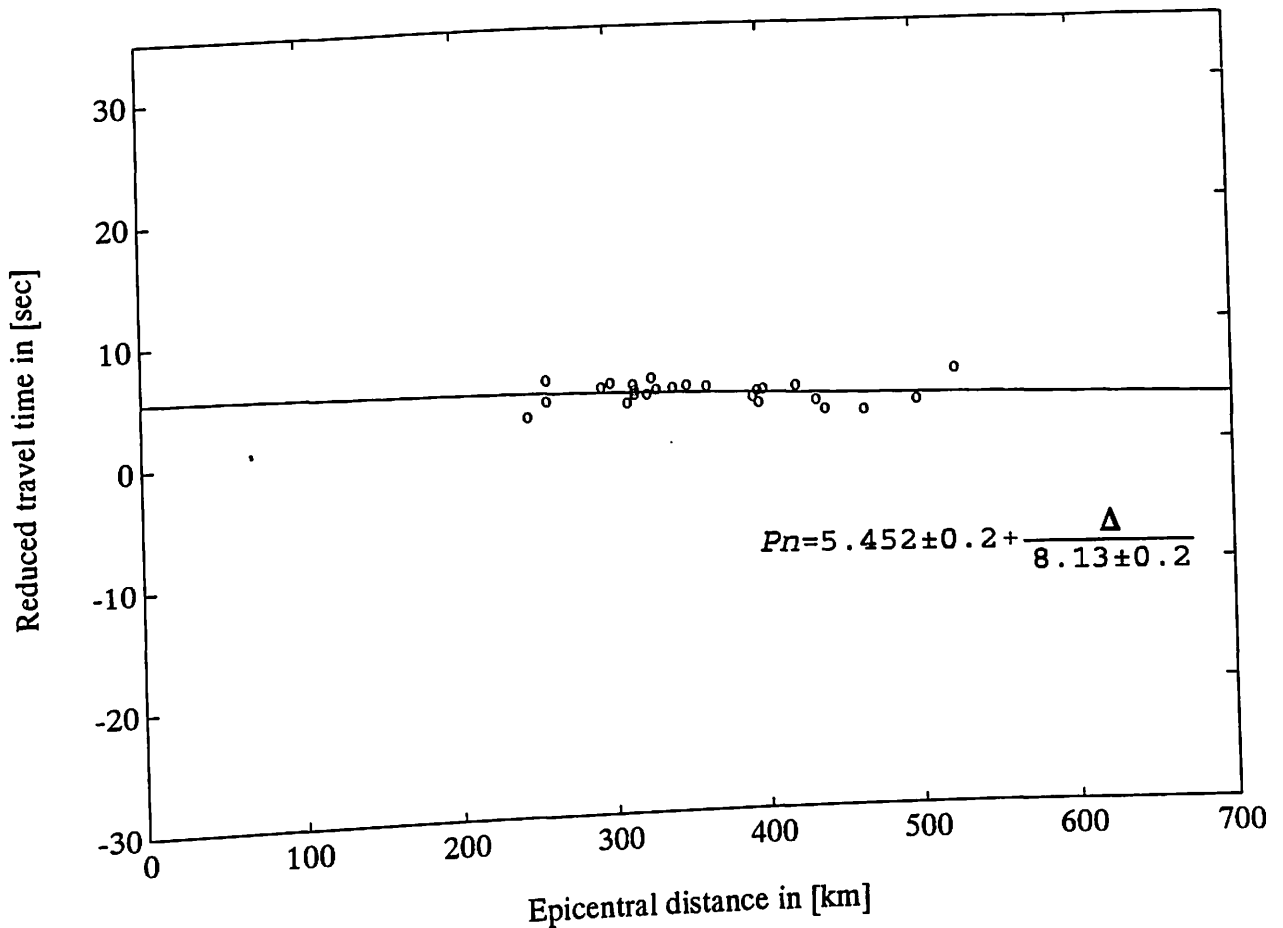
Figure (3.21) Profile 4 plot of reduced travel times against epicentral distance (upto 600 km) of Pn phase (Legend same as is Fig. 3.13).

Sn phase had thirteen events in the plot with one outlier at a distance of 803 km (assumed to belong to a different branch). The other events have been used in the regression analysis resulting in velocity of 4.72 km/s plot in Fig. 3.22 shown below.
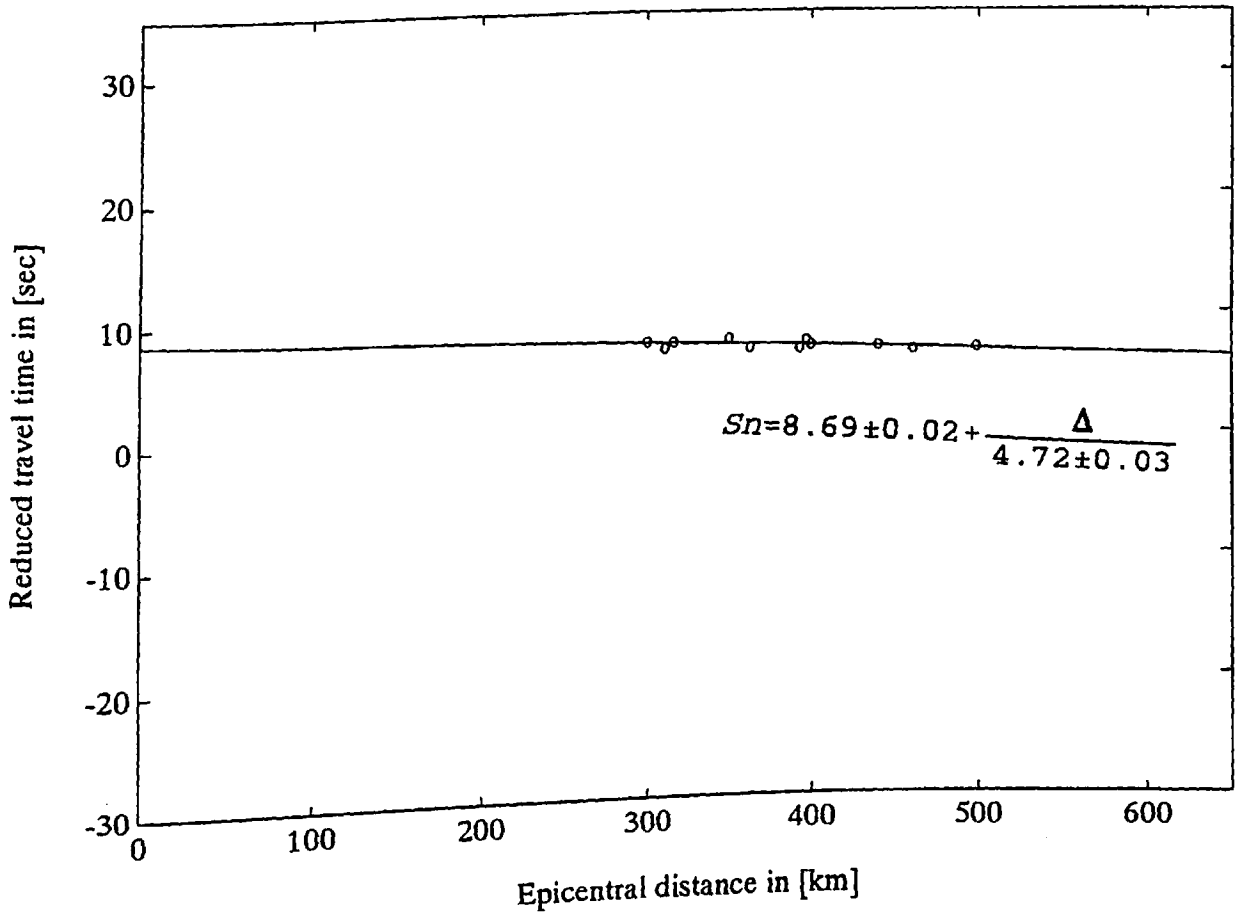
Figure (3.22) Profile 4 plot of reduced travel times against epicentral distance of Sn phase (Legend same as in Fig. 3.12).

Twenty four Pg phases were observed from the analysis. The data did not show a significant scatter and therefore all the events have been used in the computation of the coefficients. This plot resulted into a small negative intercept. The intercept was forced to zero and therefore new coefficients resulted in a velocity of 6.34 km/s, see Fig. 3.23 below for details.

$$Pg = \frac{\Delta}{6.34 \pm 0.03}$$
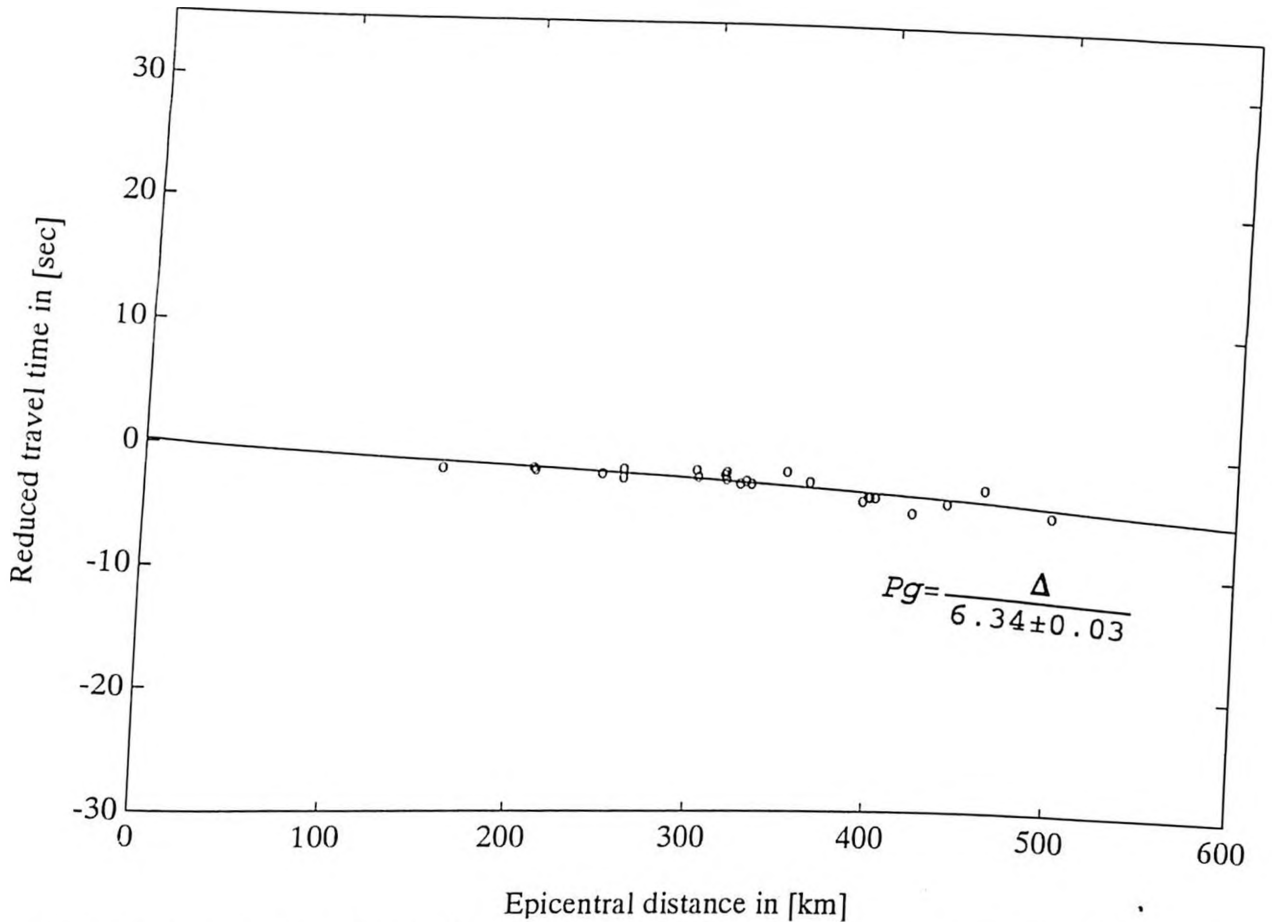
Figure (3.23) Profile 4 plot of reduced travel times against epicentral distance of Pg phase (Legend as in Fig. 3.13).

Sg phase had twenty one events from the analysis in the profile. The data did not show a significant scatter so all events could be used for the computation. A small positive time intercept was obtained. As there is no evidence of sediments in the area the intercept was forced to zero and new coefficients obtained. This resulted in a velocity of 3.64 km/s, see Fig. 3.24 below for details.
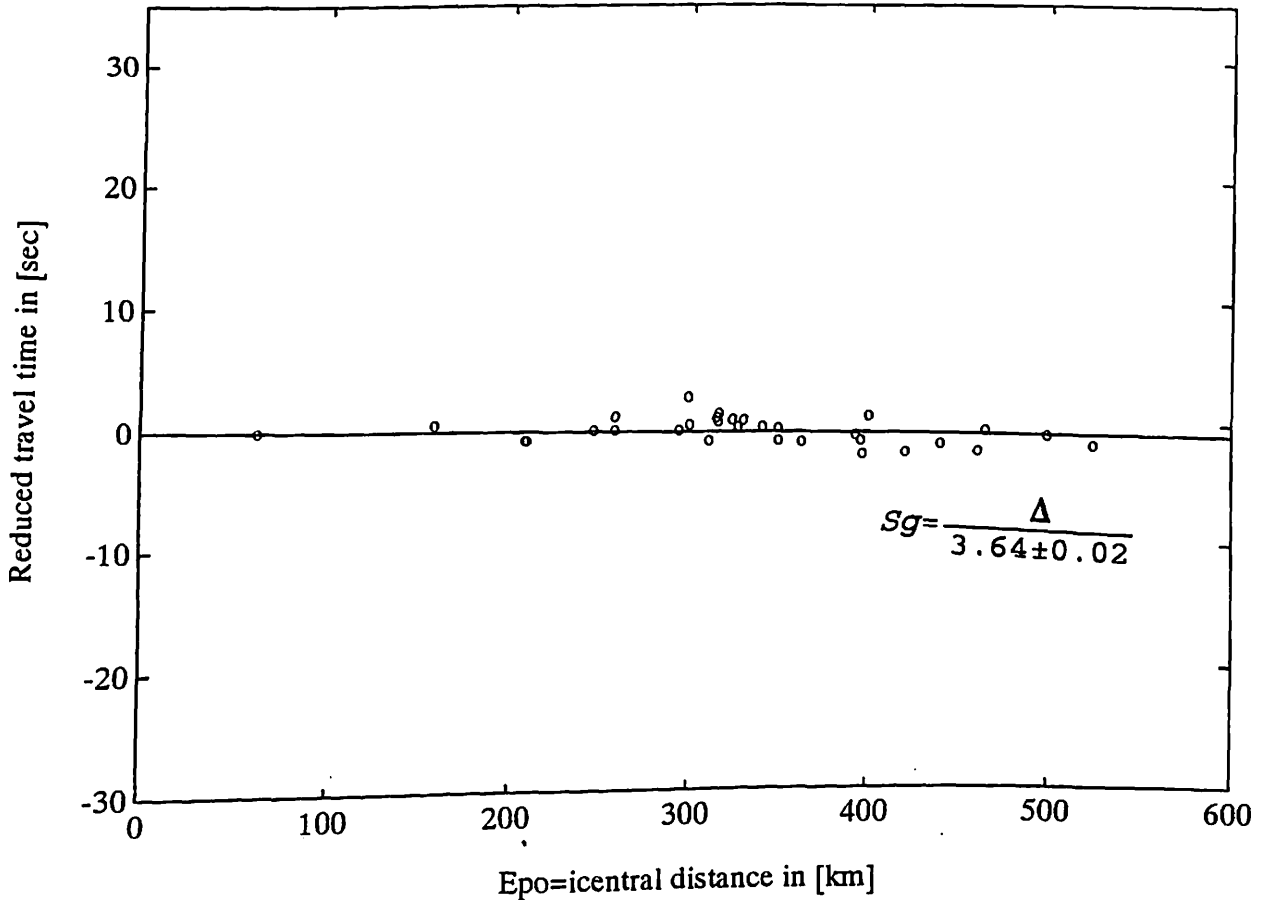
Figure (3.24) Profile 4 plot of reduced travel times against epicentral distance of Sg phase (Legend same as in Fig. 3.13).

3.4.5 P- and S- wave velocities for Profile 5

This profile extends towards the eastern flanks of the Tanzanian rift system. This extends further into the Tanzanian craton, running at an azimuth of 196^0 from NAI station.

The profile lies in sector 5 which has only eight events in the seismicity map of Olang (1992). However, thirty eight events appears in the ISC localisations. This implies that some of the events located by Olang may have been mislocated (for reasons already mentioned in section 3.4.3), thus appearing in the neighbouring sectors. Pn phase had thirty events from the analysis. There was one outlier at a distance of greater than 700 km. This was

assumed to be a phase belonging to an other branch. The plot resulted in a velocity of 8.06 km/s as it is seen in the Fig.3.25 below.
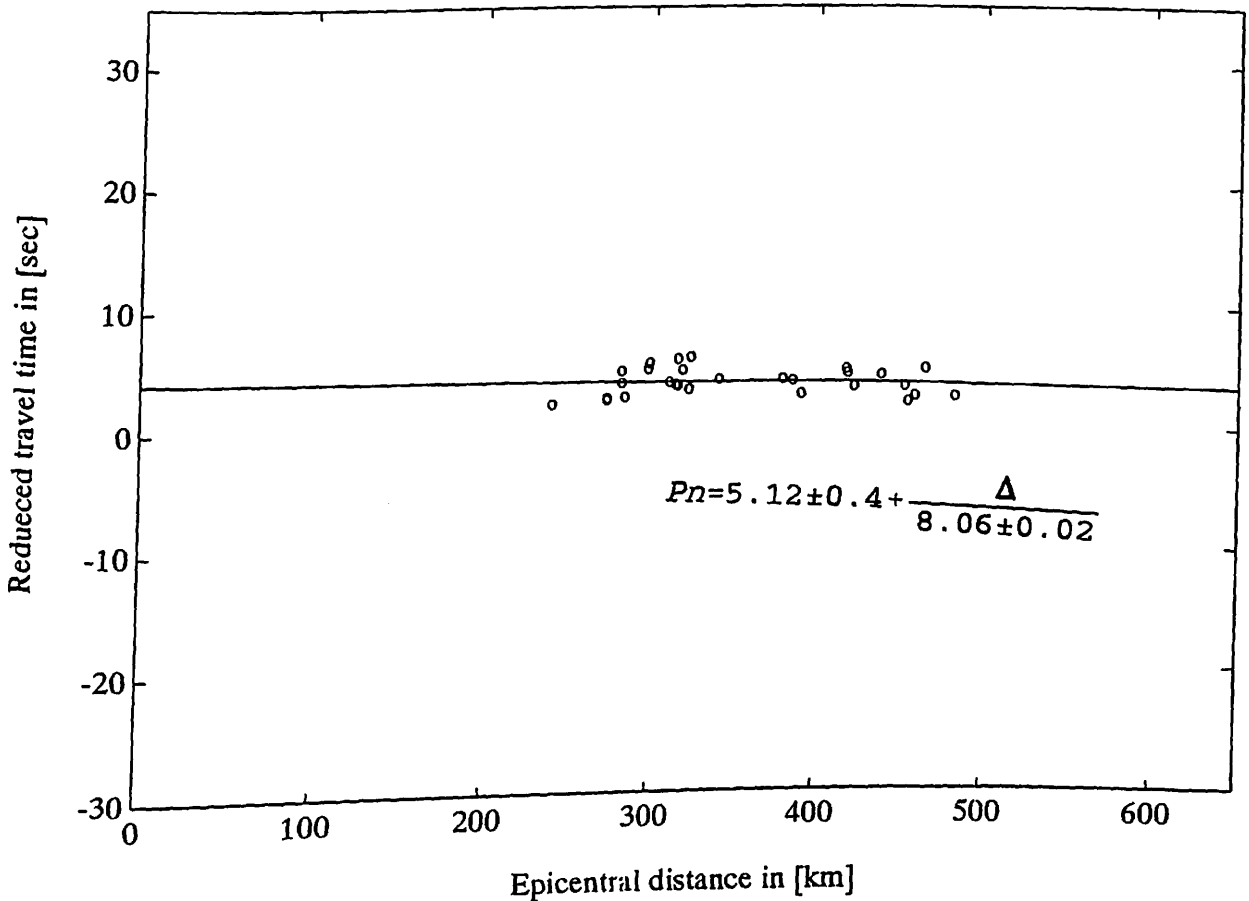
Figure (3.25) Profile 5 plot of reduced travel times against epicentral distance of Pn phase (Legend same as in Fig.3.13).

Sn phase had eleven events from the analysis. Only one event that occurred at distances greater than 700 km (for same reasons mentioned above under the Pn phase) was taken as an outlier. The regression analysis reflected a velocity of 4.66 km/s, see Fig. 3.26 below for details.

$$Sn = 9.48 \pm 0.4 + \frac{\Delta}{4.66 \pm 0.3}$$
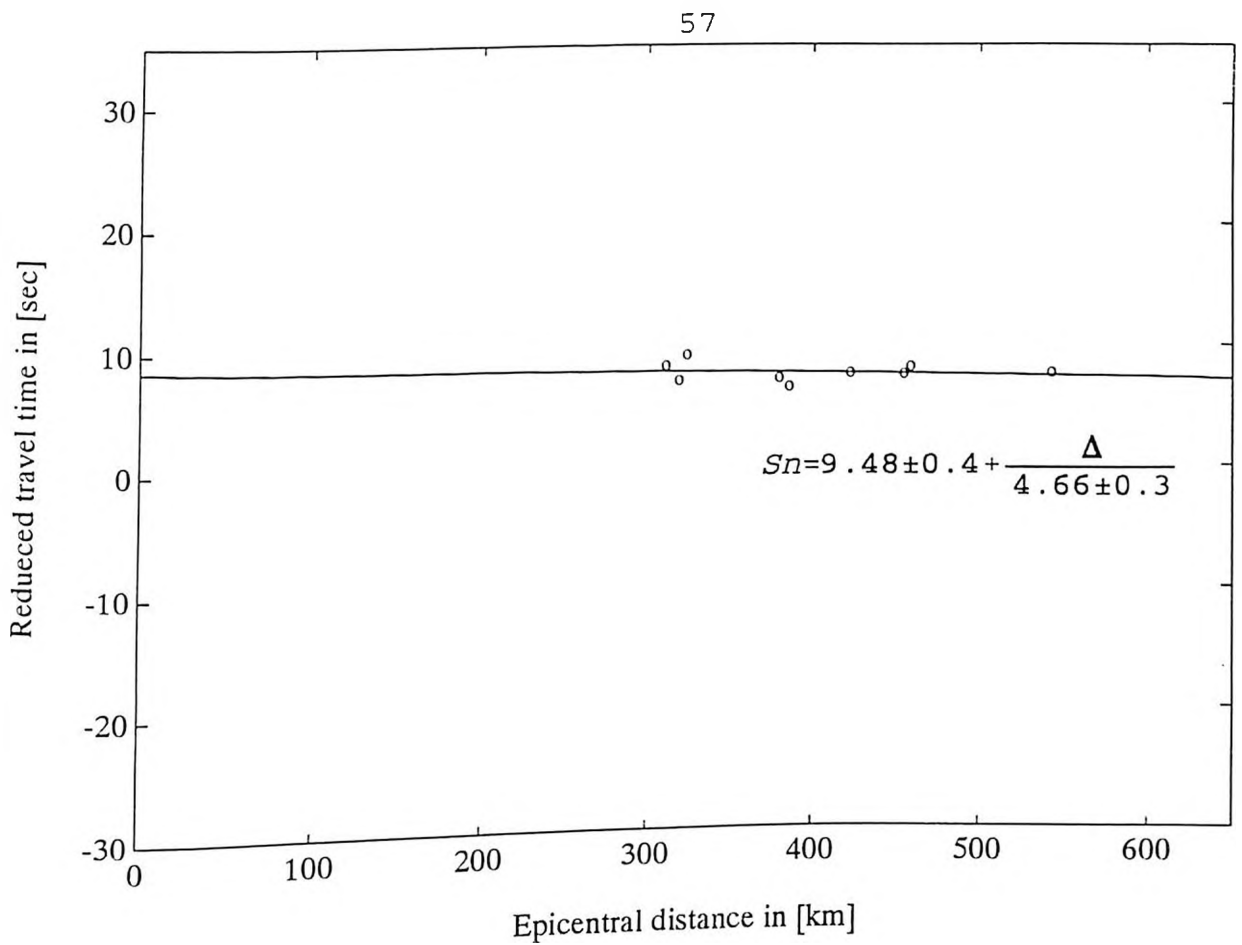
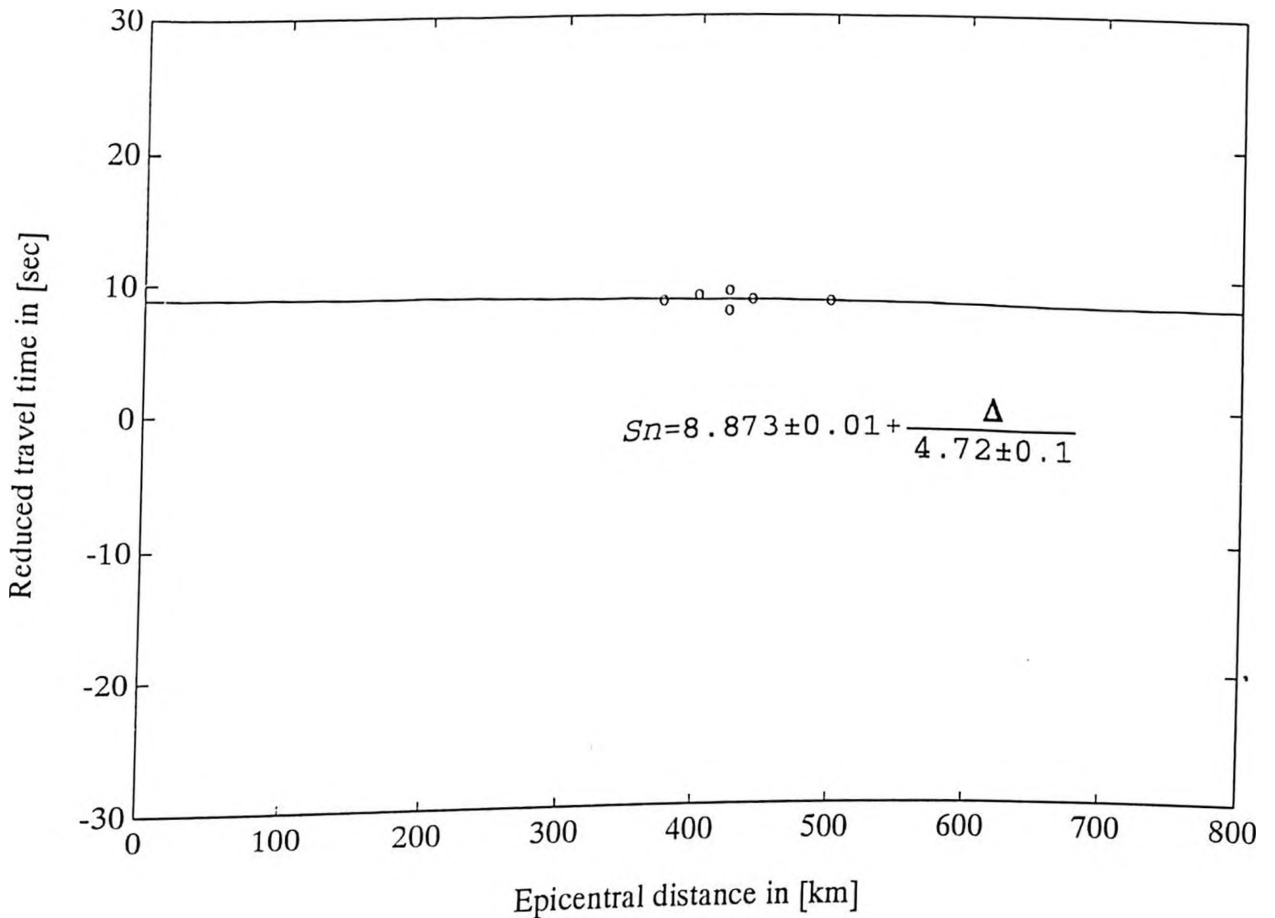*Figure (3.26) Profile 5 plot of reduced travel times against epicentral distance of Sn phase (Legend same as in Fig 3.12).*

Pg phase had twenty seven events in this profile. There was no significant scatter hence all events have been used in the analysis. This plot had a zero intercept and the velocities obtained were 6.38 km/s, see Fig. 3.27 below for details.
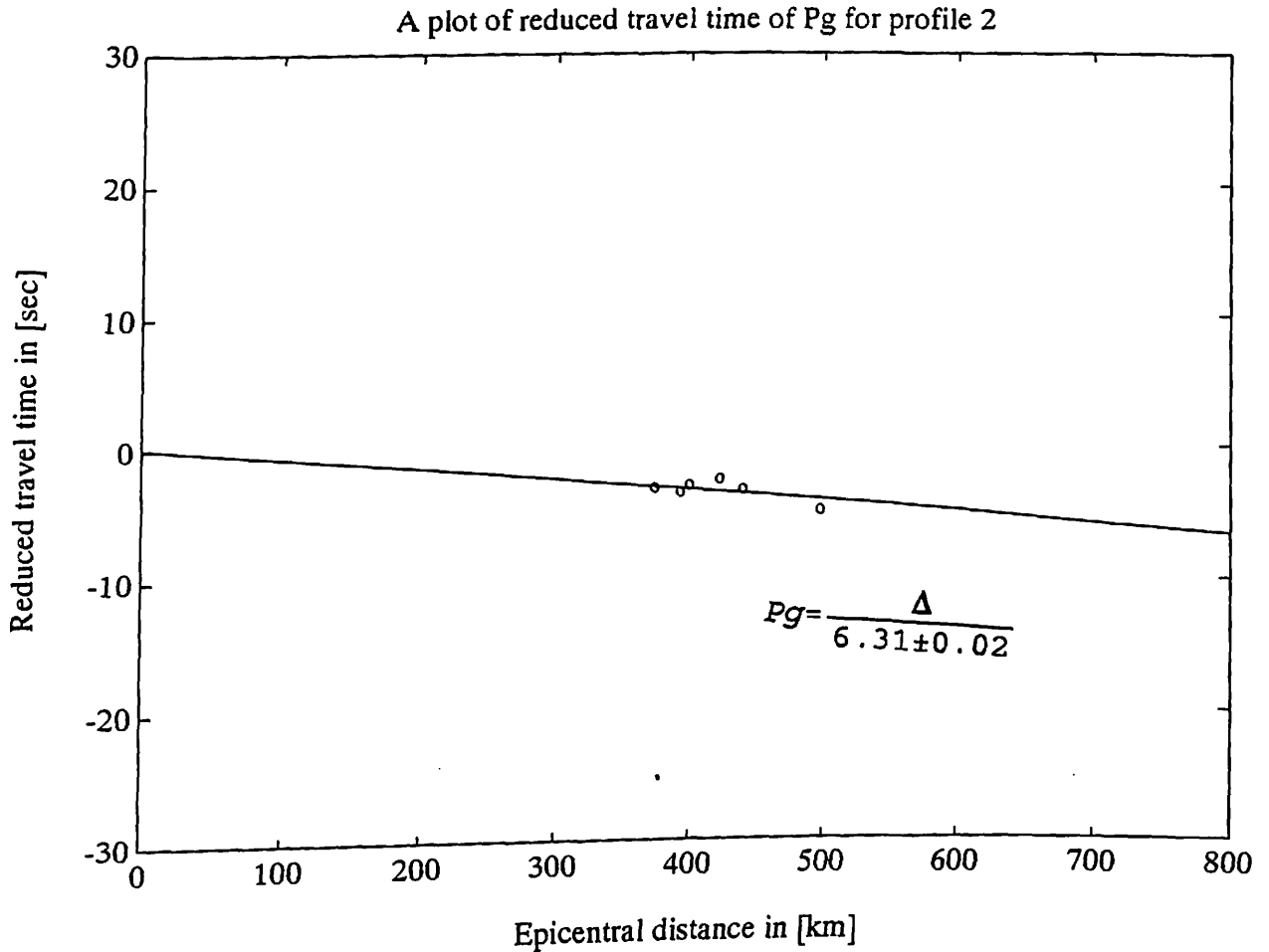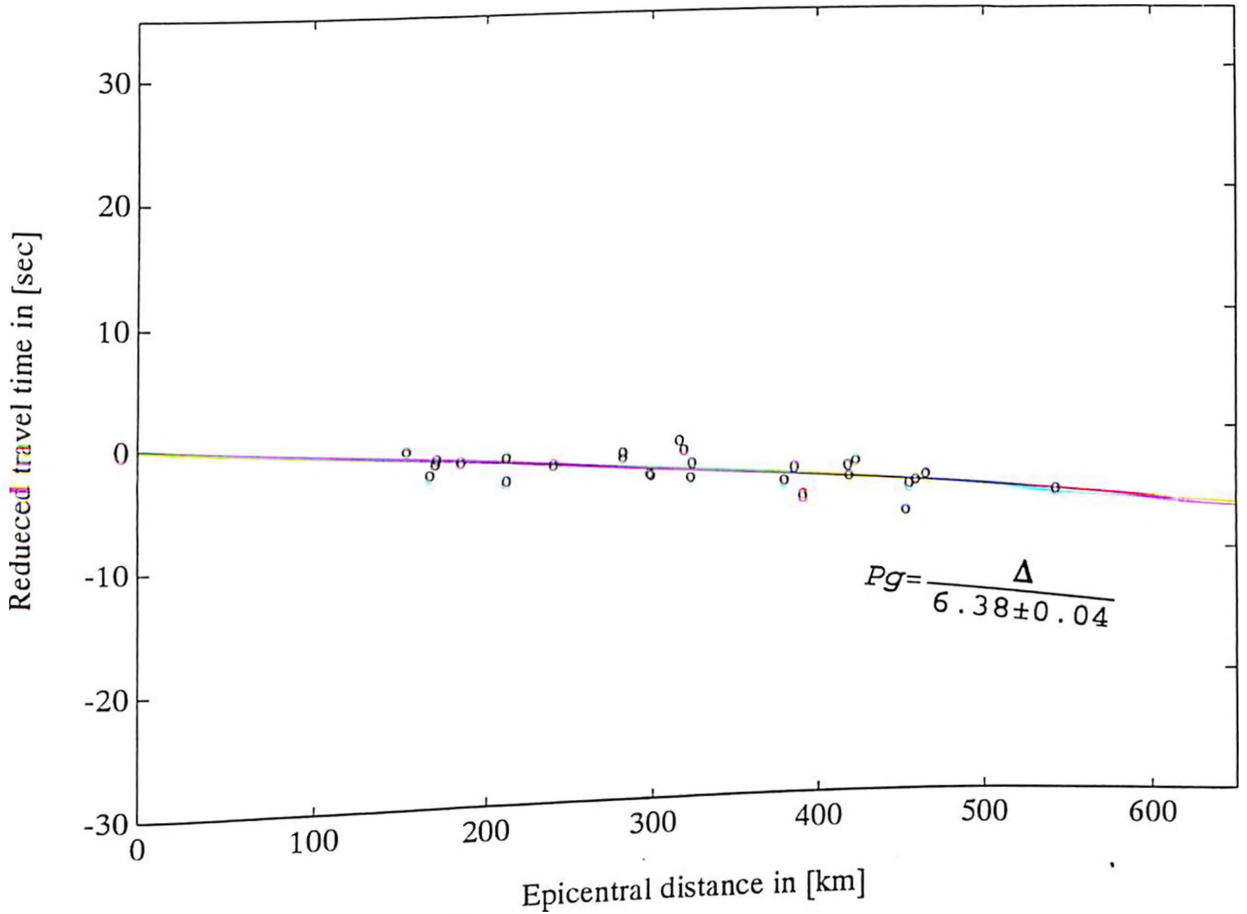
Figure (3.27) Profile 5 plot of Reduced travel times against epicentral distance of Pg phase (Legend same as in Fig. 3.13).

Sg phase had thirty four events in this profile. The scatter was not significant therefore all the events have been used in the plot. A small positive time intercept was obtained from the plot. This implies that there is some evidence of sediments which is invisible from the geology of the area. There are no results from refraction seismic study for this area to confirm this. This intercept was forced to zero and new cofficients computed resulting in a velocity of 3.67 km/s, see Fig. 3.28 below for details.
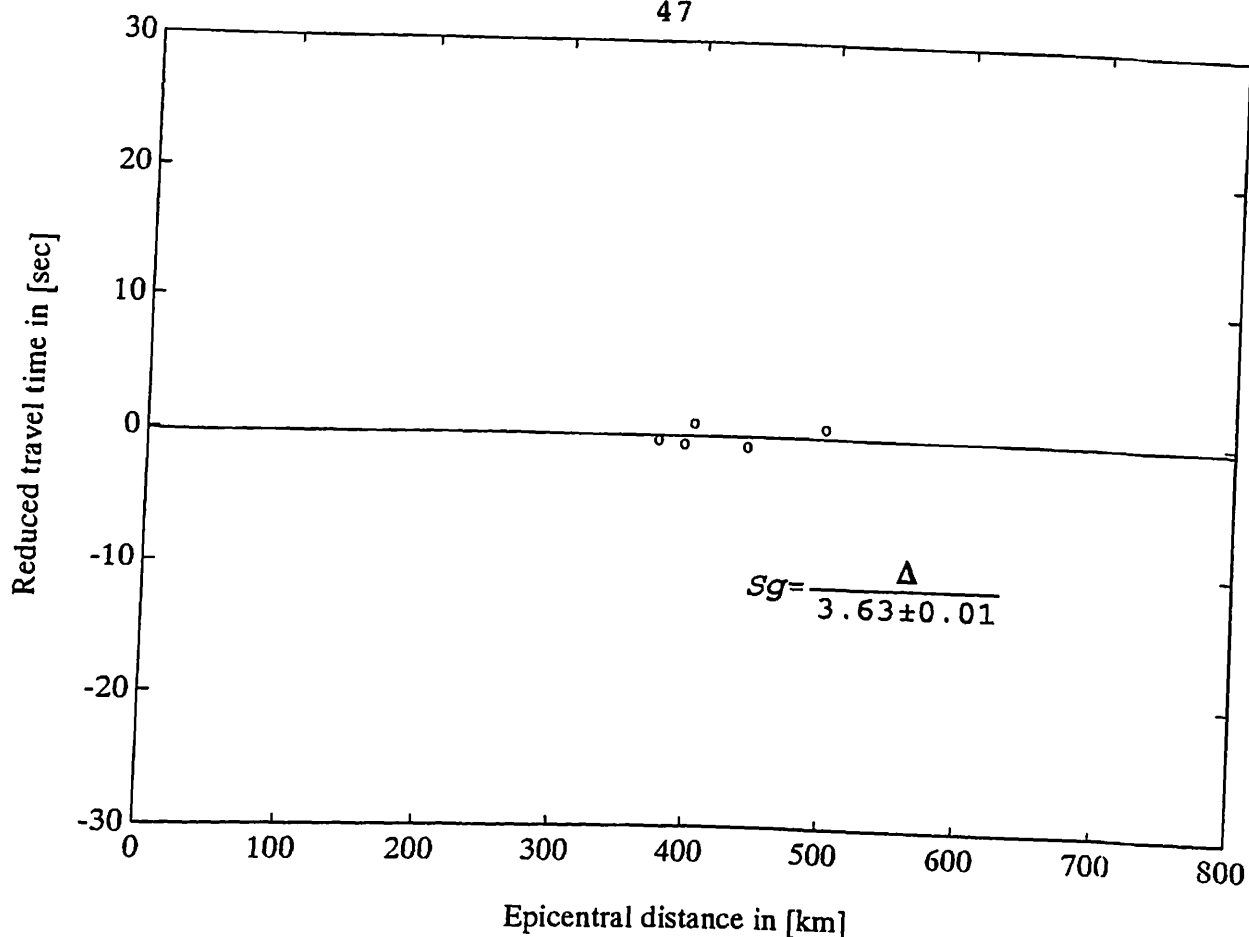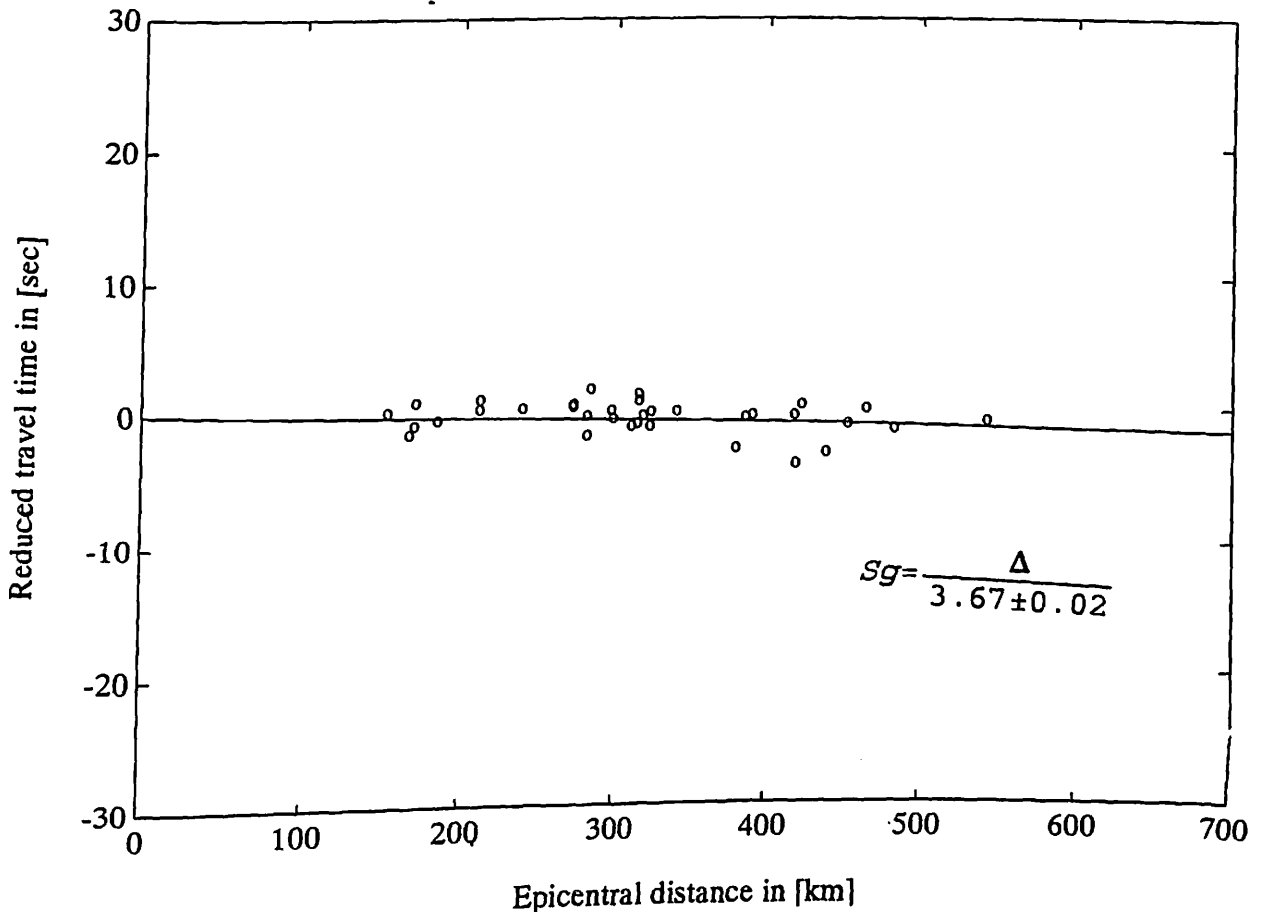
Figure (3.28) Profile 5 plot reduced travel times against epicentral distance of Sg phase (Legend same as in Fig. 3.13).

3.4.6   P- and S- wave velocities for Profile 6

This profile runs towards the coastal region of Kenya through the Chyulu hills. It transects the Mozambique belt, a region which has been found geologically to have undergone complex metamorphism and touching partly the tertiary volcanics at the coastline. This profile runs at an azimuth of 149^0 from NAI station.

The profile lies in sector 6 which has sixty eight events from Olang's localisations. Only seveteen events of them appear in the ISC localisations. This profile had very few Sn observations which therefore have not been analysed.

The profile was problematic during the analysis by showing a big scatter in the plots. It was learned from the preliminary analysis of the KRISP94 (Stangl, 1994 personal

communications) that the results show a thick crust of about 40 km. With such a thick crust the Pn phase can only be observed at distances greater than 250 km. Hence the first arrival from this profile is likely to be a Pg. This analyis is shown in Fig. 3.29 below. Pg phase had a total of thirteen events in the profile. These events did not show a significant scatter unlike the Pn. All the events were used in the plot which resulted in a small positive intercept. The intercept was forced to zero since the evidence of sediments has only been found along the coastline, and is therefore not representative of the whole profile. The new coefficients resulted in a velocity of 6.41 km/s, see Fig. 3.30 below for details.

$$Pg = \frac{\Delta}{6.41 \pm 0.02}$$
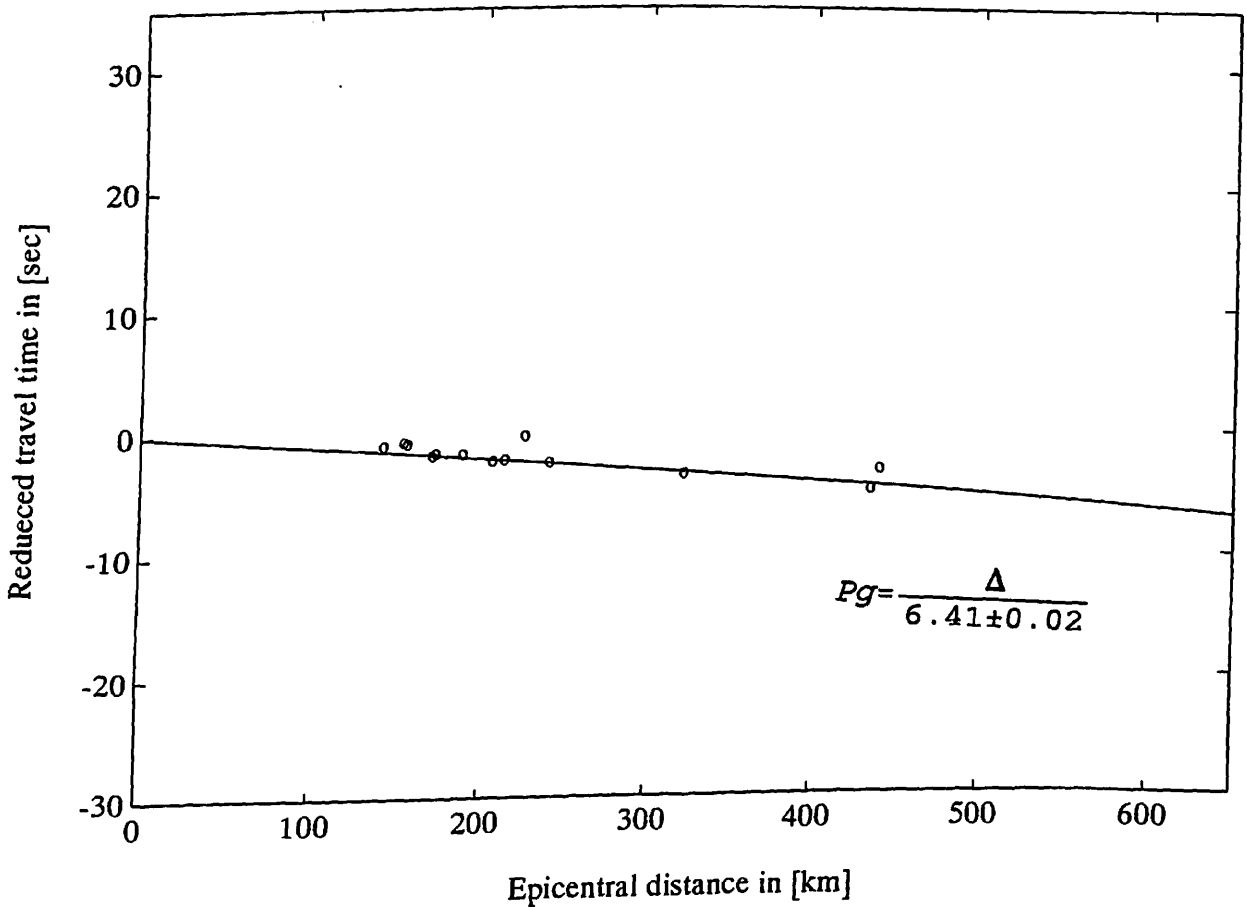
Figure (3.29) Profile 6 plot of reduced travel times against epicentral distance of Pg phase (Legend as in Fig 3.13).

Sg phase had thirteen events in this profile. These events did not show a considerable scatter

that could require omission of some events. Therefore all events have been used in the analysis with zero time intercept resulting in a velocity of 3.67 km/s as seen in Fig. 3.31 below.
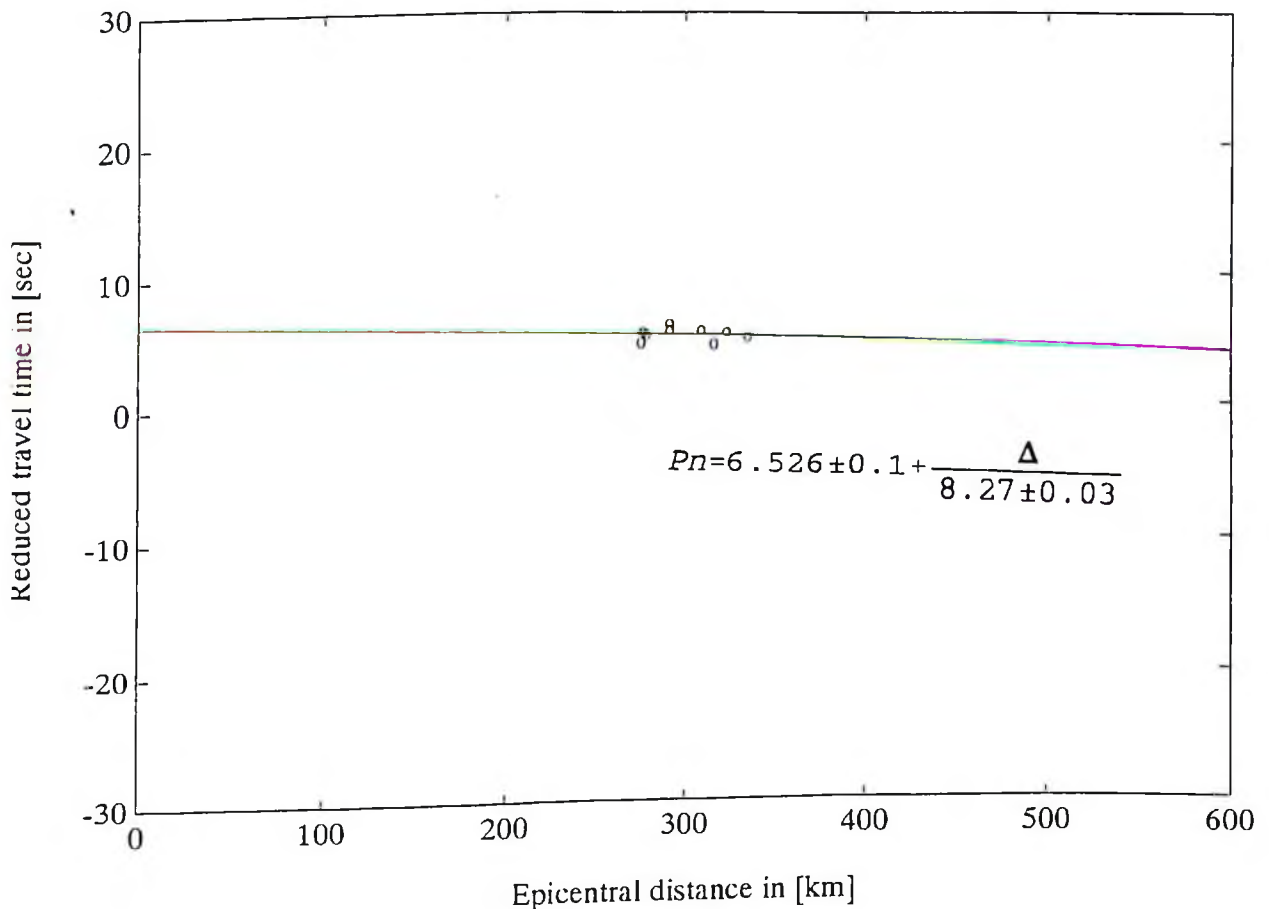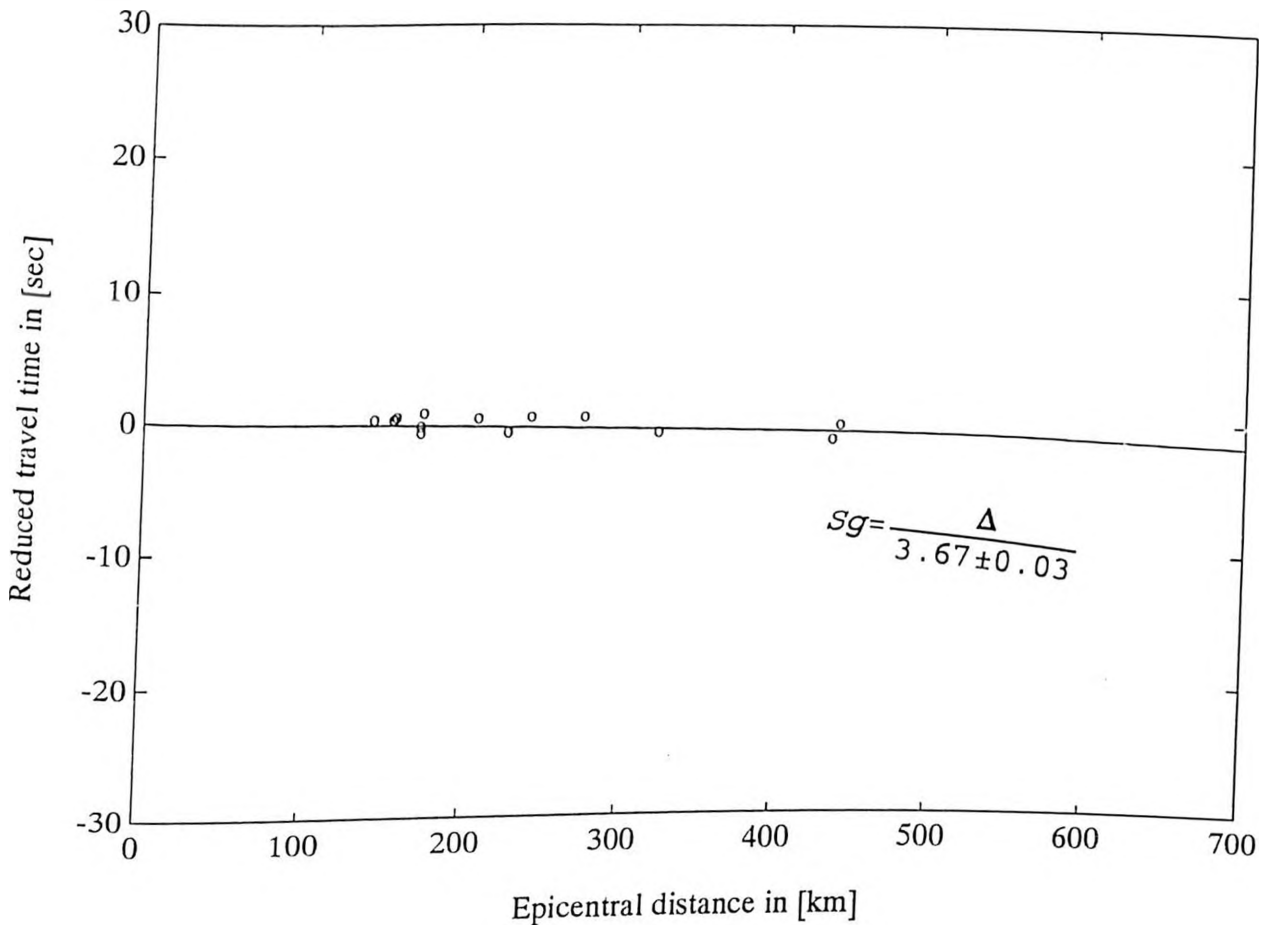

Figure (3.30) Profile 6 plot of reduced travel times against epicentral distance of Sg phase (Legend same as in Fig. 3.13).

3.4.7 P- and S- wave velocities for profile 7

The profile extends towards the eastern part of Kenya at an azimuth of 88^0 from Nairobi. This profile lies in sector 7, which has total of twenty eight events from the seismicity map, out which only seven events appear in ISC localisations.

The data points showed a considerably scatter for the Pn phase as the case of profile 6. The analysis for the Pn was therefore not done.

Pg phase had five data points which did not show a significant scatter. This plot reflected

a velocity of 6.28 km/s with a very small positive intercept that was forced to zero (see plot

in Fig. 3.32 below).
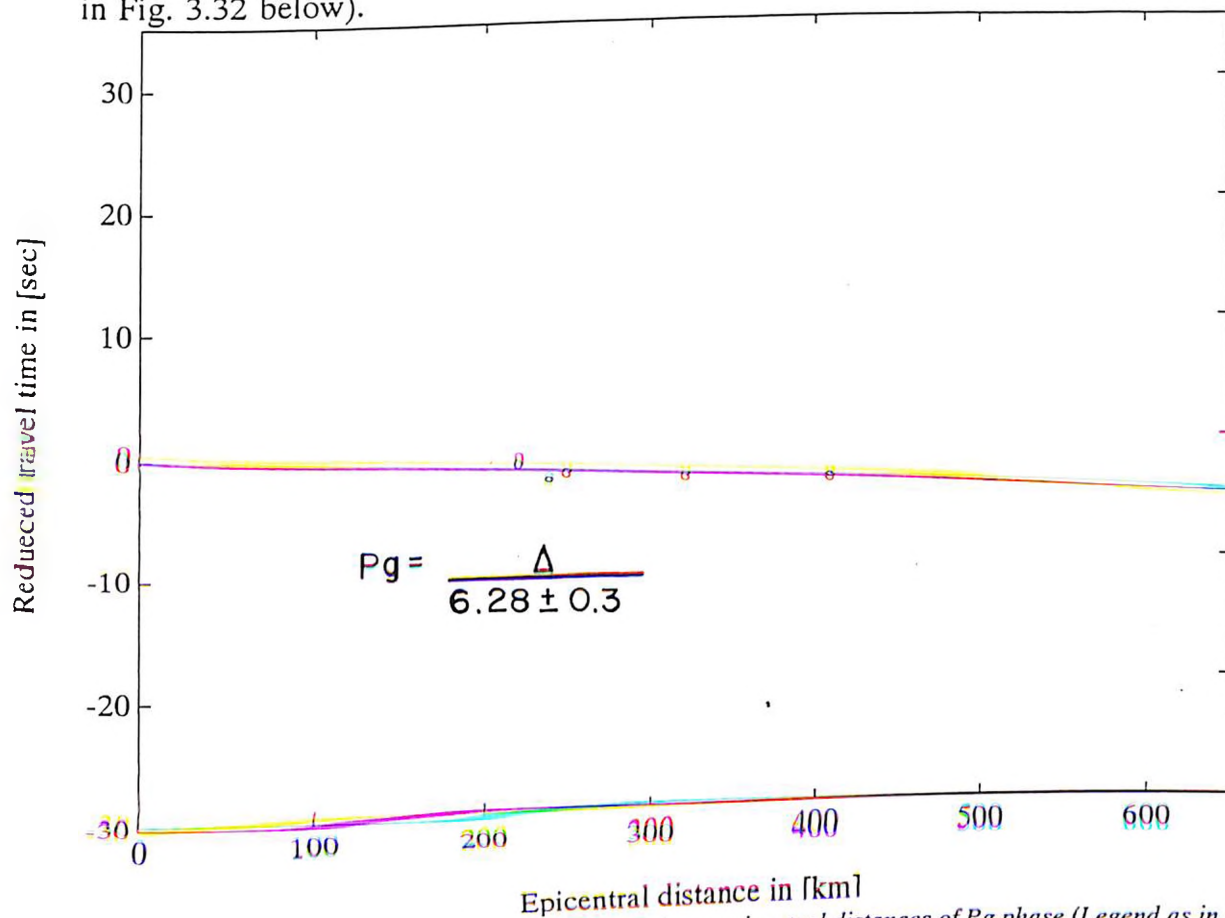
Figure (3.31) Profile 7 plot reduced travel times agianst epicentral distances of Pg phase (Legend as in Fig 3.13).

The Sg phase had six events with no significant scatter. All the data points were used in

the plot. This resulted in a small positive intercept which was forced to give a velocity of

3.66 km/s (see plot in Fig. 3.33 below).
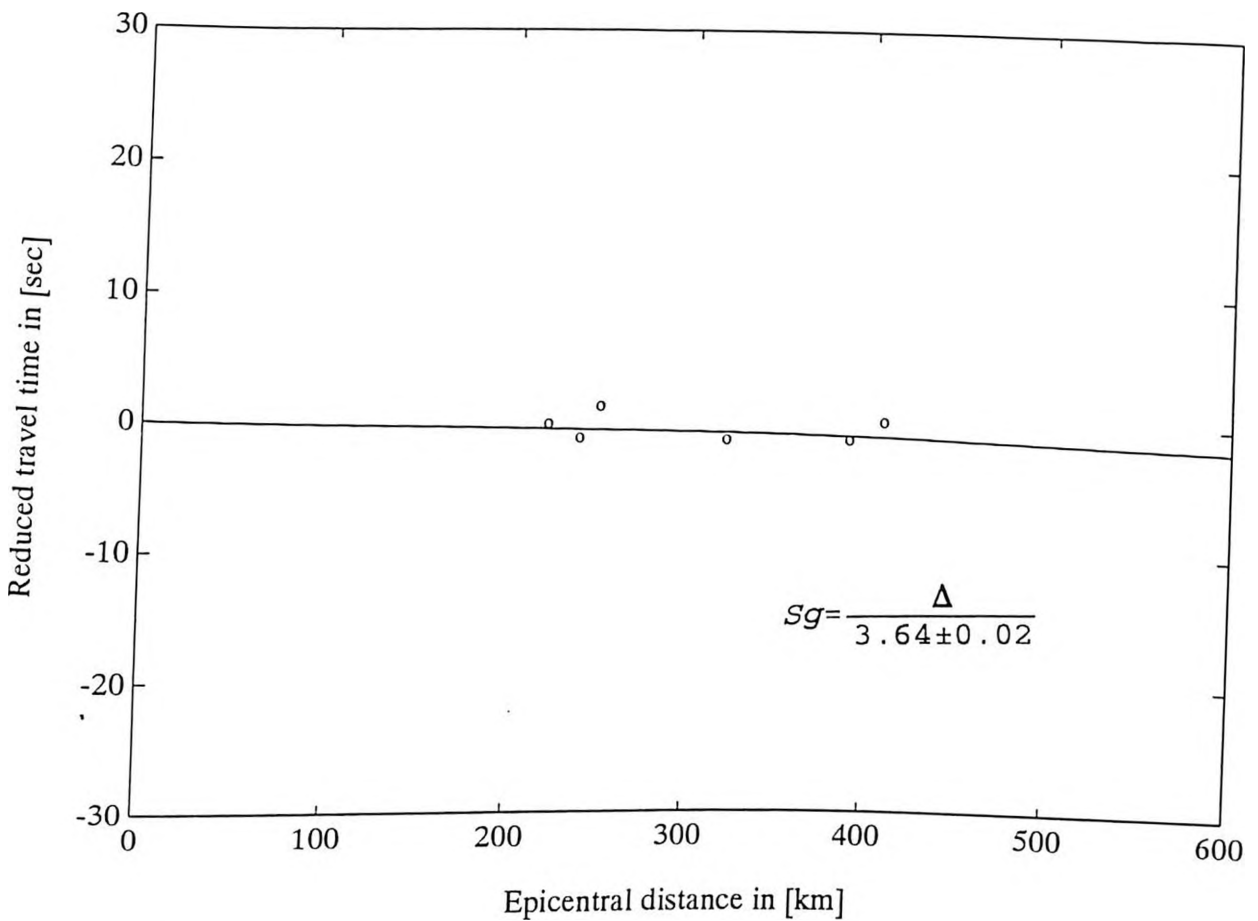
Fig. (3.32) Profile 7 plot of reduced travel time against epicentral distances of Sg phase (Legend as in Fig. 3.13).

3.4.8 P- and S- wave velocities for profile 8

The profile extends towards the northeastern part of Kenya. This lies in sector 8 which has twenty three events from the seismicity map. But there were no ISC located events in this sector, therefore no analysis was made for the P- and S- wave velocities from this profile.

3.4.9 P- and S- wave velocities for the unified dataset

A unified dataset was constructed by combining all readings from the various profiles. The velocities computed for this were to be compared with the ones from the different profiles. This was done to check the necessity of regionalisation of the seismic velocities. The unified

dataset contained all the profiles 1-7 since profile 8 did not have any ISC localised event.

Pn phase had a total of 121 events. The events from profile 6 and 7 occurred as outliers (being early by 1-2 secs.). Three different velocities could be inferred from the travel time plot. The velocities are lowered after a distance of 500 km. From 700 km the velocities then increases again.

When the full dataset was used , Pn reflected a velocity of 7.84 km/s with a time intercept of 3 secs. After removing outliers (i.e those from profile 6 and 7 and the events which occurred at a distance greater than 600 km) a velocity of 8.12 km/s were obtained.

$$Pn = 4.81 \pm 0.03 + \frac{\Delta}{8.12 \pm 0.03}$$
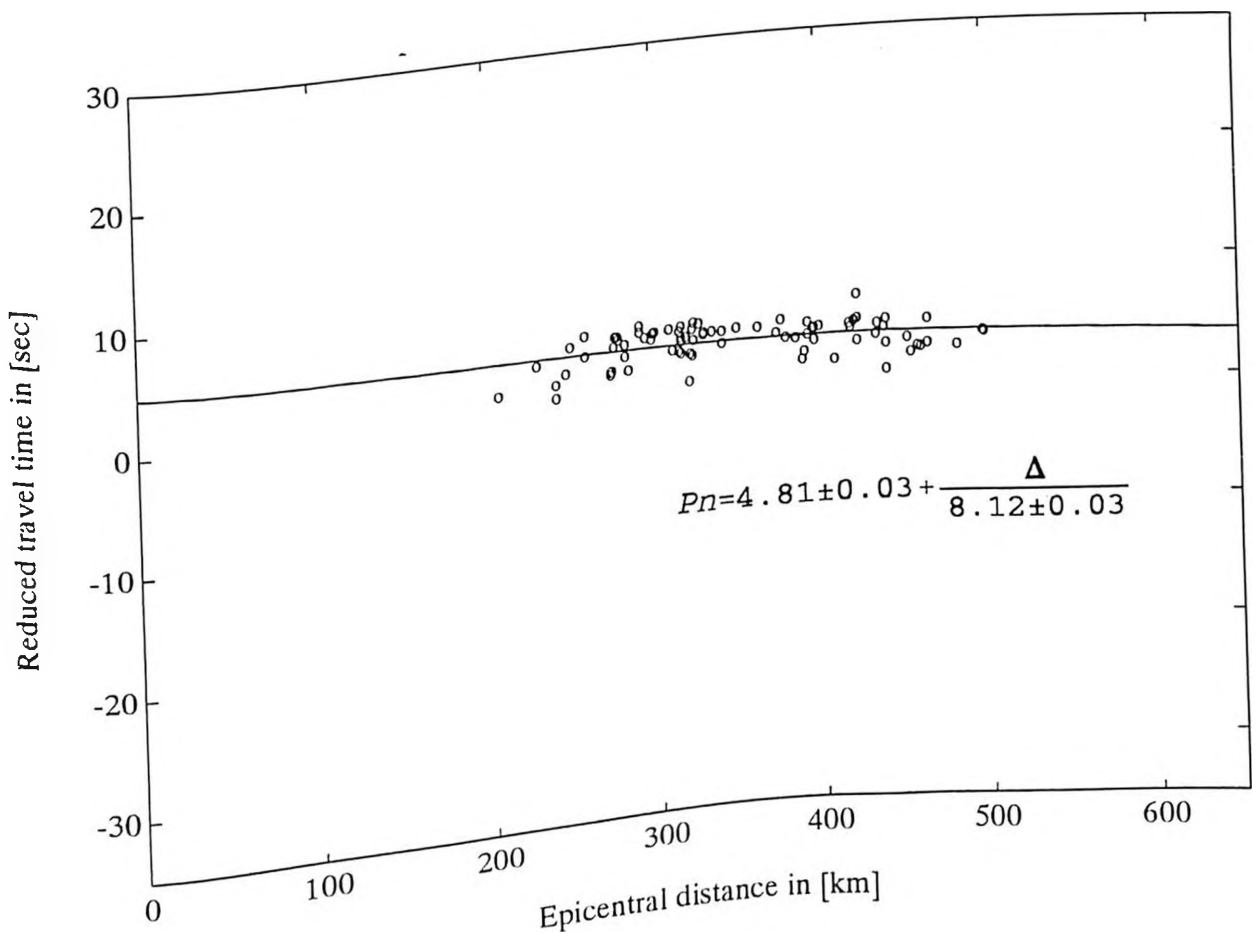
Figure (3.33) Plot of observed reduced travel time for the unified dataset against epicentral distance of Pn phase upto 600 km (legend is same as in Fig 3.13).

Sn phases had a total of fifty four events from all the profiles. There were a number of

outliers in the plot between 350-400 km distance range. The biggest scatter occurred

between 780-820 km. When these outliers were removed and data plotted upto 500 km, a

velocity of 4.68 km/s were obtained (see plot in Fig. 3.34 below for details).

$$Sn = 8.20 \pm 0.04 + \frac{\Delta}{4.68 \pm 0.03}$$
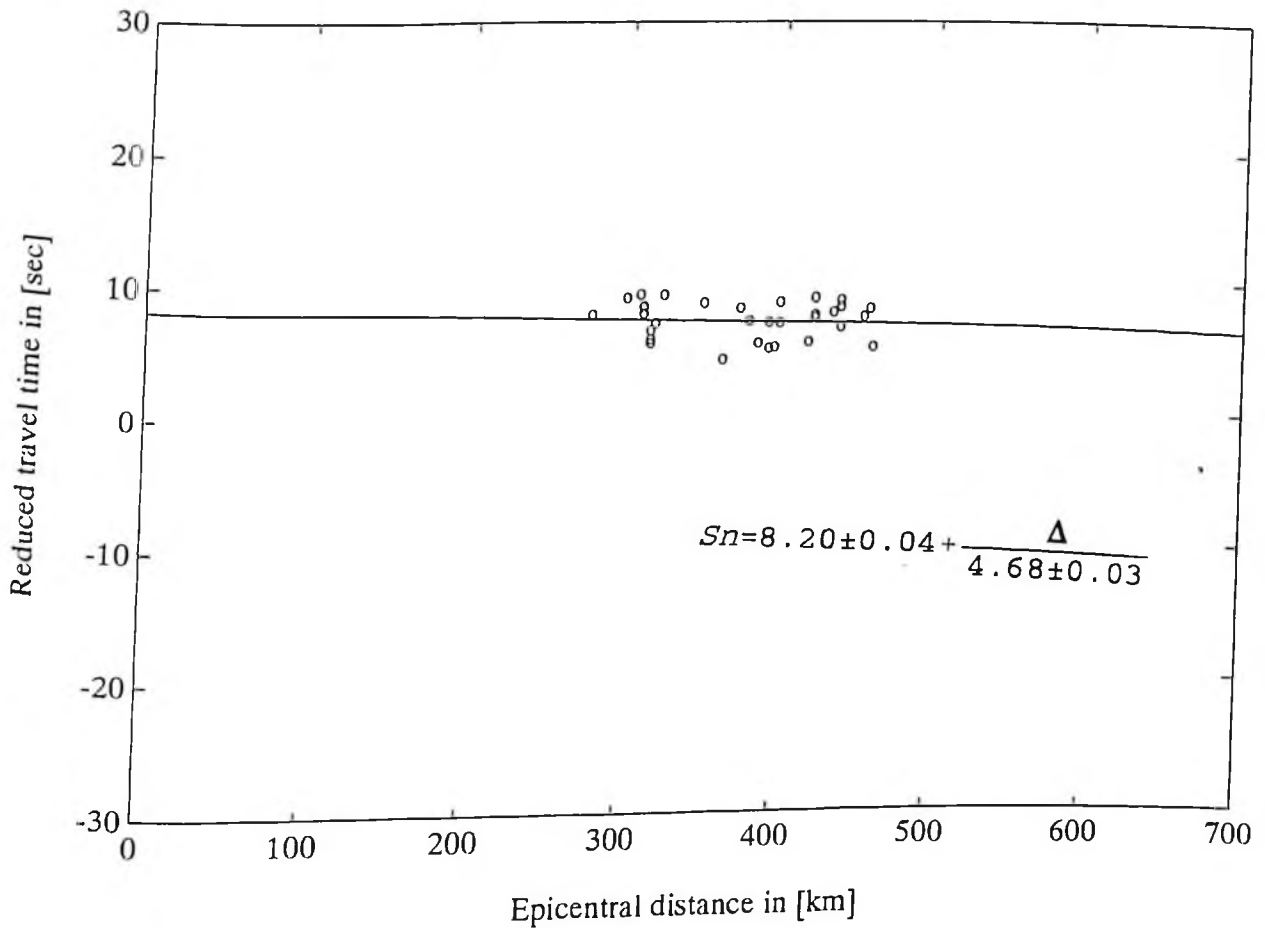
Figure (3.34) Plot of observed reduced travel times for the unified dataset against epicentral distance of Sn phase
(legend same as Fig. 3.13).

Pg plot had several outliers which could not be explained apart from those at distances

greater than 600 km that were taken to be no longer Pg phases. Without the outliers a

velocity 6.35 km/s with a very small time intercept was obtained (see plot in Fig. 3.35

below for details).
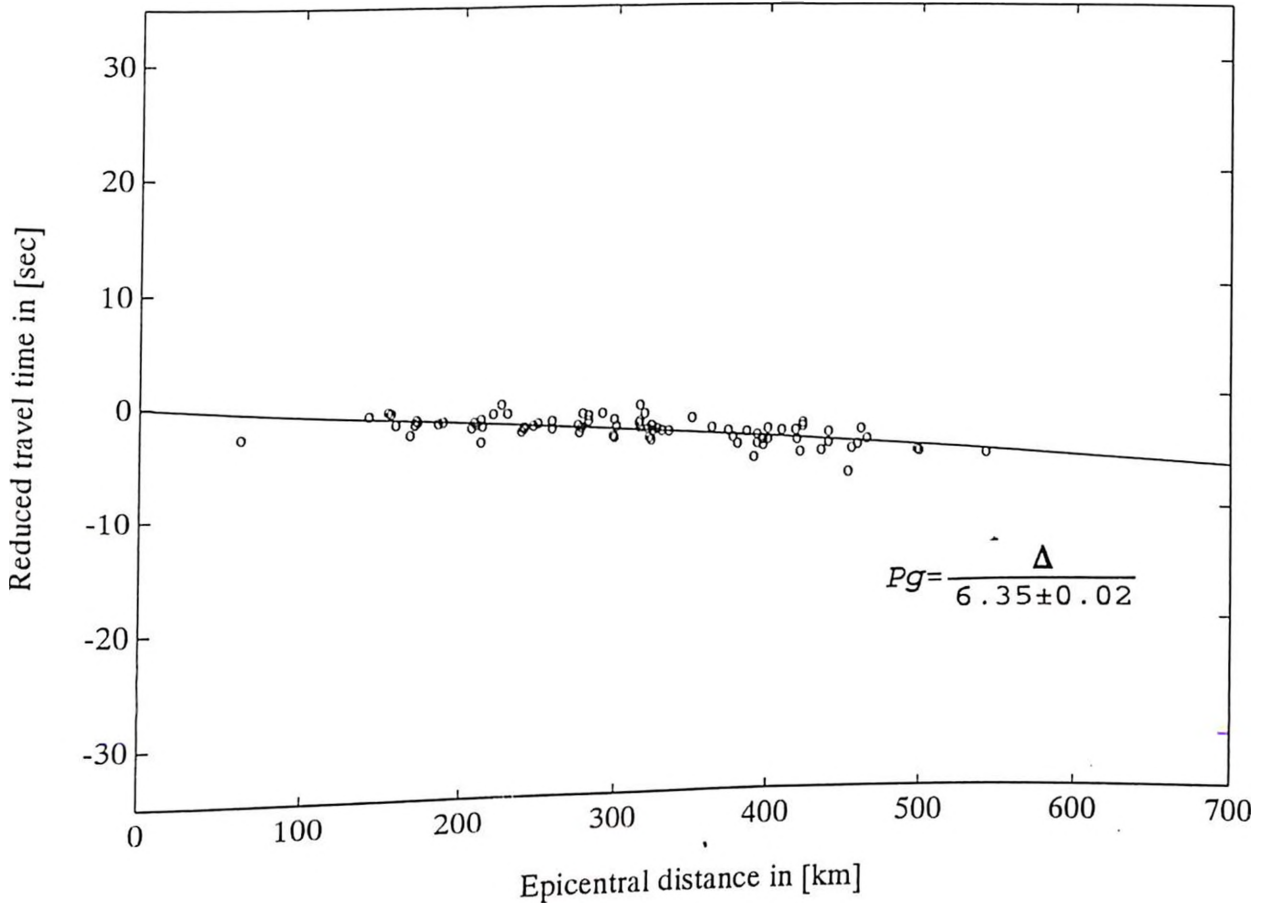
Figure (3.35) Plot of observed reduced travel times for the unified dataset against epicentral distance of Pg phase (Legend same as in Fig. 3.13).

Sg plot had also a few outliers, but their scatter was not very significant. Velocities of 3.65 km/s with very small positive time intercept were obtained. These velocity was taken to represent the average Sg crustal velocities for all the profiles.
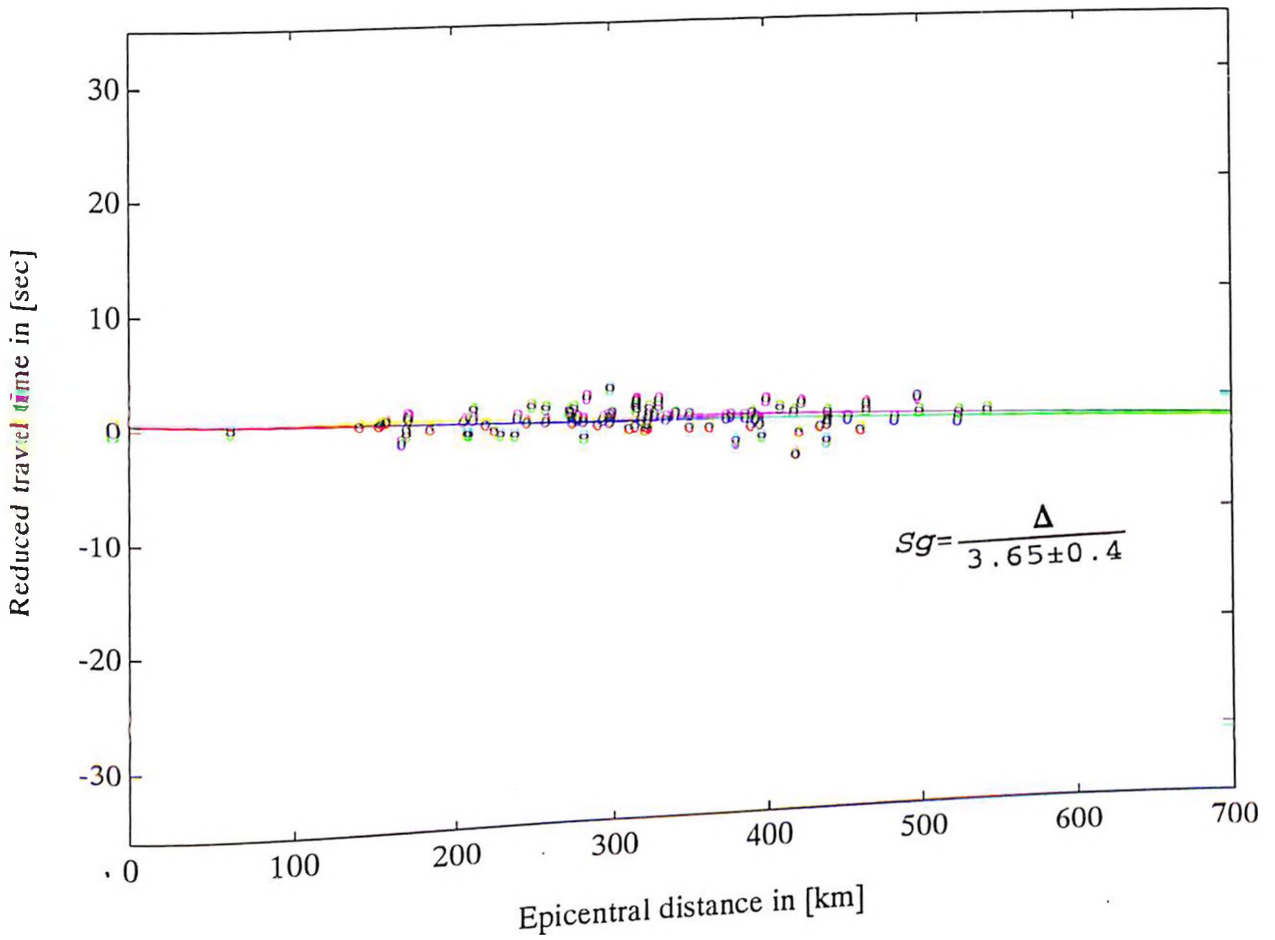
Figure (3.36) Plot of observed reduced travel times for the unified dataset against epicentral distance of Sg phase (Legend same as in Fig. 3.13).

CHAPTER FOUR

Velocity depth functions for the selected regions

This chapter tries to unravel different one-dimensional earth models for different regions of Kenya that will be used in earthquake localisations in future, from the analysis done in section 3.4. For a long time the seismology group in the Department of Geology in Kenya has used a model established for Finland (for details see Figure 4.1 below). The results of the KRISP experiments however have shown that this model does not fit for the localisations of earthquakes in Kenya as it assumes a very thick crust which is invisible (KRISP WORKING GROUP, 1991). The SEISAN software package (Havskov and Utheim, 1992) has been used to test the localisation by the Finland velocity-depth model. It was observed that this model mislocates events with errors of less than 50-60 km from that of ISC localisations.

Therefore there has been a need for establishing models to be used for future earthquake localisations in Kenya. This has been done by performing a travel time earth modelling using TRAVTIME (Stangl, 1986), for details refer to section 4.1 below. These modelling has been performed with the velocity data obtained from the profiles established in section 3.3.2.

4.1   Principles of the travel time data modelling

From the obtained velocities, modelling was done by TRAVTIME (Stangl, 1986). This is an interactive program to compute travel times for a one dimensional earth model. The model is given by discrete depth, velocity values and use a linear interpolation between neighbouring

gridpoints, to compute travel times for many ray parameters. Layers of constant velocity and discontinuities in velocity are allowed for. The travel time can be computed for a spherical earth model or for a flat one. In case of spherical model, the model is transformed to a flat one, by applying a flat earth transformation (Gerver and Markushevich, 1966). In this study a flat earth model has been taken into consideration in the modelling. Homogeneous layers are transformed to layers with a small gradient and velocity discontinuities are transformed to very thin layers. The velocity gradients are then finite and different from zero in all layers, so TRAVTIME has only to calculate the diving waves. It can also calculate the direct wave for a source at a certain depth.

During the modelling, the time intercepts for the direct waves (i.e. Pg and Sg) were taken to be zero. Positive intercepts indicates the presence of sediments, or a source at a certain depth but there has been no evidence for the existence of sediments from the refraction results (KRISP experiments) and from the geological maps. It has been shown in the section 3.3.5, that even with thick sediments the time difference is less than 0.25 secs and the velocities are the same. Therefore the travel times of these phases could be fitted with a straight line without making big errors (see section 3.3.5 for details).

As it was not possible to resolve the thickness of the upper crust and the velocity of the lower crust from the earthquake data, these two parameters have been taken from the KRISP90 results in the respective profiles. The parameter that has been modelled for the P phase travel time data was the Moho depth. This was altered to give the best fit for the dataset. For the case of the S- phases, the lower crustal velocities were obtained by taking the Vp/Vs velocity ratio to be equal to the square root of 3. Sometimes this value was slightly higher than this ratio

because the same crustal thickness obtained from a P phase for a given profile had to be obtained with the S phase. Hence the lower crustal velocity had to be altered to match the travel time data of the S phase. The focal depth was kept at 10 km for all the events assuming that most of the recorded earthquakes occurring in Kenya are shallow. This is supported by various workers e.g. Dahlheim et al. (1989) who worked around Lake Bogoria and found the earthquakes to be shallow. Secondly, for distances greater than 250 km, a surface focus and an earthquake at a depth of 10 km have almost the same travel times (as was shown in section 3.3.5). Lastly the travel time of the Pn is affected by the source depths and choosing a source depth of zero, gives very shallow Moho depths which are invisible from the refraction studies with a source depth of 10 km however the obtained models are in agreement with the KRISP90's results (see Figs. 2.4 a,b,c).

The modelling was done by setting the thickness for the upper crust and the velocity within the lower crust and varying the Moho depth to match the travel times. When the best fit was obtained, these parameters were then taken as the velocity depth model of that profile. There were always some outliers of observed travel time during this matching. Figure 4.1. shows these outliers on profile 4 for example. It can be seen that some of the Pg data are falling on the travel time curve of the phase representing PmP (encircled in Fig. 4.1a). These outliers can explain why the Pg has high velocities in some profiles. The seismograms having outliers were reread and those events which could not be improved further were then discarded as can be seen in Fig. 4.2 for the same profile 4. The reason for these outliers can be attributed to either poor known source depth or inaccuracy in phase readings, wrong phase associations or poor locations, leading to wrong epicentral calculations. From the calculations done an addition of 10 km to the epicentral distance leads to a difference in reduced time by about 1.25 secs for

8 km/s reduction velocity. This therefore confirms that mislocations of 10 km will affect the data set. The cleaned dataset was modelled, and the resulting model is seen in Fig. 4.1b.
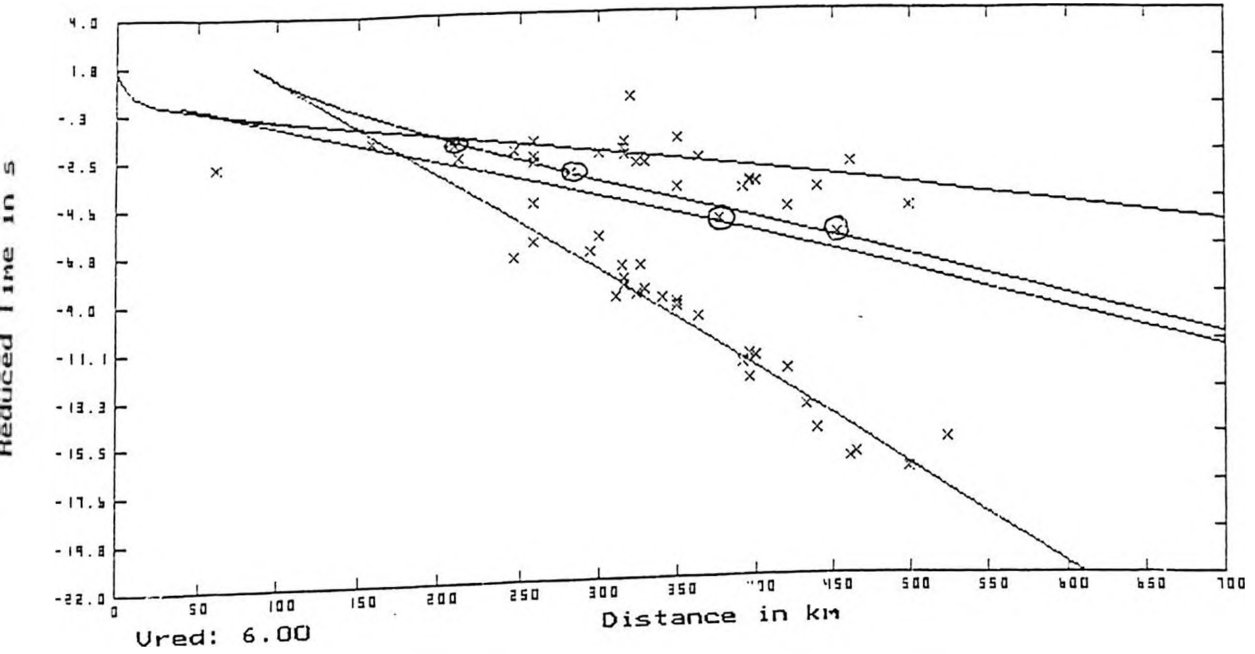
Figure (4.1) Observed reduced travel time are matched on the theoritical travel time curves of profile 4 for the P phase. The outliers can be seen falling on other curves e.g those encircled are falling on the reflected PmP phase instead of
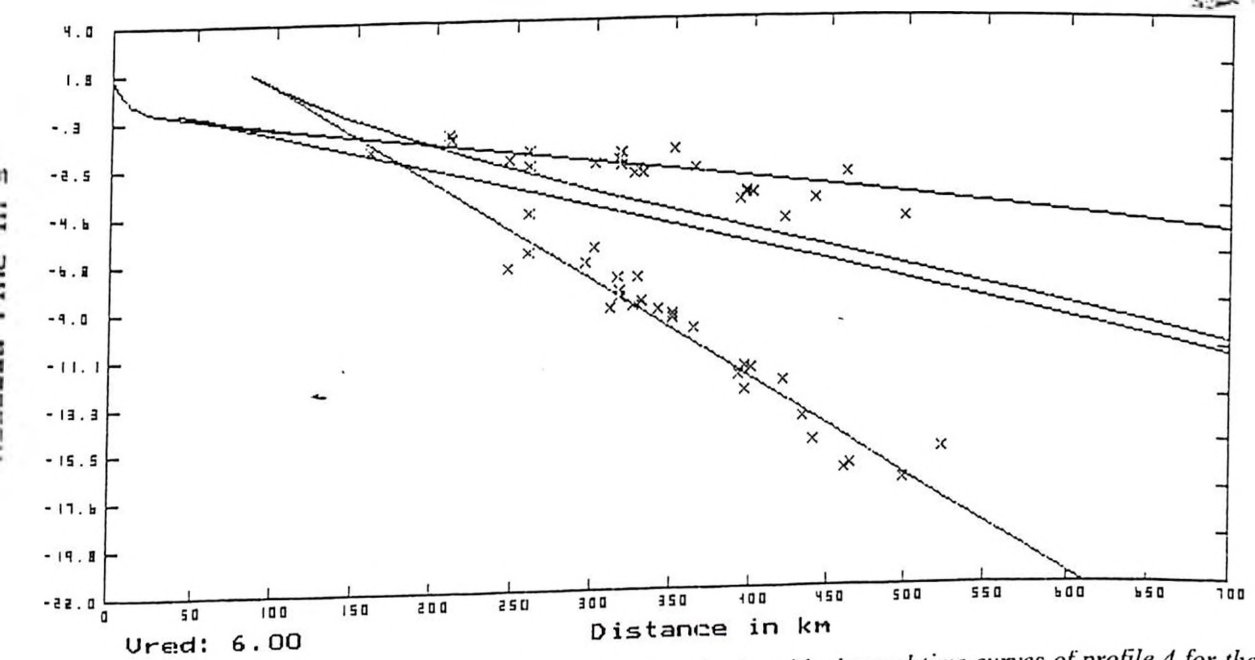
Figure (4.2) Observed reduced travel time matched on the theoritical travel time curves of profile 4 for the P phase. (all outliers have been removed and the wrongly associated phases have been rechecked and reassociated in the plot).
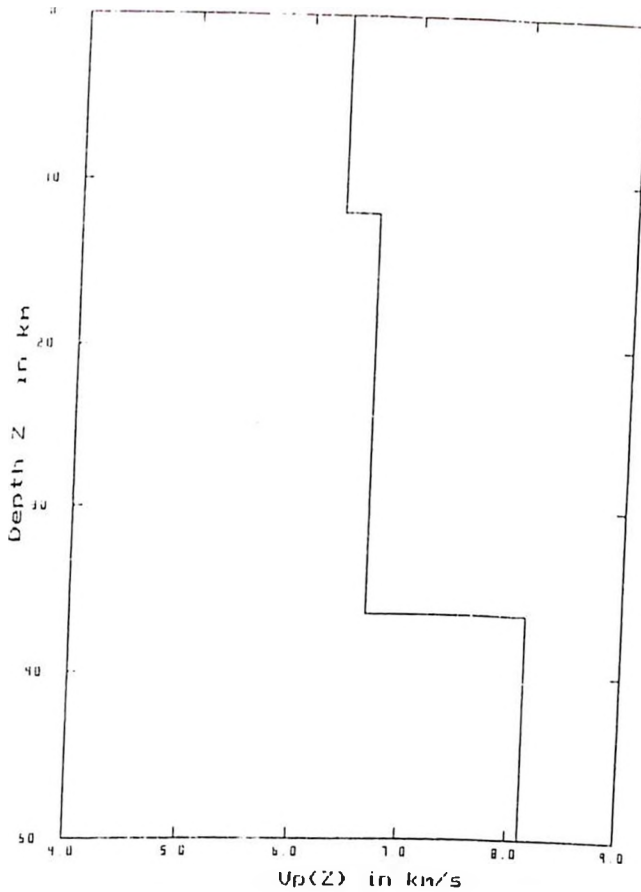
Figure (4.3) One-dimensional flat earth model of profile 4 for the P phase. The x-axis represents the velocities of these phases while the y-axis represents the depth (z) in km.

4.1.1   Model for profile 1

Not all velocities for different phases could be established from available data for this profile 1. The KRISP90 velocities for non-identified phases have been retained to be used in computation of velocity depth models (see Fig. 2.4a for details). The Pg velocity has been assumed to be 6.2 km/s and a velocity of 7.93 km/s for Pn has been used. The velocity from KRISP90 (7.75 km/s) is lower than this value. This can however be explained as being due to lack of enough data from this study and also the events that have been used are not located in the Rift Valley zone.

4.1.2 Model for profile 2

The profile reflected crustal velocities of 6.31 km/s and 3.63 km/s for Pg and Sg respectively. The upper crustal thickness for this profile was set to 15 km as was indicated by KRISP90 experiments. The average lower crustal velocities for this profile are 6.70 km/s and 3.93 km/s for P and S respectively. The 6.70 km/s results from the KRISP90 experiment (see Fig. 2.4a) while the 3.93 km/s was obtained by assuming that the velocity ratio is equal to square root of 3. But this is slightly higher than this factor because it had to be increased slightly in order to get the same model as the one obtained from the P phase travel time data. The Moho depth was found to be 37 km (see Fig. 4.6 below which shows the summary of the models obtained from this study).

4.1.3 Model for profile 3

Crustal velocities of 6.27 km/s and 3.63 km/s were obtained for the Pg and Sg respectively. The upper crustal thickness was set to 15 km (from KRISP90 results). The average for the lower crustal velocities were 6.6 km/s and 3.87 km/s for P and S respectively. A Moho depth of 39 km was obtained. The details are represented in Fig. 4.6 below.

4.1.4 Model for profile 4

Crustal velocities of 6.34 km/s and 3.64 km/s were obtained for the Pg and Sg respectively, with mantle velocities of 8.13 km/s and 4.72 km/s for Pn and Sn respectively. The upper crustal thickness was set to 15 km. There is however no control with lower crustal velocities of 6.6

km/s and 3.87 km/s for the P and S respectively and this resulted in a Moho depth of 37 km. Details of this results are represented in Fig. 4.6 below.

4.1.5   Model for profile 5

Crustal velocities of 6.38 km/s and 3.67 km/s for Pg and Sg were obtained on this profile. The average upper crustal thickness was set to be 15 km as is also indicated by KRISP90 experiment, with average lower crustal velocities of 6.8 km/s and 3.8 km/s for P and S respectively (from KRISP90 results). This model resulted in the Moho depth of 29 km. The details are shown in Fig. 4.6 below.

4.1.6   Model for profile 6

On this profile velocities for some of the phases could not be obtained since the data were not enough to give a reliable least square fit.   For this reason the velocities of this phases have been retained from the model of KRISP90 (see Fig. 2.4c for details). The Pg velocity of 6.41 km/s has been used and Sg of 3.67 km/s while a velocity of 8.0 km/s for Pn has been assumed as indicated by KRISP90. The preliminary KRISP94 analysis (Stangl, 1994 personal communication) has shown that the crust thickens to about 40-45 km. The results of this study using NAI station has reflected 6.20 km/s for Pg and 3.64 for Sg. The intermediate crustal thickness has been set to 10 km. The lower crustal velocities has been set to 6.7 km/s as indicated by KRISP90.

4.1.7   Model for profile 7

This profile reflected a velocity of 6.28 km/s for Pg. The other phases were not clear on the seismograms hence the KRISP90 results have been retained (see Fig. 2.4a,b,c in section 2.2 for details). This profile is some kilometers away from the flank line, therefore if this model has to be used then one can only speculate whether the Moho depth will remain at 30 km or the depth might increase as you move towards the eastern part of Kenya. But from the preliminary results of KRISP94 it can be assumed that the crust will become thicker eastwards.

4.1.8 Model for profile 8

This profile did not have ISC located events. Therefore the model from KRISP90 on line E (see Fig. 2.4 for details) will be retained. The Pg will be assumed to be 6.2 km/s with 8.0 km/s for the Pn and lower crustal velocities of 6.7 km/s for P phase with the lower crustal thickness of 10 km. The Moho depth will be assumed to be 30 km.

4.1.9 Model for the unified dataset (all profiles)

There was need to get a unified model for all these profiles so as to see if regionalisation of seismic velocities is justified or not. The obtained mantle velocities of 8.12 km/s and 4.71 km/s for Pn and Sn respectively from results in section 3.4.9 have been used. The average crustal velocities for this unified dataset was 6.35 km/s and 3.65 km/s for Pg and Sg respectively with the upper crustal depth being set to a depth of 15 km. Lower crustal velocities of 6.6 km/s and

3.85 km/s for the P and S respectively were used. This resulted in a Moho depths of 33 km.

The Fig. 4.4 represents a plot of synthetic travel time curves with matched observed travel times

while Fig. 4.5 represents the model for the unified dataset from all the profiles.
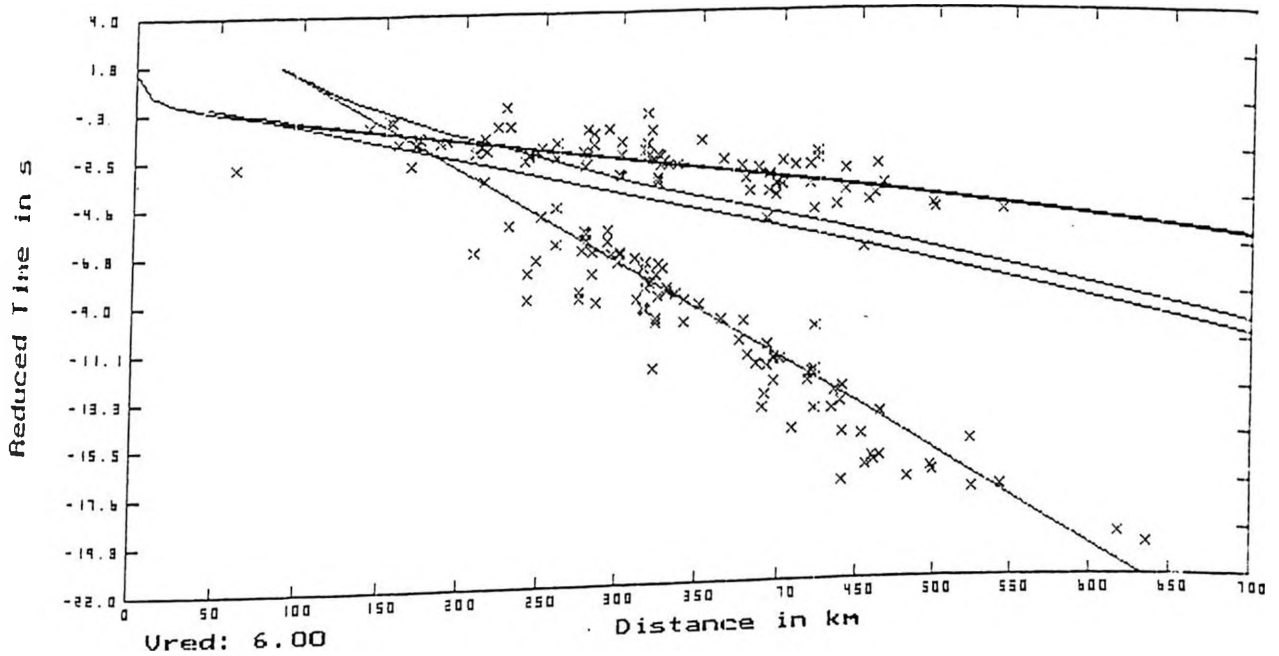
Figure (4.4) Observed reduced travel times matched on the theoritical travel times curves for unified dataset (all profiles) for the P phase (all outliers have been discarded in the plot).
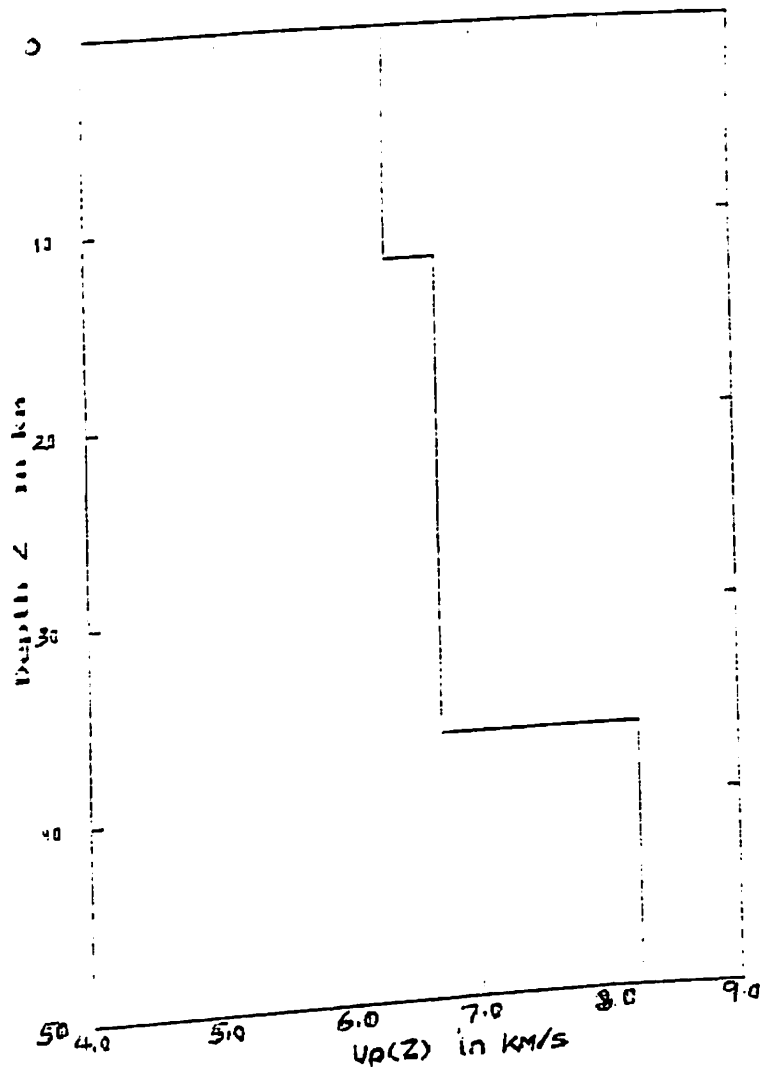
Figure (4.5) One-dimensional flat earth model for unified dataset (all profiles). The x-axis represents the velocities of these phases while the y-axis represents the depth (z) in km.

PROFILES

Figure (4.6) A summary of the established models of these profiles. The table shows different profiles with their respective phase velocities of different phases. The top of the figure is taken as the surface with increasing depth as you move to the bottom.

4.2 Discussion of the crustal models for Kenya

The crustal structure obtained from the body wave analysis has shown that the crustal structure in Kenya is not the same for the whole country. It varies in different directions as observed at Nairobi station. According to this study the Kenyan crust is typified with an average Pg-wave velocities of 6.22-6.38 km/s and 3.62-3.67 km/s Sg-wave velocities. The intermediate crustal thickness is between 10-15 km thick. The upper mantle velocities are about 8.06-8.3 km/s and 4.68-4.77 km/s for Pn and Sn respectively. The lower crustal velocities are in the range of 6.6-6.8 km/s and 3.8-3.93 km/s for P and S respectively with crustal thickness in range of 37-39 km. The southern part of Kenya and the northern part of Tanzania (the area lying in the presumed Tanzanian Rift valley) has a crustal thickness of about 29 km. The results of the unified dataset (data from all profiles) gives an average crustal thickness of 33 km. The results are comparable to those of the previous findings done by various researchers, from both earthquake data and refraction experiments done a round this area.

Dopp (1964) studied the travel times of local earthquakes in Western Rift valley and detected low velocity material in the crust at the depth between 17-39 km and P velocities of 6.7-6.8 km/s intermediate velocity. This thickness of the crust and the intermediate velocities are in close agreement with the findings from this study (see Fig. 4.6 for details). Bonjer et al. (1970) studied the structure of the earth's crust beneath stations Nairobi (NAI), Lwiro (LWI), and Addis Ababa (AAE) from the spectral behaviour of long period body waves. The models beneath these stations show that the crustal thickness varies from 35 km beneath LWI to about 40 km beneath NAI with an intermediate boundary of about 15-20 km between NAI and LWI, and about 25 km beneath AAE. The crustal thickness is in close agreement to 39 km obtained on the profile 3 extending to Lake Victoria. The intermediate crustal thickness is in the range

obtained from this study's results (see Fig.4.6). Gumper and Pomeroy (1970) obtained the intermediate boundary to be about 17.5 km with a crustal thickness of 37 km for the Afar depression. Rykouvnov et al (1972) obtained an intermediate boundary of 18 km and a crustal thickness of 36 km for southern Rift region. This results of the crustal thickness are in close agreement with those of this study except the intermediate thickness which is slightly thicker. Rodrigues (1970) obtained Pn velocity of 7.7 km/s in the Western Rift and normal velocity of 8.2 km/s from the profiles on the flanks of the Rift valley. The Sn velocities of 4.5 km/s were obtained with an average P-wave crustal velocity of 6.2 km/s. This study resulted in a total crustal thickness of 21 km in the Western Rift and 30 km for the Eastern Rift. The velocities of Pn and Sn from the flanks of the Rift are in good agreement with those of this study. But the crustal thickness of Rodrigues are much thinner than those obtained from this study.

From the detailed seismic refraction study KRISP90, the Pn velocities of 8.1 km/s were found on the flanks of the Rift valley with a crustal thickness of 20 km to the northwest part of Kenya (L. Turkana) and 35 km to the south (L. Magadi). This was in agreement with results of KRISP85 which gave the thickness of 18.5 km to the north (around L. Turkana) KRISP WORKING GROUP (1991). The results from the refraction experiment of KRISP90 showed that the velocities in the upper crystalline crust derived mainly from the analysis of the Pg phase are between 5.9 km/s and 6.2 km/s beneath all lines of all the profiles along the Rift and are consistent with a material of granitic composition (KRISP WORKING GROUP, 1991). But further south the velocity changes to 6.4-6.6 km/s which was explained as being due to an increase in the basic average composition. From the study of heat flow values in Kenya, though scattered, an increase of 200-300 degrees across the Rift margins at a depth of about 15 km is indicated (Morgan, 1982). Such temperatures would decrease the velocity by 0.1-0.2 km/s

(Birch. 1960 and Christensen. 1979). This velocity decrease could be compensated for by intrusion of more basic igneous material into the 6.4-6.6 km/s layer beneath the Rift they remarked. The anomalous upper mantle is characterised by low Pn velocity of 7.5-7.7 km/s confined along the Rift valley while the flanks have more normal velocities of 8.0-8.2 (KRISP WORKING GROUP, 1991). This KRISP90 study showed intermediate crustal thickness of about 15 km and an average crustal thickness of 35 km with 30 km in the rift valley. These velocities obtained from the Rift flanks are in good agreement with those of this study. The Pg velocities from this KRISP study showed that they were as low as 5.9 km/s unlike the results from this study which did not have velocities lower than 6.2 km/s. But the velocities obtained by the KRISP90 from the southern of 6.3-6.4 km/s are closer to the results from this study. The summary of these models are seen in Fig. 4.7 below while those of the KRISP90 study are seen in section 2.2 in Figs. 2.4a, b &c.
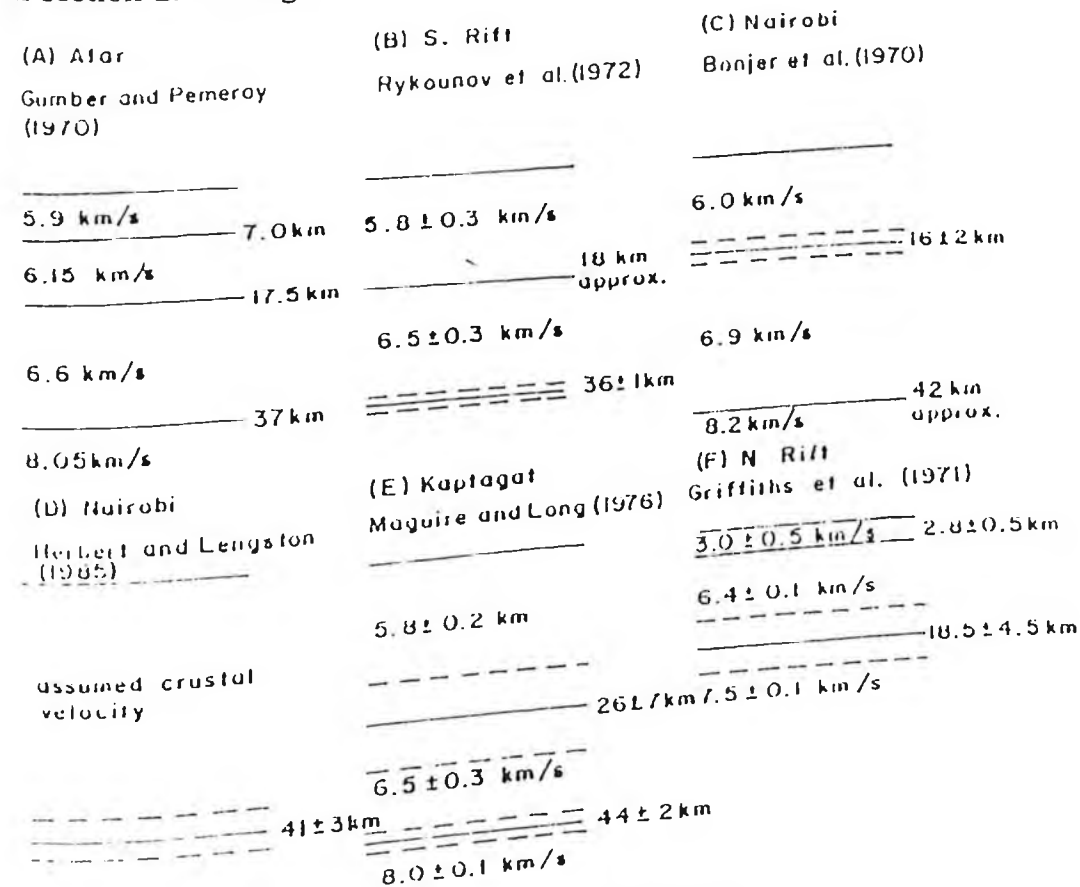
Figure (4.7) Models obtained by previous authors from thier works

4.3   Comparison of the earthquake localisation by different models using SEISAN software.

Different models have been used to compare the localisation with that of the ISC localisations, using the SEISAN software (Havskov and Utheim, 1992).

The SEISAN seismic analysis system is a complete set of programs and a simple data base for analysing earthquake phase data from analog or digital data. The earthquake localisation program is a modified version of HYPOCENTER (Lienert et al., 1988). The main modifications are that it can accept more phases, locate teleseismic events and use input in Nordic format. The program also uses observed station azimuths as given in the Nordic format. This means that the program can locate with one station if it has P, S and azimuth.

In this study the azimuth have been calculated from ISC localisations (i.e from ISC coordinates using EPIDIST program for computation). With the P and S readings and their corresponding azimuths, it was possible to locate some events from the different profiles established in this study. For each model, two plots were made; a plot with fixed depth of 10 km (for reasons already mentioned in section 3.3.5) and another one with free depth in order to see the contrast between them. It was observed that the localisations of these events showed very small or no difference at all. One reason for this could be that, these events had only two phase readings. But a further analysis showed that even for those with more than two phase readings, the changes were minimal. This therefore supports the fact that fixing of the focal depths to 10 km as already mentioned in section 3.3.5 could not result in erroneous results.

The Finnish velocity depth model assumes the crust to be 40 km thick. This model shifts the events from the Eastern Rift valley by about 50-60 km towards NAI-Station, while those from the Western Rift valley are pushed away from the NAI-Station. The model on the other hand locates the events from profile 6 (extending towards the coastal region of Kenya) on average fairly well. This therefore implies that the crust is thicker (about 40-45 km) in this profile. Fig. 4.7 below shows the localisation of this model with that of ISC. It can be observed that localistion of the events is fairly close to ISC localisation except for the event in the ocean which is expected because the crust is thinner there hence this model does not hold. This model can therefore be used for profile 6 events.
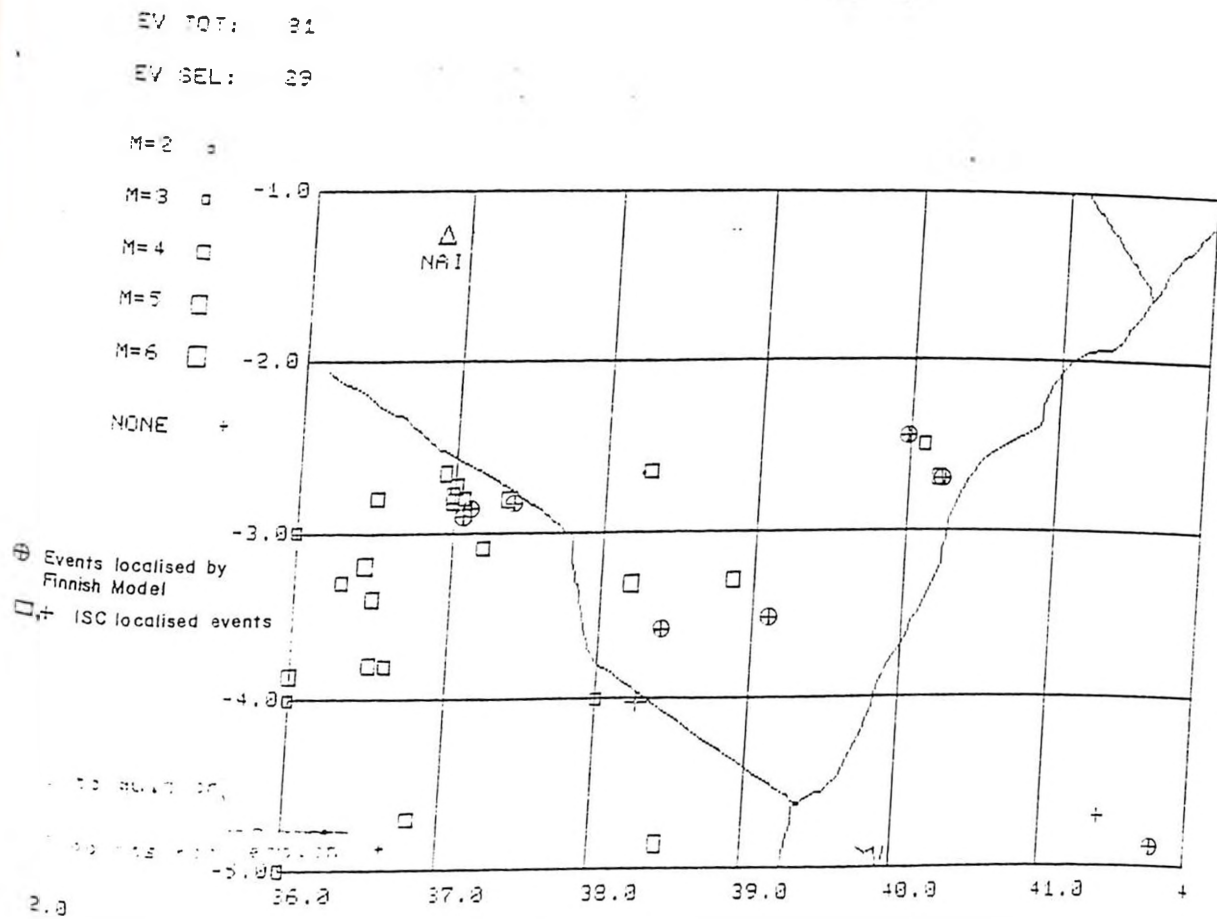
Figure (4.8) Epicentral map localised by Finnish model in comparison with the localisations of ISC.
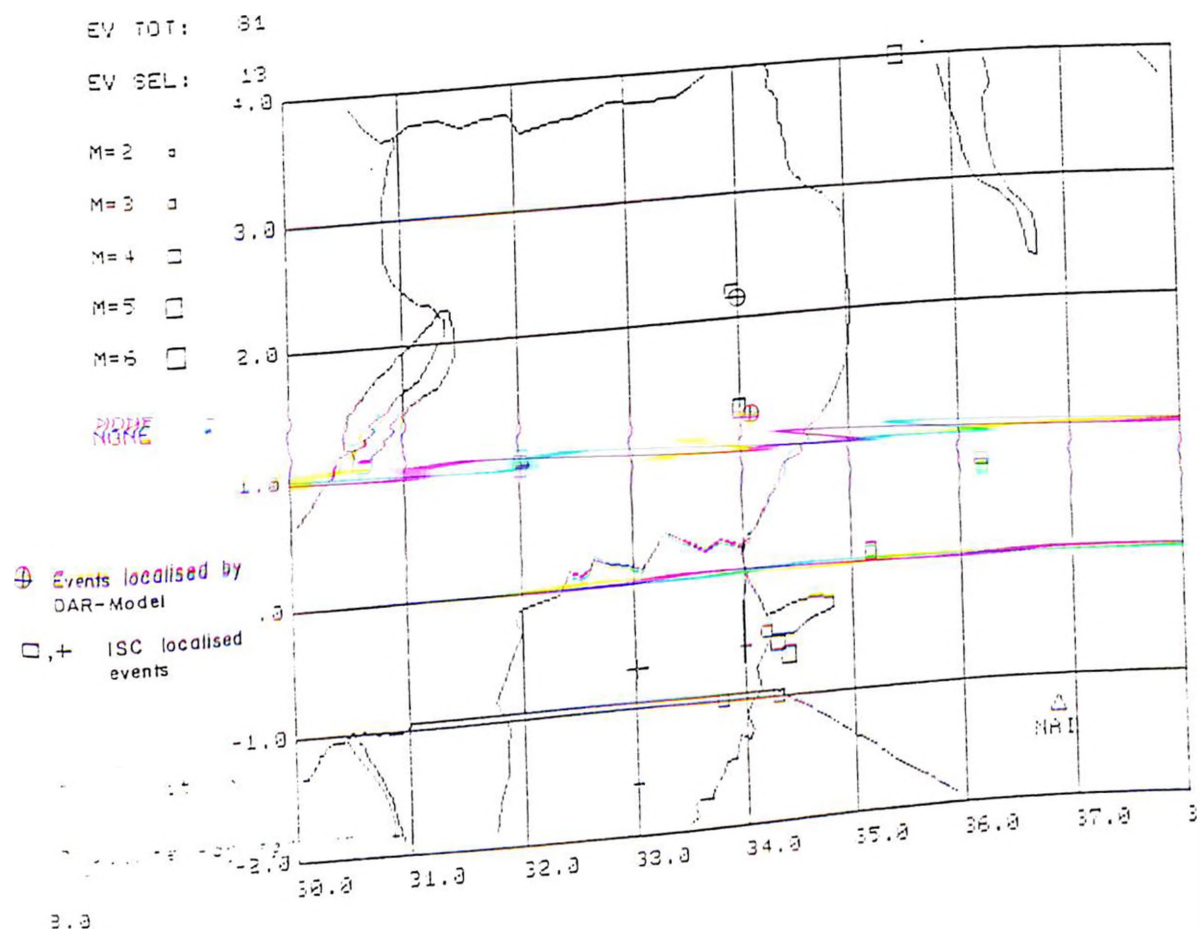
Figure (4.9) Epicentral map localised by slightly modified DAR-MODEL in comparison with the localisations of ISC.

The East African (EAF) model that has been used in the two workshops of Eastern African Region Seismological meetings (Dar-es-salaam -1993 and Nairobi-1994) sponsored by IPPS locates the events from Western Rift valley close to the ISC localisations. With some modification of the intermediate thickness from 13 km to 15 km and corresponding velocity of 6.7 instead of 6.6, the events from the Western Rift valley are better located. The localisation for the events from the southern part of Kenya and north eastern Tanzania are also roughly well located with this model.

The slightly modified NAI-East velocity depth model locates events from Lake Victoria (Homa Bay area) roughly well compared to the other models. This model could be used for events from the north eastern part of Tanzania but not Western Rift or Eastern Rift valley or profile 6, because the shift in the localisation is big. The KRISP90 velocity model established for the rift valley located the events from the rift valley better compared to other models.

The profiles 4 and 5 velocity depth models were observed to locate the events from southern part of Kenya and north eastern part of Tanzania close to ISC localisations compared to other models. But these models can not be applied to the profiles extending to Eastern and Western Rift valley because the shifts in localisations are big from these regions.

The unified velocity depth model obtained from this study, on average locates well the events from Lake Victoria (Homa Bay area) and those of profiles 4 and 5. The reasons for this could be that most of the events contributing to this model came from these profiles, hence it is biased by the dataset. But events from the western and eastern rift valley are poorly located with this model.

This study has explicitly shown that one model cannot be used to locate the earthquakes occurring in Kenya. One model will localise events from a certain profile better than the other. The results therefore show that there is need of regionalisation of seismic velocities.

It is therefore recommeded from this study that the Finnish velocity depth model can be applied for the events from profile 6 (region running towards the coast through Chyulu hills). The slightly modified EAF velocity depth model can be used for events from the western part of Kenya extending towards the western rift valley. This model can also be used for the events from the north eastern part of Tanzania and southern Kenya. But better localisation for the north eastern part of Tanzania and southern Kenya can be obtained with the velocity depth models of profile 4 or 5 or the Unified model. The modified NAI-EAST model or the Unified model can also be used to locate the events from profile 3 (Lake Victoria-Homa Bay region). The summary of these models and the corresponding velocity ratios are shown in Fig. 4.9 shown below. This models should be used to relocate all the events that have occurred in the corresponding profiles. The study further recommends that these models should be improved with the KRISP94 explosion data to make sure that errors in the earthquake localisations are minimised.

WESTERN RIFT REGION DAR — MODEL	EASTERN RIFT REGION KRISP 90 MODEL	REGION TOWARDS COASTAL REGION FINNISH MODEL	LAKE VICTORIA AND SOUTHERN PART OF KENYA EXTENDING TOWARDS TANZANIA			
			KRISP 90	PROF 4	PROF 5	UNIFIED MODEL
6.15 3.62	6.25 3.58	6.10 3.51	6.10 3.58	6.34 3.64	6.38 3.67	6.35 3.65
6.70 3.87	6.87 3.81	6.64 3.81	6.80 3.80	6.60 3.87	6.80 3.80	6.60 3.85
	7.50					
					8.06 4.66	
			8.00 4.68	8.13 4.72		8.12 4.68
8.00 4.68		8.03 4.72				

Depth scale (km): 5, 10, 15, 20, 25, 30, 35, 40

Figure (4.10) A summary of suggested models with their corresponding profiles.

CHAPTER FIVE

MAGNITUDE DETERMINATION.

5.1 Introduction.

The seismic magnitude is a measure of the energy released by an earthquake in form of seismic waves.

In general, the magnitude can be defined in the following way:

$$M = \log\left(\frac{a}{T}\right) + f(\Delta, h) + C_s + C_r \quad \ldots\ldots\ldots\ldots\ldots\ldots\ldots\ldots (5.1)$$

Where, M = magnitude, a = ground amplitude, T = wave period, Δ = epicentral distance, h = focal depth, $f(\Delta, h)$ is called the calibration function, C_s = station correction, C_r = regional correction, and log stands for log to base 10.

The three components which contribute to the size of the earthquake magnitude are:

(a)   The wave amplitude/period ratio at the measuring site.

(b)   Correction for geometrical spreading, attenution and focal depth: $f(\Delta,h)$ function is determined by a combination of theoretical and empirical results.

(c)   Station and regional correction constants: C_s, C_r

For part (a) we obtain the ground vibration of the seismic station from seismic readings. The ground amplitude can be obtained as;

$$Ground\ amplitude\ (a) = \frac{A}{V(T)} \quad \ldots\ldots\ldots\ldots\ldots\ldots\ldots\ldots\ldots (5.2)$$

where, A = trace amplitude in mm, V(T) = the magnification at period T. A and T are obtained from a seismogram according to Fig. 5.1. The figure shows how to read amplitude

and periods of body waves from a seismogram.
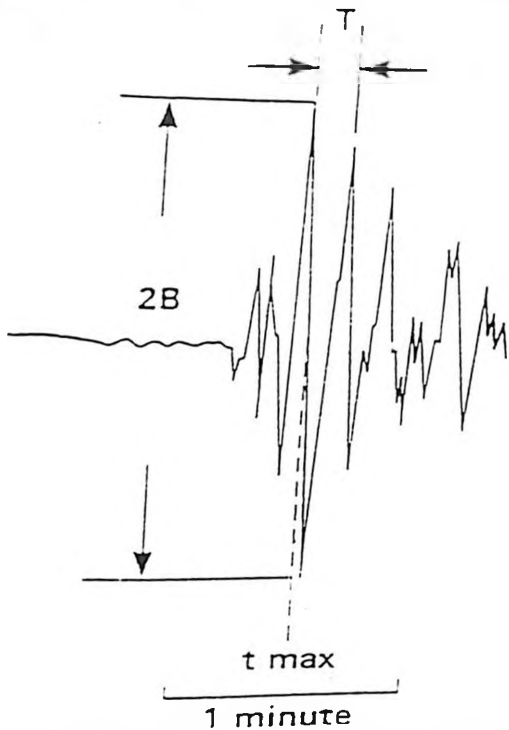
Figure (5.1) Reading amplitudes and periods of body waves from a seismogram

Log (A/T) denotes generally the first part of the magnitude formulation which accounts for the elastic wave intensity at the measuring site.

For part (b) tables are normally used while for part (c) the values are locally established for different regions.

5.2 The surface wave magnitude (M_{sz})

In order to extend the magnitude scale to large epicentral distances, the surface wave magnitude, applicable to shallow events was introduced. Here use is being made of the observation that surface wave with a period of about 20s are persistently recorded for large portion of earthquakes (Airy phase in the dispersion curve of the surface wave train) Willmore (1979). This produce large deflections on many long-period records. It suffers the disadvantage of being inapplicable to deep-focus events and from the fact that the smallest

and more numerous events are now being detected on records of short period vertical instruments. Determination based on body wave has thus gained importance (Båth 1969) The magnitude M_s is defined in equation 5.3.

Equation (5.3) below is known as the Moscow-Prague formula and applies for earthquakes with focal depths smaller than 50km and observed in distance range of 20^0-160^0. It was recommended (Båth, 1973) for general use during the 1967 Zurich General Assembly of the International Union of Geodesy and Geophysics (IUGG).

The Nairobi WWSSN station's M_{sz} is evaluated using this the Moscow-Prague formula;

$$M_{sz} = Log_{10} \frac{(1000*A)}{V_z*T} + 1.66 Log_{10}\Delta + 3.3 \dots\dots\dots\dots (5.3)$$

Where A is amplitude in mm, V_z is the magnification of the long period vertical component (LP_z). T is the period (between 10 and 25 sec). And Δ is distance in degrees.

5.3   Body wave magnitude (mb) .

In 1945 Gutenberg extended the magnitude determination also to the body waves (P,PP,S) and to earthquake of any depths. The equation below was employed;

$$mb = Log \frac{A(\Delta)}{T} + \sigma_b(\Delta, h) \dots\dots\dots\dots\dots (5.4)$$

This scale is based on the maximum ratio $(A(\Delta)/T)$ observed at the epicentral distance Δ, where $A(\Delta)$ denotes the maximum ground displacement amplitude in the respective phase

(P or S), in micrometers and T is the corresponding period in seconds. Short period

instruments with 1 sec. period are normally used for the determination of mb. The correction

function $\delta_b(\Delta, h)$ is obtained from the values in Fig. 5.2 below. Body wave magnitude (mb)

can be calculated for teleseismic events with distances $\geq 16^0$.
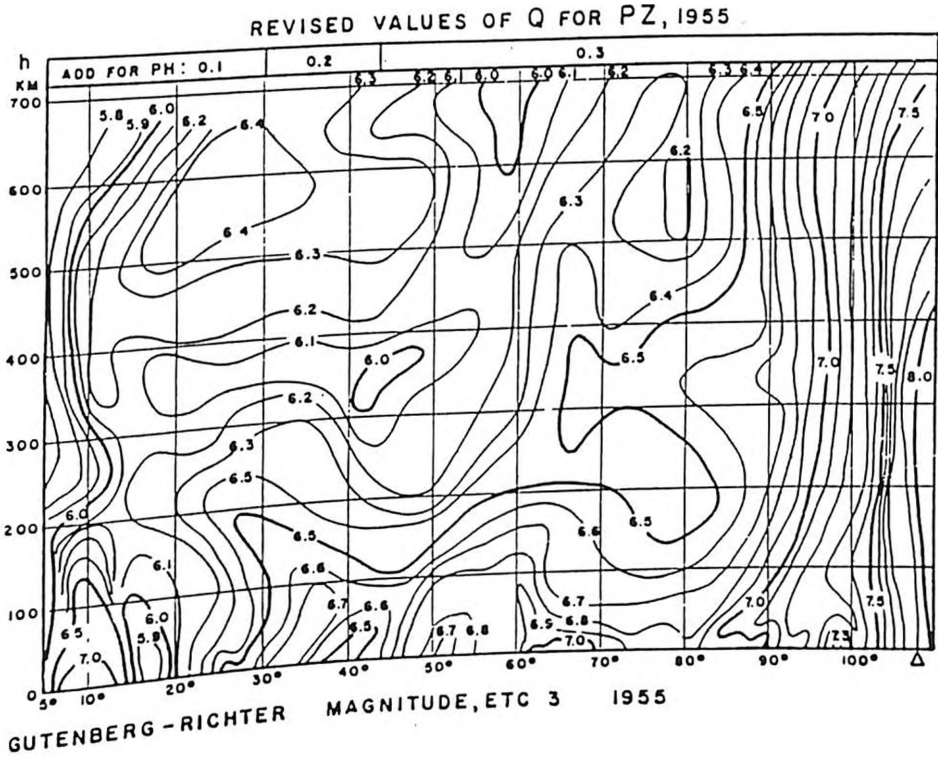
Figure 5.2 values of Q(Δ) for PZ (Gutenberg and Richter, 1956).

The following equation (5.5) is used to evaluate m_b in Nairobi WWSSN station:

$$m_b = Log\frac{(A*1000)}{V_z*T} + f(\Delta, h) \quad \dots\dots\dots\dots\dots\dots\dots\dots\dots\dots (5.5)$$

A is the amplitude of the body phase , T is its period (see Fig 5.1) and $V_{N,E}$ is the

magnification of the component used. The factor 1000 converts the mm reading into

micrometer finally. The correction value f is a function of the distance delta and source

depth h..

5.4 LOCAL MAGNITUDE (M_L) .

5.4.1 Richter's M_L definition.

Richter (1935) introduced the local magnitude (now called M_L) for southern California as the difference between the logarithm of the maximum trace amplitude and that of a calibrating event,

$$M_L = \log(A) - \log A_o(\Delta) \quad \dots\dots\dots\dots\dots\dots\dots\dots\dots\dots\dots (5.6)$$

Where, (Δ) = Distance to the epicentre.

The definition was given for a Wood-Anderson horizontal-component torsion seismometer with a maximum magnification = 2800, a free oscillation period = 0.8 and a damping ratio = 0.8 s. An earthquake of M_L = 3.0 gives an amplitude A_o of 1 mm at a distance 100 km. Richter (1935) found Log A_o as a function of distance Δ by studying several earthquakes in the region. The distance was limited to 600 km in his study.

5.4.2 Present Kenyan procedure

The above given magnitude-scale definition has several drawbacks when one tries to apply more generally. It is restricted to one region, with its special wave characteristics (absorption), to one instrument type and to a limited distance range. Recommendations on how to derive regional scales for other regions are given by many workers, e.g. Båth (1981) and Willmore, (1979). The present study does not intend to compute a regional scale as defined by Richter, but to correlate the existing M_L scale for Kenya with m_b given by ISC. It is recommended that a M_L concept should be derived following the Richter definition.

For Kenya and the existing network, the local magnitude (M_L) is computed for local earthquakes up to a distance of 1000 km as shown below.

The maximum amplitudes from peak to peak both short period horizontal components A_N and A_E are taken in mm to yield ground amplitude in mm which can be obtained from equation (5.7).,

$$a = [\frac{A_N}{V_N(T)} + \frac{A_E}{V_E(T)}] \frac{1}{2} \quad \dots \dots \dots \dots \dots \dots (5.7)$$

Where $V_{N,E}$ again denote the magnification.

If only one horizontal component is available we asssume AN = AE, i:e (from eq. 5.7)

$$a = \frac{A_N}{V_N} \quad \dots \dots \dots \dots \dots \dots \dots \dots (5.8)$$

The local magnitude is computed with formula (5.9) below.

$$M_L = Log(a*2800) + Log\mu_0 \dots \dots \dots \dots \dots \dots (5.9)$$

Log $\mu 0$ is read from table 5.1. A rapid way of getting the local magnitude is by use of the nomogram Fig (5.3). To use the figure, a straight-edge is set between the distance (S-P) interval on the left-hand scale, and the maximum trace amplitude on the right-hand scale and M_L is read where it crosses the centre scale.

TABLE 5.1 Distance dependent correction for local magnitude (-logμ0)

KM	-logμ0	KM	-logμ0
0	1.4	250-260	3.8
10	1.5	270-280	3.8
20	1.7	290-300	4.0
30	2.1	310-320	4.1
40	2.4	330-340	4.2
50	2.6	350-370	4.3
60-70	2.8	380-390	4.4
70-85	2.9	400-420	4.5
90	3.0	430-460	4.6
100	3.0	470-500	4.7
110-120	3.1	510-550	4.8
130-140	3.2	560-590	4.9
150-160	3.3	600	5.1
170-180	3.4	700	5.2
190-200	3.5	800	5.4
210	3.6	900	5.5
230	3.7	1000	5.7

Adopted from Richter 1958.
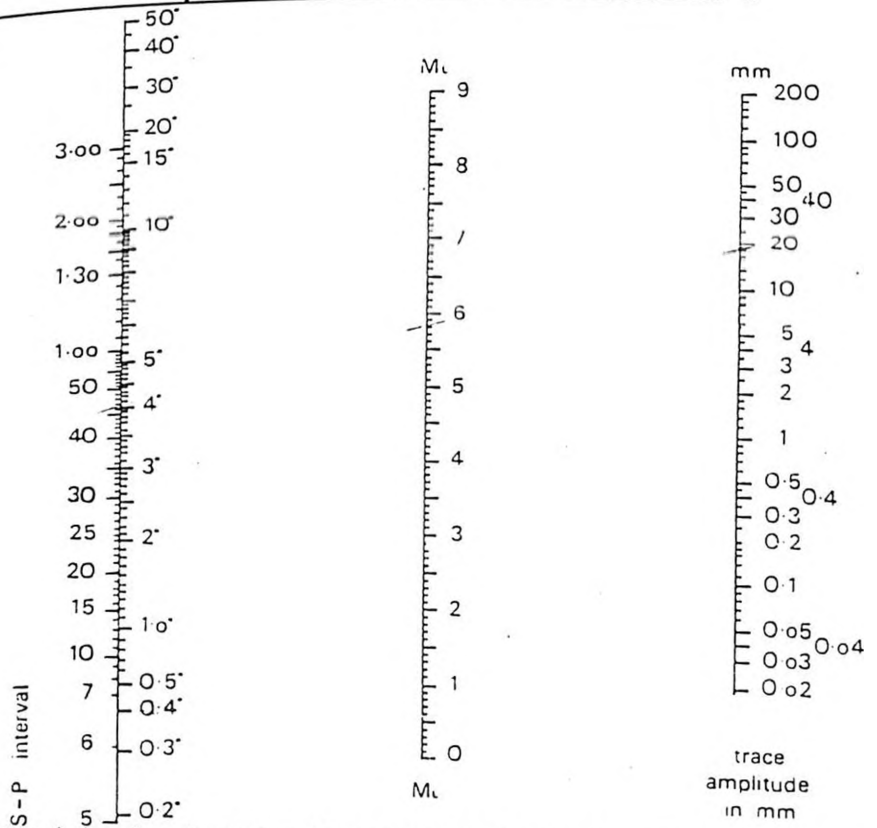
Figure (5.3) Nomogram for determining local earthquake magnitude (Ritchter, 1958, modified by Eiby and Muir, 1961)

Records from either short period seismographs can be used if the difference of magnification is allowed for (equation 5.9). For this purpose, a magnification curve for the standard Wood-Anderson instrument is neccessary. If the magnification of an available seismograph is plotted on this chart, the separation of the curves for earth motion of any given period will be a measure of the amplitude ratio expected on records taken by the two instruments Willmore (1979).

5.5   Duration Magnitude

Bisztricsany (1958) proposed the use of the duration of the surface-wave train for the determination of magnitude, and obtained the following formulae for Wiechert Seismographs at the Budapest station (Willmore, 1979)

(i) for shallow shocks ....(5.10)

$$MD = 2.72\log(F\text{-}eL) + 0.0065(\Delta) + 2.66$$

(ii) for deeper shocks ....(5.11)

$$MD = 1.58\log(F\text{-}eL) + 0.002(\Delta)\ 0.0007h + 4.02$$

Where F and eL are the end and commencement in minutes of the recorded surface waves, Δ is the epicentral distance in degrees and M is the magnitude determined at Praha station.

Eaton et al (1970) discussed some of the difficulties encountered when attempting to establish a suitable magnitude scale for a network of highly sensitive seismometers. The problems usually encountered are:

(i)   The difference in response characteristics between the Wood-Anderson seismometer (upon which the magnitude schemes is based) and the modern high sensitive short

period instruments.

(ii)   The difficulty in getting the resolution of high frequency coda of small earthquake into their component waves, and with this to attain the correct magnification for instruments with high-gradient amplitude response in the period domain of interest.

(iii)   The fact that large lateral variations in attenuation and elastic properties of the crust may produce significantly different signals at different stations.

(iv)   The often only moderately sized earthquakes will produce saturation of the amplification of recording equipment, as a result of the practical limitation of dynamic range. This can also happen at some distances.

(v)   The problem that the fault dip orientation of the same fault relative to the station affects the wave magnitude.

After analysing these problems in using amplitude data for the standard method of local magnitude determination (Richter, 1935), it was decided to use the signal duration as a way of obtaining the local mgnitude (Eaton et al, 1970; Lee et al, 1972; Crosson, 1972; Real and Teng, 1973). The method consists of establishing a magnitude scale based on the relation between the coda length and conventionally defined magnitudes. Thus the method has been adopted recently at many seismological stations with their own definition of the duration time and the empirical magnitude formula. The method is convenient for local shocks in determining the magnitude without requiring an exact knowledge of epicentral distance (Willmore, 1979). Wahlström (1980) and others have found the dependance on the distance to be almost negligible.

Kenya is at times hit by local earthquakes whose local magnitudes cannot be defined because the seismograms get saturated and therefore duration magnitude can be the only

solution for a such a case. In the Nairobi WWSSN-station, the duration coda is defined as the time interval from the onset of the first p- arrival to the point at which the earthquake signals falls to just twice the noise level for the first time. The duration magnitude is obtained using the equation;

$$Fmag = -0.87 + 2 \log (F - P) + 0.0035 (\Delta) \dots\dots\dots\dots\dots\dots (5.12) \text{ (Willmore, 1979)}$$

Where, $(F - P)$ = Duration time, (Δ) = Distance

In the present work, the duration of coda was defined as the time interval from the onset of the first P - arrival to the point at which the earthquake signal does not fall to twice the noise level for the first time (this was also adopted by Shah, 1986). From the previous work, the duration time of the same earthquake has been found to vary from reader to the other in the order of a few seconds (Wahlström, 1980). Therefore the uncertainity of getting correct duration time cannot be ruled out since the reading was done by one person and may be subjective. On the other hand the consistency of the definition if maintained then the magnitudes should be the same but the problem should arise if the reader A and B do the reading alternately then their definitions are bound to differ, hence the magnitude values.

The equation (5.12) above is used to evaluate the duration magnitude from Nairobi WWSSN station and the values are higher than the local magnitude hence the need for correction.

A graph of duration magnitude was plotted against the local magnitude M_L (see Fig. 5.4 below) and it can be seen that the duration magnitude was higher than the M_{LNA} and hence requires correction. Preliminary corrections are listed below. The correction of duration magnitudes to unified local magnitude could not be done because of the fear of high errors

that could be involved.

$$MD = -0.87 + 2 * \log10(TD) + 0.0035 * Delta$$
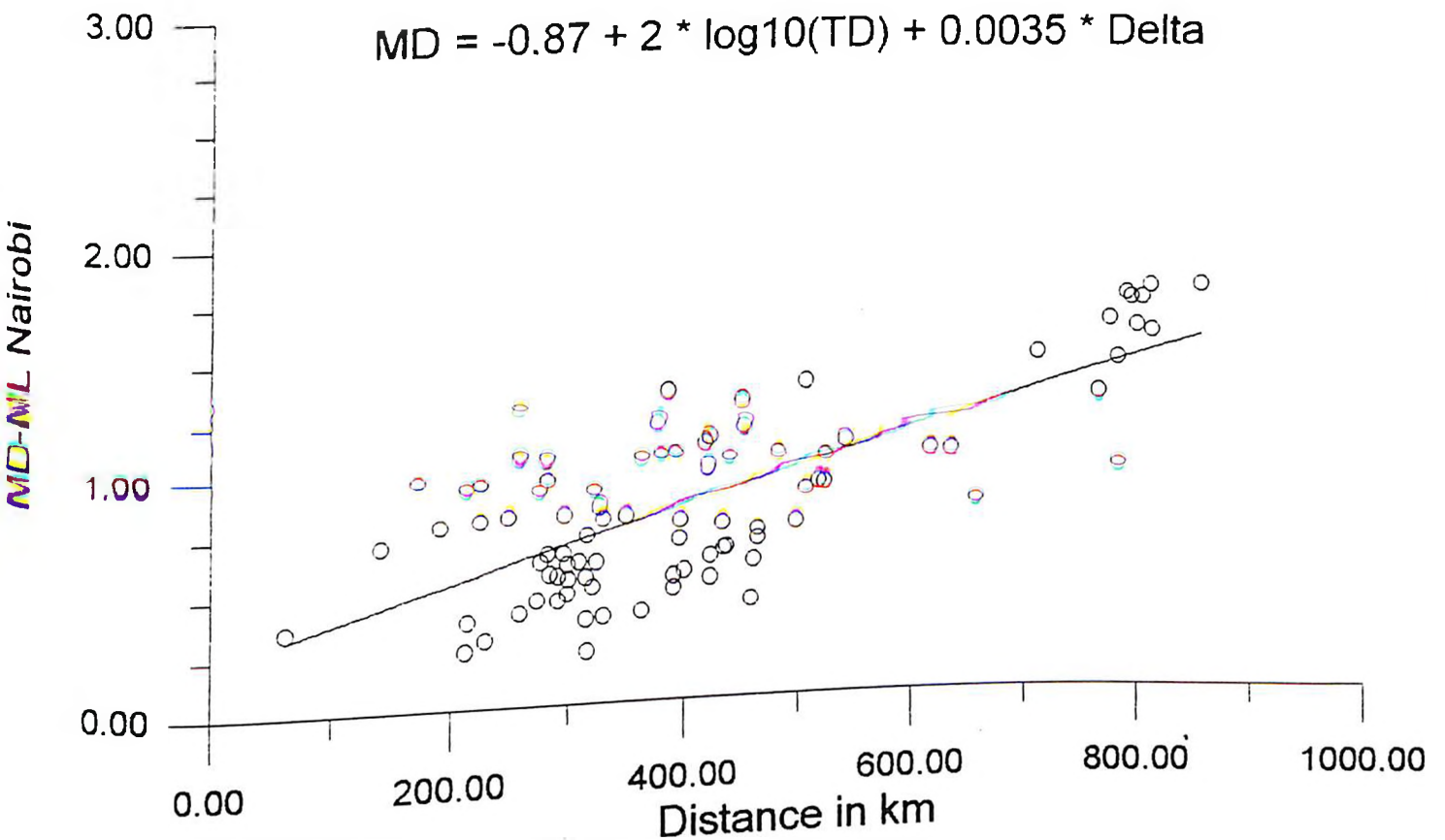
Figure 5.4 Plot of MD - M_L against the epicentral distance.

5.6 Unification of magnitudes.

The availability of a reliable scale is important in studying the seismic risk caused by earthquakes. As per now, the determination of magnitude is still subject to discussion and several different magnitude scales are in current use (Shah, 1986). With the same earthquake in question, magnitude calculated by different stations may differ appreciably. In infact the difference in the magnitude is admirable, being significant and consistent from various stations which assume the same scale.

Båth (1981), Chung and Bernreuter (1981) and Shah (1986) gave a review on assignment

of magnitudes. In any study, it is also necessary to specify clearly which magnitude is used since relations are often magnitude dependent.

In order to unify magnitudes the Nairobi local and duration magnitudes were calculated using the formula 5.12 and 5.6 respectively. The local magnitude of Nairobi (M_{LNAI}) was compared with that of m_{bISC}. The Nairobi local magnitude was corrected to the m_{bISC} by making a plot of m_{bISC} against the M_{LNAI} and a least square fit was obtained. The Fig. (5.4) below shows the obtained plot.

A plot af mb [ISC] against ML [NAI]
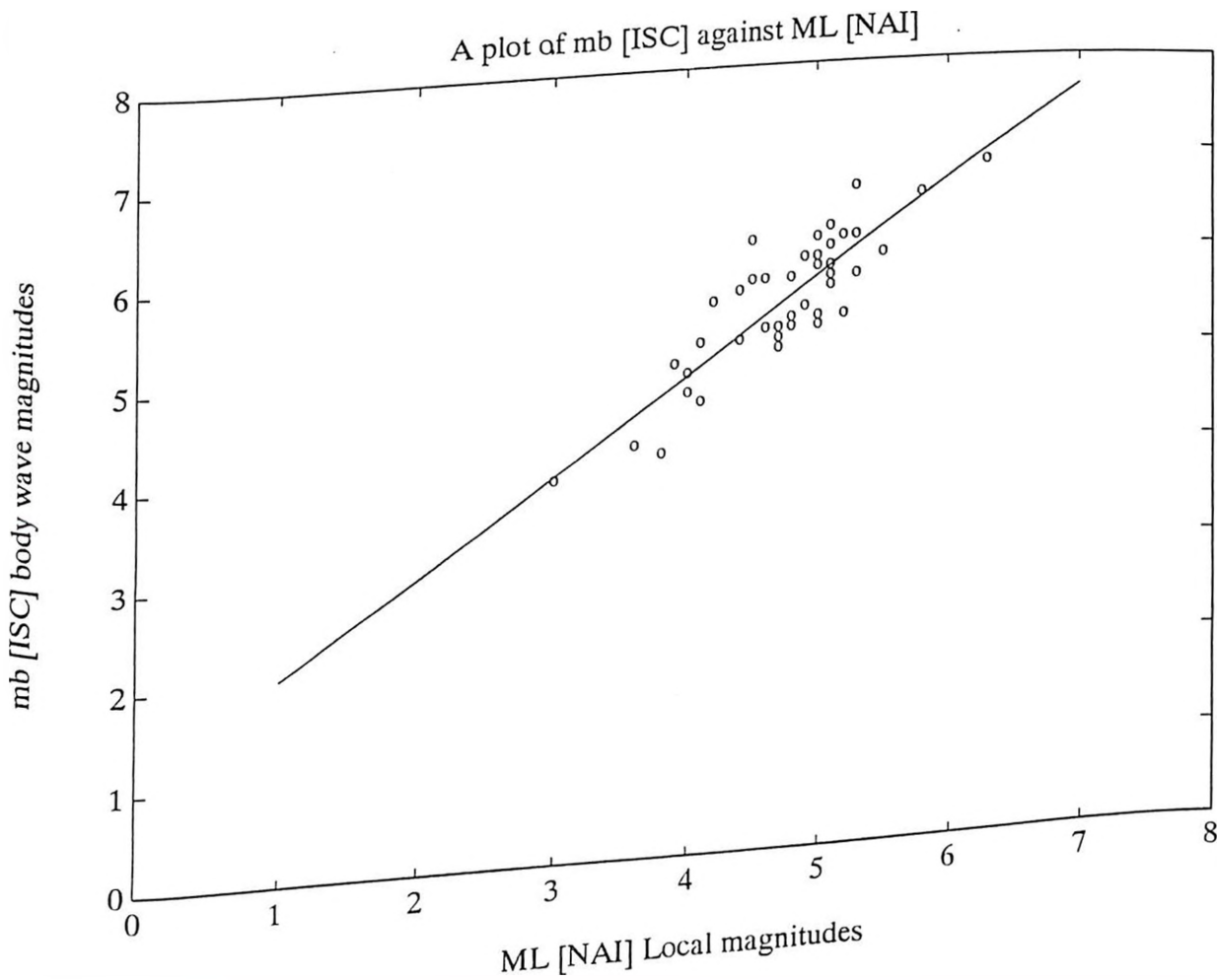
Figure (5.4) plot of m_{bISC} against the M_{LNAI} magnitudes.

The plot gave the following least square fit;

$$mb_{(ISC)} = 0.7837 \pm 0.03 ML_{(NAI)} + 0.3905 \pm 0.01 \ldots \ldots \ldots \ldots$$

The ML_{NAI} was then corrected to the mb_{ISC} to get the unification magnitude which was included in the Appendix I.

CHAPTER SIX

DISCUSSIONS AND CONCLUSIONS

6.1 DISCUSSIONS

6.1.1 Pn and Sn propagation and the structure of the upper mantle

Pn and Sn travel through the uppermost part of the mantle, and their frequency and amplitudes are strongly affected by structural irregularities along the path (Rodrigues, 1970). This effect is more pronounced for Sn than Pn. This is due to the fact that Pn has high velocity and is able to propagate through deeper portions of the mantle thus eliminating to some extent the constraining effects of anomalous condition that may be present in the less dense portions of the mantle (Rodrigues, 1970). Sn being a shear wave is very much affected by departures from the ideal elastic body.

From this study it was seen that at distances up to 300-320 km Sn is clearly distinguished and becomes almost non existent between 400-600 km, while further on it is more easily recognized again. This is in agreement with the findings of Dopp (1964) and Rodrigues (1970).

The Pn velocities have been found to be strikingly higher for profiles on the flanks of the Rift Valley of about 8.0-8.27 km/s while Sn velocities are in the range of 4.68-4.77 km/s comparable to the velocities obtained on the Rift Valley flanks by the refraction seismic results. The rift zones showed velocity of 7.93 km/s.

There was a big discrepancy from the results of the rift valley in Kenya and those of Tanzania as is exemplified on profile 5 (Tanzania rift valley) and the KRISP90 for Kenyan rift valley. This Profile 5 extends towards the southern part of Kenya connecting with the northern part of Tanzania as already mentioned in section 3.4.1. The greater length of this profile is within the rift valley, although the term "rift" cannot really be used to describe tectonic structure in Tanzania (Rodrigues, 1970). Mantle velocities of 8.06 km/s for Pn and Sn of 4.66 km/s with a Moho depth of 29 km were obtained. These results agrees well with those of the KRISP90 except that the velocities for the Pn are higher than the 7.5 km/s obtained in the rift valley by KRISP90 experiments. Therefore it might be unlikely that the same lower velocities will be obtained in Tanzanian rift when KRISP extends its study in Tanzania. The reasons for this discrepancies could be that the low velocities in the mantle obtained by KRISP90 are only for a narrow zone in the rift valley but since it is difficult to define the rift valley 'proper' in Tanzania, then most of this events fall out of this narrow rift zone. Alternatively the intrusion of mafic material could be the source of this high velocities in Tanzanian rift.

It was of interest to compare the Poisson ratio deduced from the natural-earthquake data of the Tanzanian rift and those of seismic data from the KRISP experiments. Using the velocities 7.5 km/s and 4.5 km/s for KRISP90 (KRISP WORKING GROUP, 1991). The relation below was used (Rodrigues, 1970);

$$\frac{(V_p)^2}{(V_s)^2} = \frac{2(1-\delta)}{(1-2\delta)} \quad \dots\dots\dots\dots\dots\dots\dots\dots\dots\dots\dots\dots\dots\dots\dots\dots (6.1)$$

The value of the Poisson ratio, ∂ from the above earthquake data is 0.2489 and that of the refraction data is 0.2187. A value from the natural earthquake data is in agreement with that

obtained from other parts of world (usually the ideal value is taken to be equal to 0.25). But the refraction results were restricted to the Rift Valley which has been found to have an anomalous low Pn velocity unlike the Pn for this study which takes a profile that falls in rift zone which is not well defined. Therefore possibly, most of these events fall out of the rift zone as already explained above.

6.1.2 Pg and Sg propagation in the crust

The results have clearly shown that the Kenyan crust is typified by crustal velocities of 6.22-6.38 km/s and 3.62-3.67 km/s for Pg and Sg respectively. This is comparable with velocities of 6.1-6.3 km/s from individual earthquake study obtained by Rodrigues (1970) for the East African crust and 5.9-6.2 km/s for the KRISP90 refraction experiments and S of 3.62-3.64 km/s. while the lower crustal velocities are in the range of 6.6-6.8 km/s and 3.78-3.85 km/s for P and S respectively. These are averages velocities obtained by the refraction experiments KRISP90.

6.1.3 Implication of velocities and seismic wave character to the Geology

The time delay of seismic waves can be expounded by many reasons. In a tectonically disturbed region, the distinction between the crust and the mantle is not clear leading to the problem that has been referred to as the " Crust-mantle mix " (Rodrigues, 1970). The possibility of referring to it as anomalous basal crust or abnormal upper mantle can not be ruled out (Rodrigues, 1970). Loss of energy occurs at such planes and the other likely reason is the effect of high temperatures relatively lower the velocities and this could be due the molten mantle material (KRISP WORKING GROUP, 1991).

Previous studies done in parts of East Africa have shown the same time delay. Rodrigues (1970) observed the time delay of the teleseismic events recorded at the Nairobi station. Dahlheim et al (1989) and Green et al (1991) studies showed that teleseismic data produced evidence of high lower crustal velocities in the upper mantle depths of 20 km and the were indications of axial variability above 60 km. The KRISP85 data showed a thinned (30-35 km) but typical continental crust beneath the Rift and considerable relief observed on the basement surface could account for a significant portion of local gravity and teleseismic delay time anomalies KRISP WORKING GROUP (1987); Henry et al. (1990). In other previous workings (e.g Baker and Wohlenberg, 1971; Savage and Long, 1985) stated that a broad axial dike of mafic material rising nearly to the surface was the model preferred for explaining gravity and teleseismic delay time anomalies. Axial variability in crustal structure which could affect the interpretation of the gravity and teleseismic data was also indicated.

6.2 Crustal structure in Kenya

Crustal structure has been determined from earthquake body wave analysis. The results have shown that the crustal structure in Kenya is not constant. The rift system has a thin crust of about 30 km, while the flanks of the rift are thicker, being in a range of 35-39 km thick. The intermediate crustal thickness is between 10 and 15 km. The crustal thickness around Lake Victoria has been found to be 39 km and the crustal thickness on the profile extending to the coastal region through the Chyulu hills has been found to be thicker. The unified model reflected an average crustal thickness of 33 km. It was observed that this model cannot be used as an average model for the whole Kenyan crust. Some profiles are not as well localised with this model as others. This model is good for localisation of earthquakes from Lake Victoria-

Homa Bay area and those from northeastern part of Tanzania and southern part of Kenya because it is biased by dataset since most of the profiles contributing events for this model are from these areas.

6.3   CONCLUSIONS

This study shows that the area in the western part of Kenya and extending towards the Western Rift Valley and covering a small part the Eastern Rift, depicts average velocities of 6.31 km/s and 3.63 km/s for Pg and Sg wave velocities respectively. This values are in good agreement with the previous earthquake and refraction studies from thess areas. The upper mantle velocities are about 8.03 km/s and 4.72 km/s for Pn and Sn respectively. The intermediate crustal thickness is about 15 km and a total crustal thickness of 37 km. The region extending to Lake Victoria centered at NAI-Station has crustal velocities of 6.27 km/s and 3.63 km/s for Pg and Sg respectively. The average intermediate crustal thickness of 15 km and an average total crustal thickness of 39 km. The southwestern part of Kenya and the northern part of Tanzania has crustal velocities of 6.34 km/s and 3.64 km/s for Pg and Sg respectively. The intermediate crustal thickness is about 15 km and total crustal thickness of 37 km. The northern part of Tanzania (an area presumably lying in the Tanzanian Rift Valley) has crustal velocities of 6.38 km/s and 3.67 km/s for Pg and Sg respectively and the upper mantle velocities of 8.06 km/s and 4.66 km/s. The intermediate crustal thickness is about 15 km and Moho depth of 29 km. The area extending towards the coastal region of Kenya passing through the Chyulu hills has an upper mantle velocities of 6.41 km/s and 3.67 km/s for Pg and Sg respectively. The eastern part of Kenya has crustal velocities of 6.28 km/s and 3.66 km/s for Pg and Sg respectively. The northwest part of Kenya extending towards Lake Turkana (this is in the Kenyan rift valley) has

an upper mantle velocity of 7.93 km/s for Pn. The average crustal velocities as per the results of the unified dataset is about 6.35 km/s and 3.65 km/s for Pg and Sg respectively. The upper mantle velocities are 8.12 km/s and 4.68 km/s for Pn and Sn. The intermediate crustal thickness is about 15 km while the total crustal thickness is about 33 km. The Tanzanian rift valley has velocities of 8.06 km/s unlike the low anomalous velocities of 7.5 km/s of Pn for the Kenyan rift as per the results of the KRISP90 seismic refraction experiments. Therefore it might be unlikely that the same low velocities will be obtained when this seismic study is extended to Tanzanian rift. These results are summarised in Fig.4.7 in section 4.1.

In summary, the results from section 4.3 has shown that localisations of the earthquakes in Kenya can not be done by one model hence regionalisation of seismic velocities is necessary. The Finnish velocity depth model can be used to locate events from profile 6 which extends towards the coastal region through the Chyulu hills. The localisations from this profile are on average close to those of ISC when this model is used. This implies that the crust is thicker about 40 km on this profile. While the other parts of Kenyan crust is much thinner than 40 km which the Finnish velocity depth model assumes therefore the earthquakes will be mislocated by this model. The western part of Kenya extending towards the western rift valley can be located by the modified EAF model. The events from the eastern rift valley can be located by the modified NAI-EAST model as well as those from profile 3 (especially Homa Bay area). The area in the southern Kenya extending towards Tanzania will be located with models from profiles 4 and 5. The details of this results are represented in Fig. 4.9 in section 4.3. The unified model is biased by the dataset thus only being useful for the regions towards Lake Victoria and southern part of Kenya extending into Tanzania. This model cannot be used as an average model of Kenya. This study recommends that the data from KRISP94 should be used to

improve these velocity depth models in order to minimise the mislocation of earthquakes from different parts of Kenya.

The study on the local magnitudes and body wave magnitude from ISC shows that the Nairobi local magnitude (ML_{NAI}) are higher than the ISC body wave magnitudes (mb_{ISC}) in the order of 0.6-0.7 units on Richter scale. There is therefore need for the correction of these local magnitude scale following the normal procedures of the Richter's way of calibration of magnitudes and the duration magnitude should then be corrected to this corrected local magnitude scale.

REFERENCES

Ambrasseys, N.N., 1972. The seismicity of stiegler's gorge, 'Tanzania, Unpublished report for NOROCONSULTS, A.S., 126pp.

Baker, B.H. and Wohlenberg, J., 1971. Structure and evolution of the Kenya Rift Valley. NATURE, Vol. 229:538.

Båth, M., 1966. Earthquake energy and magnitude Phys. Chem. Earth., 7:117.

Båth, M., 1967. Observations of teleseismic Pn phases. Pure Appl. Geophys., (PAGEOPH), 66 30-36.

Båth, M., 1969. Handbook on earthquake Magnitude determinations, VESIAL. Sp. Rep. 77885-36 -X, 2 ed, 158pp.

Båth, M., 1973. INTRODUCTION TO SEISMOLOGY. Birkhauser, 395pp.

Båth, M., 1975. Seismicity of Tanzania region. Tectonophysics, 27:353.

Båth, M., 1979a. INTRODUCTION TO SEISMOLOGY. Birkhauser 2 ed., 428 pp.

Båth, M., 1981. Earthquake magnitude - recent research and current trends. Earth. Scu. Rev., 17:315.

Birch. F., 1960. Compressional waves velocities in rocks down to 10 kilobars, part 1 Journal 6 Geophy. Res., 65, 1083-1102.

Bisztricsany, E., 1958. A new method for the determination of magnitude of earthquake. Geofiziki Kotcleményck, VII:69.

Bonjer, K.P., K.Fuchs and J. Wohlenberg , 1970. Crustal structures of the East African Rift System from spectral response ratios of long period body waves. Z. Geophysik, 36, 287-287 pp.

Bullen, K.E. and Bolt, B.A. 1985. An introduction to the theory of seismology. Cambridge University Press, Fourth edition, 499pp.

Bungum, H., and Ringdal, F., 1982. Turkwell gorge multipurpose project. Further seismological investigation. Unpublished report for NORAD.

Bungum, H., and Nnko, A.A., 1984. Seismicity and Tectonics of the Stiegler's Gorge Area, Tanzania. J. Geophy. Res. 89, 1874-1888pp.

Chung, D.H. and Bernreuter, D,L., 1981. Regional relationships among earthquake magnitude scales. Rev. Geophys. Space Phys., Vol, 19:649.

Christensen N. L. 1979. Compressional wave velocities in rocks at high temperatures and pressures, critical thermal gradienst and crustal low velocity zones. Journal of Geophys. Res. 84, 6849-6857

Crosson, R.S., 1972. Small earthquakes, structure and tectonic of Pugent Sound region. Bull. Seism. Soc. Am., 82:1133.

Dahlheim, H.A., Davies, p. and Achauer, V., 1989. Teleseismic investigation of the East African rift Kenya. Journal of Africa Earth sci. 8, 461-470.

De Bremaecker, J. Cl., 1959. Seismicity of the West African Rift Valley. J Geophys. Res., 64:1961.

Dopp, S. 1964. Preliminary Note on a refracted P phase in the Western Rift Valley of Africa.

Eaton, J.P., O'Nell, M.E. and Murdock, J.N., 1970. Aftershocks of the 1966 Parkfield-Cholame, California, earthquake. A detailed study. Bull. Seism. Soc. Am., 60:1151.

Fairhead, J.D., 1968. The seismicity of the East African rift system 1955 to 1968. M.sc. Dissertation, University of New Castle Upon Tyne.

Fairhead, J.D. and Girdler, R.W., 1971. The seismicity of Africa. Geophys. J.R. Astr. Soc., 24:271.

G'D souza 1968. Structural sketch map of part of the rift zone of Eastern Africa. Printed by the East African press Ltd. Nairobi Kenya.

Gervev, M. and Markushevich, V., 1966. Determination of a seismic wave velocity from the travel time curve, Geophys. J. R. Astron. Soc., 11, 165-173,.

Girdler, R.W., (ed), 1972. East African Rifts. Tectonophysics, 15:1.

Gorshkov, G.P., 1961. Seismicity of Africa. UNESCO publ. provisional NS/NR/2. Add. I, Paris.

Gouin, P., 1979. Earthquake History of Ethiopia and the Horn of Africa. Ottawa, Ont., IDRC, 259pp.

Gumper, F. and P.W. Pomeroy, 1970. Seismic wave velocities and earth structures on the African continent. Bull. Seism. Soc. Am. 60, 651-668 pp.

Gutenberg, B. and Richter, C.F., 1942. Earthquake magnitude, intensity, energy and acceleration. Bull. Seism. Soc. Am., 32:163.

Gutenberg, B., 1944. Travel times of principal P and S waves over small distances in Southern California. Bull. Seism. Soc. Am., Vol. 34 pp 13-32.

Gutenberg, B. and Richter, C.F., 1954. SEISMICITY of the EARTH. Princeton. University press, 2 ed., 310 pp.

Gutenberg, B. and Richter, C.F., 1956. Magnitude and energy of earthquakes. Ann. Geofis.,9:1

Green, V.W., Achauer, U. and Meyer, R.P. 1991. A three dimensional seismic image of the crust and upper mantle beneath the Kenya rift. Nature, 354: 199-203

Hamilton, R.M., Smith, B.E. and Knapp, F., 1973. Earthquakes in geothermal areas near lake Naivasha and Hannington, Kenya. Unpublished report.

Havskov and Utheim (1992). SEISLOG and SEISAN: A complete system for seismic acquisition and analysis. Cashier du Centre European de Geodynamique et de Seismologie, Vol.5, 67-74.

Henry W.J., Mechiie, J., Maguire, R.K.H., Khan, M.A., Prodehl, C., Keller, G.R., and Patel, J., 1990. A seismic investigation of the Kenya rift valley. Geophys. J. Inst., 100: 107-130.

Jeffreys, H. and Bullen, K.E., 1958. Seismological tables British Assoc. Adv. Science, 50pp.

Kataka, M.O. and Stangl, R. 1994. Special departmental report University of Nairobi (unpublished).

KRISP Working Group, 1987. Structure of the Kenya rift from seismic refraction. Nature 325 (no. 6101): 239-242.

KRISP Working Group, 1991. Large Scale variation in lithospheric structure along and across the Kenya Rift. Nature, 354: 223-227.

Krenkel, E., 1921. Die Erdbeben Ostafrikas, Centralbatt fur Mineralogie, Geologie und Palaontologie. Stuttgart, no 23:705.

Kulhánek, O., 1990. ANATOMY OF SEISMOGRAMS, Elsevier science publishing company.

Lahr, J. C and Pomeroy, P. W., 1970. The foreshock - aftershock sequence of march 20 1966 earthquake in the republic of Congo Proc. Sym. II, XXII Inst. Geol. Congr., 19:87.

Lee, W.H.K and Lahr, J.C., 1971. HYPO71: A computer program for determining hypocentre magnitude and first motion pattern of local earthquakes. U.S. Geological survey. Open file report.

Lee, W.H.K., Bennet, R.E and Meager, K.L., 1972. A method of estimating magnitude of local earthquakes from signal duration U.S. Geol. Survey, Open file report.

Lienert, B., Berg, R.E., and Fraser, L.N., 1988. Hypocenter: an earthquake location method using centred scaled, and adaptively damped least squares, Bull. Seism. Soc. Am. 76, 771-783.

Loupekine, I.S. and Wohlenberg, J., 1966. The Toro earthquake of 20 March 1966. UNESCO, Paris 80pp.

Lomax ,A., 1989. User manual for SeisGram, in "Digital Seismogram Analysis and Waveform Inversion", Editor W.H.K Lee, IASPEI Software Library Vol., 2 IASPEI $ SSA, El Cerito, 13.75.

Loupekine, I.S., 1971. A catalogue of felt earthquakes in Kenya 1892 - 1969. Seismological unit. Geology Dept. University of Nairobi. Unpublished report, 129pp.

Maasha, N., 1975. The seismicity and tectonics of Uganda. Tectonophysics, 27:381.

Molnar, P. Fitch, J. and Asfaw, L.M., 1970. A microearthquake survey in Ethiopian rift. E.S.S.A., Earthquake notes, 41 (2):37

Molnar and Aggarwal, 1971. A microearthquake survey in Kenya. Bull. Seism. Soc. Am., 61:195.

Morgan, P. 1982. International Continental and Oceanic Rifts (ed.Paimasong) Am. Geophys. UnGeody Ser 8, 107-122s

Olang, O., 1992. Seismicity and Tectonics of Kenya. M.sc thesis, University of Nairobi.

Real, C.R. and Teng, T.I., 1973. Local Richter magnitude and total signal duration in southern California. Bull. Seism. Soc. Am. 63:1809.

Richter, C.F., 1935. Instrumental earthquake magnitude scale IBID., 25:1.

Rodrigues, E.D., 1970. Seismological studies of the east African rift system. ph.D. thesis University college, Nairobi.

Rothé, J.P., 1954. La Zone Sismique Médiane Indo-Atlantique Proc. Roy. Soc. (England), A222 London.

Rykounov, L.N., Sedov, V.V., Saurina, L.A. and Bourmin, V. Ju., 1972. Study of microearthquake in the rift zones of East Africa. Tectonophysics, 151:123.

Scholz, C.A., Rosendahl, B.R., Versfelt, J.W. and Rach, N., 1990. Results of high resolution echo sounding of Lake Victoria. J.Afr. Earth Sc., 11: 25-35.

Shah, E.R., 1986. The seismicity of Kenya. Procedure for compilation of the map. Seismol. Inst. Uppsala Tech. Report.

Shah, E.R., 1986. The Seismicity of Kenya. ph.D thesis. University of Nairobi.

Seiberg, A. 1904. Handbuch der Erdbebenkunde Vieweg, Braunschweig.

Seiberg, A., 1923. Erdbebenkunde Seismischtektonishe Übersichtskarte der Welt. Berlin, Geologische Physikalische Und angewandte Erdbenkunde. Mit Beiträgen Von. Dr. Beno Gutenberg, 101pp.

Stangl, R., 1984. EPIDIST program for azimuth and epicentral distance calculation (Unpublished).

Stangl, R., 1986. TRAVTIME program for travel time calculation, University of Kalshruhe (unpublished).

Stangl, R., 1992. TRAVTAB program for making travel time tables (unpublished).

Suhadoc, P., 1978. Total duration and local magnitude for small shocks in Friulli, Italy. Bull. Geof. Teo. Appl. 20:203.

Suteau, A.M. and Whitcomb. J.H., 1979. A local earthquake coda magnitude and its relation to duration moment Mo., and local Richter magnitude, ML. Bull. Seismol, Soc. Am. 69:353.

Sutton, G.H. and Berg. E., 1958. Seismological studies of the Western rift valley of Africa. Trans. Am. Geophys. Union, 39:474.

Sykes, L.R., and Landisman, M., 1964. The Seismicity of East Africa, the gulf of Aden and the Arabian and Red Seas. Bull. Seism. Soc. Am., 54:1927.

Tongue, J., Maguire, P.K.H., and Young, P.A.V., 1992. Seismicity distribution from temporary recording networks in Kenya. In: R. Altherr (Editor), The Afro-Arabian Rift System. Tectonophysics, 204 (spec. sect.): 71-79.

Wadati, K., 1931. Shallow and deep earthquakes (3rd paper). Geophysical mag., 1, 162-202 pp.

Wahlström, R., 1980. Duration magnitude for Swedish earthquakes. Geophysica (Helsinki) 16:171

Willmore, P.L (ed) 1979. Manual of Seismological Observatory Practice. "World Data Centre A, Rep. Se-205, 166pp.

Wohlenberg, J., 1968. Untersuchungen der Erdbebentätigkeit der Ostafrikanischen Grabenzonen. Africa, Henke, 21:319.

Wohlenberg, J., 1969. Remarks on the seismicity of East Africa between 4^0 N - 12^0 S and 23^0 E -40^0 E. Tectonophysics, 6:567

Wohlenberg, J., 1970. On the seismicity of the East African Rift System. Inst.Upper mantle Proj., Sci. Rep. 27:290.

Young, P.A.V., Maguire, P.K.H., Laffolet, N.d'A. and Evans, J.R., 1991. Implications of the distribution of seismicity near Lake Bogoria in Kenya rift. J.R. Astron. Soc., 105: 665-674.

APPENDIX I

XII FORMAT NOTATIONS

The format of the listing is as follows:

Column 1   MONTH, DATE and YEAR.

Column 2   ORIGIN TIME in hours, minutes and seconds.

Column 3   EPICENTRAL COORDINATES (Latitude and Longitude)

Column 4   AZIMUTH

Column 5   DISTANCE

Column 6   LOCAL MAGNITUDE OF NAIROBI

Column 7   TYPE

Column 8   BODY WAVE MAGNITUDE and LOCAL MAGNITUDES FROM ISC

Column 9   AGENCY TYPE

Column 10   FOCAL DEPTH, generally instrumental depth. The depth is given in kilometres.

Column 11   UNIFIED MAGNITUDE from Nairobi local magnitudes to ISC corrected magnitudes.

Column 12   Calculated DURATION MAGNITUDES OF NAIROBI

XIII   Notation used in the Appendix and the text

ISC   International Seismological Centre.

ISS	British Association Seismological Bulletins and International Seismological Summary.
BUL.	Zimbabwe / Rhodesia Meteorological Service Seismological Bulletin, Bulawayo.
UmbN.	Unified body magnitude
mb	Body wave magnitude
ML	Local magnitude
DIST.	Epicentral distance.
DEP	Depth in km
MD	Duration magnitude
AGMAG	Agency magnitude

Date:	EVT_TIME	LAT	LONG	AZIM	DIST	MAG	TYP	AG
03/05/64	105700.0	-3.400	35.000	220	309	0.0	ML	
05/07/64	054531.9	-3.880	35.060	213	348	4.9	ML	
04/28/65	123926.0	4.000	35.500	346	604	4.9	ML	
01/01/66	131351.0	-5.000	35.000	205	459	5.2	ML	
01/30/66	204130.6	-3.860	36.000	197	363	0.0	ML	
08/01/66	180639.0	1.000	31.000	0		0.0		
02/10/66	095450.0	-3.930	35.700	202	319	4.8	ML	
02/15/66	013047.9	-4.000	38.000	156	330	4.8	ML	
02/22/66	195834.8	-4.000	38.000	156	225	4.2	ML	
02/25/66	234816.0	-4.500	35.400	203	391	4.2	ML	
02/25/66	234816.4	-4.500	35.400	0	391	4.2	ML	
03/01/66	204130.6	-4.000	35.000	213	363	4.2	ML	
03/09/66	031247.6	2.270	31.420	0		0.0		
03/21/66	092349.9	0.840	30.000	287	790	6.2	ML	
03/21/66	092349.9	0.800	29.810	0	792	0.0		
03/21/66	094349.9	0.580	29.930	0	792	0.0		
03/21/66	013038.0	0.800	29.810	0	811	4.7	ML	
03/25/66	215808.0	-0.300	30.100	0		0.0		
04/01/66	075940.0	0.600	29.500	0		0.0		
04/07/66	000910.7	0.580	29.930	284	791	5.3	ML	
04/07/66	105127.0	-4.000	35.240	0		0.0		
04/11/66	101227.0	-4.860	29.900	242	437	5.9	ML	
04/13/66	021600.0	0.990	30.070	288	790	6.0	ML	
04/15/66	030815.5	0.770	29.980	286	792	6.0	ML	
04/16/66	144317.8	0.760	29.860	286	796	6.3	ML	
04/16/66	013059.0	-4.700	34.700	0		0.0		
04/26/66	084026.0	-4.700	41.400	126	636	5.2	ML	
04/30/66	203847.9	0.730	29.830	285	806	5.4	ML	
05/10/66	215328.0	1.600	31.100	0		0.0		
06/14/66	123744.0	0.000	31.000	0		0.0		
06/14/66	235052	0.000	31.000	0		0.0		
06/22/66	054605	0.000	31.000	0		0.0		
07/10/66	235435.1	-3.540	35.350	212	299	4.3	ML	
07/14/66	043447.7	0.600	29.900	285	796	5.7	ML	
07/15/66	221407.3	-4.000	35.000	213	315	4.4	ML	
07/21/66	083153	-3.900	35.530	0		0.0		

GMAG	TYPE	DEP	UmbN	MD
0.0	mb		·	5.5
6.3	mb	49	5.8	4.7
5.1	mb		4.2	
0.0	mb		4.4	5.7
4.4	ML			
0.0				
0.0	mb	00	4.1	4.6
3.6	ML		4.1	5.3
3.7	ML		4.1	4.6
3.5	ML			
3.5	mb		3.7	4.6
3.6	ML		3.7	4.6
5.4	mb	06	5.3	7.6
5.0	mb			
5.3	mb			
0.0				
5.3	mb	01	4.1	4.7
4.3	mb		3.7	4.5
0.0				
4.8	mb	33	4.5	6.5
0.0				
4.0	mb		5.0	6.8
5.5	mb	17	5.1	
5.3	mb	26	5.1	7.7
5.1	mb	11	5.2	7.8
0.0				
0.0	mb		4.5	6.3
4.8	mb	33	4.6	
5.4	mb			
4.0	mb			
4.4	mb			
3.8	mb			
0.0	mb		3.7	4.8
5.1	mb		4.8	6.2
3.7	ML		3.8	4.9
0.0		33		

07/22/66	025124.8	0.620	29.730	284	814	5.8	ML
07/23/66	202117.0	-4.000	36.000	196	315	3.7	ML
07/23/66	020255.0	-6.000	32.000	0		0.0	
07/24/66	102503.0	-3.000	36.000	205	212	3.9	ML
07/31/66	151900.0	-5.570	35.700	194	492	5.4	ML
07/31/66	174451.1	0.670	30.020	285	784	6.1	ML
08/15/66	071937.9	-4.000	34.000	266	396	4.6	ML
09/02/66	000916.0	0.600	31.600	0		0.0	
09/04/66	033950.0	-4.000	33.000	0		0.0	
09/08/66	223416.0	-3.300	35.400	214	274	3.5	ML
09/24/66	132928.0	0.700	36.200	342	229	4.6	ML
10/02/66	201131.8	-5.300	35.800	194	461	4.6	ML
10/05/66	083440.1	0.020	29.940	280	777	6.2	ML
10/30/66	050535.2	-3.620	29.970	0	813	6.2	ML
10/30/66	013039.5	0.000	0.000	0	811	0.0	ML
10/30/66	050535.2	-3.620	29.970	251	803	6.2	ML
10/30/66	044756.0]	-1.600	33.000	0		0.0	
10/30/66	050535.2	-3.620	29.970	0		0.0	
11/04/66	072719.8	0.000	0.000	0	400	4.9	ML
11/12/66	102215.0	-4.000	34.000	225	434	4.1	ML
11/14/66	161042.5	-5.080	35.800	194	437	5.0	ML
11/20/66	104429.0	-4.500	35.400	203	391	4.7	ML
11/23/66	041738.0	3.800	31.300	0		0.0	
11/25/66	212859.6	0.800	30.000	0	788	5.4	ML
12/02/66	002331.6	-3.400	39.500	0	350	4.8	ML
12/10/66	204515.0	-5.000	36.000	192	423	4.5	ML
12/14/66	175820	2.000	31.000	0		0.0	
12/17/66	180343.8	5.830	37.100	0		0.0	
01/12/67	222210.0	2.100	31.210	0		0.0	
04/06/67	084613.0	1.000	31.000	0		0.0	
04/16/67	070220.8	-3.000	36.000	205	212	3.5	ML
04/16/67	170137.6	-4.200	37.000	0	324	5.2	ML
04/16/67	070220.0	-3.000	36.000	0		0.0	
05/08/67	135950.0	-3.000	36.000	205	618	5.5	ML
05/23/67	190344.2	4.200	37.000	2	330	4.2	ML
05/08/67	135827.0	4.100	35.400	281	618	0.0	ML
06/28/67	223819.0	-3.800	36.500	186	282	4.8	ML

	DEP	UmbN	MD
4.8 mb			
3.2 ML	33	4.9	7.2
0.0	3.3	3.3	4.2
3.4 ML		3.4	4.1
4.3 ML	06	4.6	6.1
5.0 mb	00	5.2	6.1
4.1 ML		4.0	
4.0 mb			
3.5 mb			
3.5 ML		3.1	
4.2 ML	00	4.0	4.9
3.8 mb		3.5	5.2
5.3 mb	28	5.2	7.8
5.2 mb	33	5.2	7.9
0.0			
5.2 mb		5.2	7.9
0.0			
5.2 mb		4.3	5.6
0.0		3.5	4.9
3.8 ML			
4.2 ML	00	4.3	5.6
4.0 ML		4.1	5.2
0.0 mb			
0.0		4.6	6.0
4.3 mb		4.0	5.2
3.9 ML		3.9	5.0
4.1 mb			
4.9 mb			
0.0			
0.0			
3.9 ML		3.2	3.8
4.0 mb		4.5	5.3
0.0			
0.0			5.7
0.0		3.7	4.6
4.7 mb			
4.5 ML		4.1	5.4

07/08/67	163959.0	-3.000	36.000	205	212	4.5 ML
09/09/67	233554.0	4.000	32.300	0		0.0
09/15/67	170135.6	-3.990	35.740	201	324	4.7 ML
10/14/67	232931.6	-3.320	38.190	145	274	4.7 ML
10/30/67	212241.0	2.600	31.200	0		0.0
10/30/67	195545.0	1.800	35.400	0		0.0
10/31/67	135235.0	1.990	31.210	300	720	5.9 ML
11/29/67	053209.0	3.000	33.000	0		0.0
12/02/67	125317.0	4.000	36.000	351	316	4.5 ML
12/17/67	180347.5	-5.830	37.100	2	796	6.3 ML
12/29/67	160703.0	1.300	34.000	312	423	4.7 ML
12/29/67	233913.0	1.300	34.000	312	423	4.4 ML
12/29/67	130432.0	1.300	34.000	283	525	5.1 ML
12/29/67	134630.0	3.000	31.400	0		0.0
12/29/67	154301.0	2.800	31.200	0		0.0
12/30/67	102708.3	-2.100	29.950	263	767	5.3 ML
01/15/68	182320.0	-2.700	40.200	112	409	5.3 ML
02/17/68	070420.0	-5.200	36.700	181	453	5.2 ML
03/14/68	194416.8	-1.000	33.800	275	374	0.0
03/16/68	070227.9	-0.610	34.000	295	277	0.0
03/18/68	231403.9	-1.000	34.300	285	323	0.0 ML
03/21/68	032602.0	-0.500	34.200	286	291	4.2 ML
03/21/68	025936.0	-0.600	34.300	0		0.0
03/21/68	033503.0	-0.500	34.300	287	291	4.3 ML
03/31/68	233557.4	4.700	35.000	287	377	5.1 ML
04/01/68	035608.0	-0.660	34.400	284	276	4.2 ML
05/10/68	080416.0	-0.690	34.400	283	275	4.6 ML
05/20/68	130017.7	-3.170	37.100	171	213	4.5 ML
06/06/68	200810.0	-3.800	36.600	184	282	4.1 ML
06/07/68	161154.0	-4.000	35.000	213	363	5.2 ML
06/10/68	200553.0	-3.800	35.300	210	327	4.7 ML
06/10/68	20053.3	-3.800	35.300	0	327	4.7 ML
06/13/68	165350.0	2.210	33.950	320	508	4.8 ML
06/13/68	165349.5	2.210	33.950	0		0.0
06/24/68	032200.5	-0.400	29.900	0	775	0.0
07/03/68	191832.5	-4.810	34.980	207	393	4.8 ML
07/06/68	073758.7	0.061	35.170	196	419	5.0 ML

3.8 ML	DEP	UmbN	MD
0.0		3.2	4.8
0.0 mb		4.1	5.4
5.1 mb	33	4.5	6.1
4.8 mb			
4.4 mb			
5.1 mb	33	5.0	
0.0			
3.9 ML		3.9	4.7
4.9 mb	19	4.4	
4.0 mb	00	4.1	5.3
4.1 mb		3.8	5.9
4.2 mb	00		
4.4 mb	00	4.3	6.1
4.4 mb			
4.7 mb		4.4	6.6
4.5 ML		4.5	5.7
0.0 mb	33	4.5	5.7
4.1 ML			
0.0			
3.9 ML			
4.0 ML	41	3.7	4.7
4.5 mb	33		
4.0 ML		38	4.8
3.9 ML	33	44	6.3
4.9 ML	00	3.7	4.8
4.9 ML	18	4.0	5.2
0.0 mb	33	3.9	5.4
3.8 ML		3.7	4.8
5.1 ML	00	4.4	6.0
4.4 ML	00	4.1	5.5
4.4 mb			
-4.3 ML	66	4.1	5.6
0.0			
4.5 ML	00		
4.4 ML	00	4.1	5.9
4.4 ML		4.3	6.1

APPENDIX II

X km	Pg m	Pg s	P* m	P* s	Pn m	Pn s	Sg m	Sg s	S* m	S* s	Sn m	Sn s
0	0	1.6	0	0.0	0	0.0	0	2.8	0	0.0	0	0.0
20	0	3.6	0	0.0	0	0.0	0	6.2	0	0.0	0	0.0
40	0	6.6	0	6.6	0	0.0	0	11.5	0	0.0	0	0.0
60	0	9.7	0	9.6	0	11.0	0	17.0	0	16.9	0	19.6
80	0	12.9	0	12.6	0	13.5	0	22.5	0	22.4	0	23.8
100	0	16.1	0	15.6	0	16.0	0	28.1	0	27.8	0	28.1
120	0	19.3	0	18.6	0	18.4	0	33.6	0	33.2	0	32.3
140	0	22.5	0	21.6	0	20.9	0	39.2	0	38.6	0	36.6
160	0	25.6	0	24.6	0	23.4	0	44.8	0	44.0	0	40.8
180	0	28.8	0	27.6	0	25.8	0	50.4	0	49.5	0	45.0
200	0	32.0	0	30.7	0	28.3	0	55.9	0	54.9	0	49.3
220	0	35.2	0	33.7	0	30.8	1	1.5	1	0.3	0	53.5
240	0	38.4	0	36.7	0	33.2	1	7.1	1	5.7	0	57.7
260	0	41.6	0	39.7	0	35.7	1	12.7	1	11.1	1	2.0
280	0	44.8	0	42.7	0	38.2	1	18.3	1	16.6	1	6.2
300	0	48.0	0	45.7	0	40.6	1	23.8	1	22.0	1	10.4
320	0	51.2	0	48.7	0	43.1	1	29.4	1	27.4	1	14.7
340	0	54.4	0	51.7	0	45.6	1	35.0	1	32.8	1	18.9
360	0	57.6	0	54.8	0	48.0	1	40.6	1	38.2	1	23.2
380	1	0.8	0	57.8	0	50.5	1	46.2	1	43.7	1	27.4
400	1	4.0	1	0.8	0	53.0	1	51.8	1	49.1	1	31.6
420	1	7.2	1	3.8	0	55.5	1	57.4	1	54.5	1	35.9
440	1	10.4	1	6.8	0	57.9	2	2.9	1	59.9	1	40.1
460	1	13.6	1	9.8	1	0.4	2	8.5	2	5.3	1	44.3
480	1	16.8	1	12.8	1	2.9	2	14.1	2	10.8	1	48.6
500	1	20.0	1	15.8	1	5.3	2	19.7	2	16.2	1	52.8
520	1	23.2	1	18.9	1	7.8	2	25.3	2	21.6	1	57.1
540	1	26.4	1	21.9	1	10.3	2	30.9	2	27.0	2	1.3
560	1	29.6	1	24.9	1	12.7	2	36.4	2	32.4	2	5.5
580	1	32.8	1	27.9	1	15.2	2	42.0	2	37.9	2	9.8
600	1	36.0	1	30.9	1	17.7	2	47.6	2	43.3	2	14.0
620	1	39.2	1	33.9	1	20.1	2	53.2	2	48.7	2	18.2
640	1	42.4	1	36.9	1	22.6	2	58.8	2	54.1	2	22.5
660	1	45.6	1	39.9	1	25.1	3	4.4	2	59.5	2	26.7
680	1	48.8	1	42.9	1	27.6	3	10.0	3	5.0	2	31.0
700	1	52.0	1	46.0	1	30.0	3	15.6	3	10.4	2	35.2

Travel time table for the Rift Valley (slightly modified KRISP90 model)

X km	Pg m	Pg s	P* m	P* s	Pn m	Pn s	Sg m	Sg s	S* m	S* s	Sn m	Sn s
0	0	1.6	0	0.0	0	0.0	0	2.8	0	0.0	0	0.0
20	0	3.7	0	0.0	0	0.0	0	6.2	0	0.0	0	0.0
40	0	6.8	0	6.7	0	0.0	0	11.5	0	0.0	0	0.0
60	0	10.0	0	9.7	0	11.1	0	17.0	0	16.9	0	19.6
80	0	13.2	0	12.7	0	13.6	0	22.5	0	22.4	0	23.8
100	0	16.5	0	15.7	0	16.1	0	28.1	0	27.8	0	28.1
120	0	19.7	0	18.7	0	18.6	0	33.6	0	33.2	0	32.3
140	0	23.0	0	21.7	0	21.0	0	39.2	0	38.6	0	36.6
160	0	26.3	0	24.7	0	23.5	0	44.8	0	44.0	0	40.8
180	0	29.6	0	27.8	0	26.0	0	50.4	0	49.5	0	45.0
200	0	32.8	0	30.8	0	28.5	0	55.9	0	54.9	0	49.3
220	0	36.1	0	33.8	0	31.0	1	1.5	1	0.3	0	53.5
240	0	39.4	0	36.8	0	33.5	1	7.1	1	5.7	0	57.7
260	0	42.7	0	39.8	0	36.0	1	12.7	1	11.1	1	2.0
280	0	45.9	0	42.8	0	38.5	1	18.3	1	16.6	1	6.2
300	0	49.2	0	45.8	0	41.0	1	23.8	1	22.0	1	10.4
320	0	52.5	0	48.8	0	43.5	1	29.4	1	27.4	1	14.7
340	0	55.8	0	51.9	0	45.9	1	35.0	1	32.8	1	18.9
360	0	59.0	0	54.9	0	48.4	1	40.6	1	38.2	1	23.2
380	1	2.3	0	57.9	0	50.9	1	46.2	1	43.7	1	27.4
400	1	5.6	1	0.9	0	53.4	1	51.8	1	49.1	1	31.6
420	1	8.9	1	3.9	0	55.9	1	57.4	1	54.5	1	35.9
440	1	12.1	1	6.9	0	58.4	2	2.9	1	59.9	1	40.1
460	1	15.4	1	9.9	1	0.9	2	8.5	2	5.3	1	44.3
480	1	18.7	1	12.9	1	3.4	2	14.1	2	10.8	1	48.6
500	1	22.0	1	15.9	1	5.9	2	19.7	2	16.2	1	52.8
520	1	25.3	1	19.0	1	8.4	2	25.3	2	21.6	1	57.1
540	1	28.5	1	22.0	1	10.9	2	30.9	2	27.0	2	1.3
560	1	31.8	1	25.0	1	13.3	2	36.4	2	32.4	2	5.5
580	1	35.1	1	28.0	1	15.8	2	42.0	2	37.9	2	9.8
600	1	38.4	1	31.0	1	18.3	2	47.6	2	43.3	2	14.0
620	1	41.7	1	34.0	1	20.8	2	53.2	2	48.7	2	18.2
640	1	44.9	1	37.0	1	23.3	2	58.8	2	54.1	2	22.5
660	1	48.2	1	40.0	1	25.8	3	4.4	2	59.5	2	26.7
680	1	51.5	1	43.1	1	28.3	3	10.0	3	5.0	2	31.0
700	1	54.8	1	46.1	1	30.8	3	15.6	3	10.4	2	35.2

Travel time table for the region extending towards the coastal region (Finnish model)

X km	Pg m	Pg s	P* m	P* s	Pn m	Pn s	Sg m	Sg s	S* m	S* s	Sn m	Sn s
0	0	1.6	0	0.0	0	0.0	0	2.8	0	0.0	0	0.0
20	0	3.6	0	0.0	0	0.0	0	6.2	0	0.0	0	0.0
40	0	6.7	0	6.6	0	0.0	0	11.5	0	0.0	0	0.0
60	0	9.9	0	9.6	0	11.0	0	17.0	0	16.9	0	19.6
80	0	13.1	0	12.6	0	13.5	0	22.5	0	22.4	0	23.8
100	0	16.3	0	15.6	0	16.0	0	28.1	0	27.8	0	28.1
120	0	19.6	0	18.6	0	18.5	0	33.6	0	33.2	0	32.3
140	0	22.8	0	21.5	0	21.0	0	39.2	0	38.6	0	36.6
160	0	26.1	0	24.5	0	23.5	0	44.8	0	44.0	0	40.8
180	0	29.3	0	27.5	0	26.0	0	50.4	0	49.5	0	45.0
200	0	32.6	0	30.5	0	28.5	0	55.9	0	54.9	0	49.3
220	0	35.8	0	33.5	0	31.0	1	1.5	1	0.3	0	53.5
240	0	39.1	0	36.5	0	33.5	1	7.1	1	5.7	0	57.7
260	0	42.3	0	39.5	0	36.0	1	12.7	1	11.1	1	2.0
280	0	45.6	0	42.4	0	38.5	1	18.3	1	16.6	1	6.2
300	0	48.8	0	45.4	0	41.0	1	23.8	1	22.0	1	10.4
320	0	52.1	0	48.4	0	43.5	1	29.4	1	27.4	1	14.7
340	0	55.3	0	51.4	0	46.0	1	35.0	1	32.8	1	18.9
360	0	58.6	0	54.4	0	48.5	1	40.6	1	38.2	1	23.2
380	1	1.8	0	57.4	0	51.0	1	46.2	1	43.7	1	27.4
400	1	5.1	1	0.3	0	53.5	1	51.8	1	49.1	1	31.6
420	1	8.3	1	3.3	0	56.0	1	57.4	1	54.5	1	35.9
440	1	11.6	1	6.3	0	58.5	2	2.9	1	59.9	1	40.1
460	1	14.8	1	9.3	1	1.0	2	8.5	2	5.3	1	44.3
480	1	18.1	1	12.3	1	3.5	2	14.1	2	10.8	1	48.6
500	1	21.3	1	15.3	1	6.0	2	19.7	2	16.2	1	52.8
520	1	24.6	1	18.3	1	8.5	2	25.3	2	21.6	1	57.1
540	1	27.8	1	21.2	1	11.0	2	30.9	2	27.0	2	1.3
560	1	31.1	1	24.2	1	13.5	2	36.4	2	32.4	2	5.5
580	1	34.3	1	27.2	1	16.0	2	42.0	2	37.9	2	9.8
600	1	37.6	1	30.2	1	18.5	2	47.6	2	43.3	2	14.0
620	1	40.8	1	33.2	1	21.0	2	53.2	2	48.7	2	18.2
640	1	44.1	1	36.2	1	23.5	2	58.8	2	54.1	2	22.5
660	1	47.3	1	39.2	1	26.0	3	4.4	2	59.5	2	26.7
680	1	50.6	1	42.1	1	28.5	3	10.0	3	5.0	2	31.0
700	1	53.8	1	45.1	1	31.0	3	15.6	3	10.4	2	35.2

Travel time table for the region extending towards the Western Rift Valley (Dar- model)

X km	Pg m	Pg s	P* m	P* s	Pn m	Pn s	Sg m	Sg s	S* m	S* s	Sn m	Sn s
0	0	1.6	0	0.0	0	0.0	0	2.8	0	0.0	0	0.0
20	0	3.5	0	0.0	0	0.0	0	6.2	0	0.0	0	0.0
40	0	6.5	0	6.5	0	0.0	0	11.5	0	0.0	0	0.0
60	0	9.6	0	9.5	0	11.0	0	17.0	0	16.9	0	19.6
80	0	12.7	0	12.6	0	13.5	0	22.5	0	22.4	0	23.8
100	0	15.9	0	15.6	0	15.9	0	28.1	0	27.8	0	28.1
120	0	19.0	0	18.6	0	18.4	0	33.6	0	33.2	0	32.3
140	0	22.1	0	21.7	0	20.9	0	39.2	0	38.6	0	36.6
160	0	25.3	0	24.7	0	23.3	0	44.8	0	44.0	0	40.8
180	0	28.4	0	27.7	0	25.8	0	50.4	0	49.5	0	45.0
200	0	31.6	0	30.7	0	28.2	0	55.9	0	54.9	0	49.3
220	0	34.7	0	33.8	0	30.7	1	1.5	1	0.3	0	53.5
240	0	37.9	0	36.8	0	33.2	1	7.1	1	5.7	0	57.7
260	0	41.0	0	39.8	0	35.6	1	12.7	1	11.1	1	2.0
280	0	44.2	0	42.9	0	38.1	1	18.3	1	16.6	1	6.2
300	0	47.3	0	45.9	0	40.5	1	23.8	1	22.0	1	10.4
320	0	50.5	0	48.9	0	43.0	1	29.4	1	27.4	1	14.7
340	0	53.7	0	52.0	0	45.5	1	35.0	1	32.8	1	18.9
360	0	56.8	0	55.0	0	47.9	1	40.6	1	38.2	1	23.2
380	0	60.0	0	58.0	0	50.4	1	46.2	1	43.7	1	27.4
400	1	3.1	1	1.0	0	52.8	1	51.8	1	49.1	1	31.6
420	1	6.3	1	4.1	0	55.3	1	57.4	1	54.5	1	35.9
440	1	9.4	1	7.1	0	57.8	2	2.9	1	59.9	1	40.1
460	1	12.6	1	10.1	1	0.2	2	8.5	2	5.3	1	44.3
480	1	15.7	1	13.2	1	2.7	2	14.1	2	10.8	1	48.6
500	1	18.9	1	16.2	1	5.1	2	19.7	2	16.2	1	52.8
520	1	22.0	1	19.2	1	7.6	2	25.3	2	21.6	1	57.1
540	1	25.2	1	22.3	1	10.1	2	30.9	2	27.0	2	1.3
560	1	28.3	1	25.3	1	12.5	2	36.4	2	32.4	2	5.5
580	1	31.5	1	28.3	1	15.0	2	42.0	2	37.9	2	9.8
600	1	34.7	1	31.3	1	17.4	2	47.6	2	43.3	2	14.0
620	1	37.8	1	34.4	1	19.9	2	53.2	2	48.7	2	18.2
640	1	41.0	1	37.4	1	22.4	2	58.8	2	54.1	2	22.5
660	1	44.1	1	40.4	1	24.8	3	4.4	2	59.5	2	26.7
680	1	47.3	1	43.5	1	27.3	3	10.0	3	5.0	2	31.0
700	1	50.4	1	46.5	1	29.7	3	15.6	3	10.4	2	35.2

Travel time table for the region extending towards the southern part of Kenya and northern part of Tanzania (Profile 4 model)

X km	Sg-Pg m	s	Sg-P* m	s	Sg-Pn m	s	S*-P* m	s	Sn-Pn m	s
0	0	1.2	0	0.0	0	0.0	0	0.0	0	0.0
20	0	2.5	0	0.0	0	0.0	0	0.0	0	0.0
40	0	4.8	0	0.0	0	0.0	0	7.4	0	0.0
60	0	7.1	0	0.0	0	7.5	0	9.5	0	10.6
80	0	9.4	0	9.1	0	10.5	0	11.7	0	12.5
100	0	11.7	0	11.5	0	13.5	0	13.9	0	14.3
120	0	14.0	0	14.0	0	16.5	0	16.0	0	16.1
140	0	16.4	0	16.4	0	19.6	0	18.2	0	18.0
160	0	18.7	0	18.8	0	22.6	0	20.4	0	19.8
180	0	21.0	0	21.3	0	25.6	0	22.5	0	21.6
200	0	23.3	0	23.7	0	28.7	0	24.7	0	23.5
220	0	25.7	0	26.1	0	31.7	0	26.9	0	25.3
240	0	28.0	0	28.6	0	34.7	0	29.0	0	27.2
260	0	30.3	0	31.0	0	37.8	0	31.2	0	29.0
280	0	32.6	0	33.5	0	40.8	0	33.4	0	30.8
300	0	35.0	0	35.9	0	43.9	0	35.5	0	32.7
320	0	37.3	0	38.4	0	46.9	0	37.7	0	34.5
340	0	39.6	0	40.8	0	49.9	0	39.8	0	36.3
360	0	42.0	0	43.3	0	53.0	0	42.0	0	38.2
380	0	44.3	0	45.7	0	56.0	0	44.2	0	40.0
400	0	46.6	0	48.2	0	59.1	0	46.3	0	41.9
420	0	48.9	0	50.6	1	2.1	0	48.5	0	43.7
440	0	51.3	0	53.1	1	5.1	0	50.7	0	45.5
460	0	53.6	0	55.5	1	8.2	0	52.8	0	47.4
480	0	55.9	0	57.9	1	11.2	0	55.0	0	49.2
500	0	58.3	1	0.4	1	14.3	0	57.2	0	51.0
520	1	0.6	1	2.8	1	17.3	0	59.3	0	52.9
540	1	2.9	1	5.3	1	20.4	1	1.5	0	54.7
560	1	5.2	1	7.7	1	23.4	1	3.7	0	56.6
580	1	7.6	1	10.2	1	26.4	1	5.8	0	58.4
600	1	9.9	1	12.6	1	29.5	1	8.0	1	0.2
620	1	12.2	1	15.1	1	32.5	1	10.1	1	2.1
640	1	14.6	1	17.5	1	35.6	1	12.3	1	3.9
660	1	16.9	1	20.0	1	38.6	1	14.5	1	5.7
680	1	19.2	1	22.4	1	41.7	1	16.6	1	7.6
700	1	21.6	1	24.9						

Travel time table for the Unified model